ELECTRIC POWER SYSTEM FOR HIGH ALTITUDE UAV TECHNOLOGY SURVEY

POWER COMPUTING SOLUTIONS, INC.
2001 Aerospace Parkway
Brook Park, Ohio 44142

CONTRACT NAS2-96011
NASA Ames Research Center
Moffett Field, California

November 16, 1997

Table of Contents

Table of Figures

Table of Tables

EXECUTIVE SUMMARY

In support of the National Aeronautics and Space Administration's Environmental Research Aircraft and Sensor Technology (ERAST) Program, Power Computing Solutions, Inc. (PCS) completed a nine month contract to assess electric powertrain technologies with application to high altitude Unmanned Aerial Vehicles (UAV). The contract objectives were to determine the feasibility of achieving the aircraft mission requirements outlined in Table 1 using electric powertrain components that were available on January 1, 1997 and using electric powertrain components that are projected to be available on January 1, 2001.

PCS, Inc. assembled the performance data base for the 1997 technology baseline and projected the performance for the 2001 technology baseline for those powertrain components listed in Table 2. For both the 1997 and 2001 performance baselines, PCS, Inc. devised performance characteristic profiles to estimate mass, volume, and efficiency for each powertrain component listed in Table 2. Building upon a previously devised solar electric UAV simulation platform, PCS, Inc. included the performance characteristic profiles and added flight simulation capabilities for Liebeck, Wortman, and Clark Y airfoils. One hundred twenty five solar electric UAV configurations and missions were simulated. In addition to those requirements listed in Table 1, the simulations were carried out for both span loaded and twin boom airframes at latitudes of 0 deg, 25 deg, and 40 deg with mission start dates of March 15 and June 15. Since there was no time-of-day requirement for reaching the maximum altitude, all aircraft took off at dawn. Throughout the analyses, synergistic design opportunities were investigated with the premise that specific benefits may be realized, for example, if a single component can serve multiple functions, such as a battery being used for energy storage as well as for a structural component of the aircraft.

For each UAV mission simulation, the airframe structure, powertrain configuration (type of solar cells, energy storage options) and performance baseline (1997 or 2001) were specified. The output of each simulation included the smallest wing area (for specified aspect ratio) needed to accomplish the specified mission. All of the candidate aircraft were able to meet the mission requirements which included the 0 km radius of action using solar cell power with no energy storage. For the 1000 km radius of action requirement, only the lowest efficiency (amorphous silicon) photovoltaic system was unable to achieve the missions. Those results dictated that in general, photovoltaic power alone was best for the missions of interest and energy storage capability yielded modest benefit. Exceptions to

this were calculated for the most challenging missions. For example, for the low altitude (90 kft.), high payload mass (225 kg), long radius of action (1,000 km) case at 40 deg latitude, the use of primary batteries allowed a reduction of approximately 15% in wing area compared to the analogous aircraft using only solar power. For those cases using primary batteries, the aircraft wing loading increased slightly, from about 1.02 lb/ft^2 to about 1.09 lb/ft^2. Rechargeable energy storage systems were not beneficial for any of the mission simulations mainly because the 35 minute required time at altitude was too small to warrant the need for rechargeable systems.

One synergistic design opportunity was found to have significant benefits for these missions. By using a mylar substrate, the amorphous silicon solar cells could also be used as the outer airfoil covering. This enabled these relatively low efficiency cells to produce aircraft with wing areas comparable to their higher efficiency solar cell (single junction and multi-junction) counterparts, thereby allowing tremendous cost savings. One of the most important conclusions from this effort was that the use of the high efficiency (multi-junction) solar cells or the use of the synergistic amorphous silicon solar cell configuration yields aircraft that can accomplish the majority of the missions of interest for any latitude between 0 deg, and 55 deg. Hence, instead of oversizing a single aircraft or procuring several different aircraft with less effective solar cell configurations, a single versatile aircraft can be constructed and implemented to accomplish a majority of the solar electric UAV missions of interest.

INTRODUCTION

The first solar electric Unmanned Aerial Vehicle (UAV) program started over 20 years ago with the Sunrise I and has continued to the present. Table 3.0 shows the progression of solar powered aircraft from the early Sunrise I and II aircraft with wing spans of about 30 feet to Aerovironment's Pathfinder aircraft with a wing span of 100 feet. The capabilities of each successive aircraft has also increased dramatically. This is best shown by Aerovironment's success in setting a world altitude record of over 71,000 ft. with Pathfinder in July of 1997. This increase in capabilities can be directly related to the improvements in energy source technology as well as the introduction of lightweight materials with which the aircraft are made. Aerovironment, under funding by the National Aeronautics and Space Administration (NASA) Environmental Research Aircraft and Sensor Technology (ERAST) program is now developing two new solar electric aircraft. One of these new aircraft is designed to fly at 100,000 ft while the other is designed to be

capable of continuous flight (day and night during a narrow range of seasons and latitudes) by adding an energy storage system to a solar cell power generation system.

While all of these systems have pushed the current State-of-the-Art (SOA) for both aircraft design and energy source technology, it is still a challenge to develop a solar powered aircraft which is inexpensive, capable of sustained flight over a wide range of seasons and latitudes, and capable of carrying significant payloads. The rapid advancements in energy storage and electric drivetrain technologies being achieved through electric vehicle and renewable energy development programs worldwide may enable a more cost effective and capable electric aircraft in the future.

In support of NASA's ERAST Program, Power Computing Solutions, Inc. (PCS) completed a nine month contract to assess electric powertrain technologies with application to high altitude Unpiloted Aerial Vehicles (UAV). This study was specifically designed by NASA Ames Research Center to ascertain which, if any, technologies would enable the all electric aircraft to perform the missions outlined by the ERAST Leadership Committee. The contract objectives were to determine the feasibility of achieving the aircraft mission requirements outlined in Table 1 using electric powertrain components that were available in 1997 and using electric powertrain components that are projected to be available in 2001. This effort included a survey and characterization of energy source technologies, a survey and characterization of drive system technologies, an analysis of airframe concepts, and an analysis of aircraft component integration concepts. The most promising energy sources, drive components, and aircraft structures were then integrated to produce conceptual UAV designs for which mission simulations were conducted. Throughout the analyses, synergistic design opportunities were investigated with the premise that specific benefits may be realized, for example, if a single component can serve multiple functions, such as a battery being used for energy storage as well as for a structural component of the aircraft.

For the energy source and drive system technology surveys, candidate systems were identified, ranked for UAV suitability, and downselected for further analysis and incorporation into the integrated aircraft mission simulations. The detailed analyses resulted in standard characteristic profiles that were used to estimate the mass, volume, and efficiency of the individual components that were selected. Two technology baselines were required for each standard characteristic profile, one baseline for performance demonstrated and/or predicted in 1997 and one baseline for performance predicted in 2001. PCS, Inc. assembled the performance data base for the 1997 technology baseline and projected the performance for the 2001 technology baseline for those powertrain components listed in Table 2. Performance of the integrated total powertrain was considered to be much more

important than performance of a single isolated powertrain component, hence a total systems approach was undertaken for all of the analyses performed for this contract. The powertrain analyses included all of those items in Table 2 and the fundamental performance characteristics of each of those items was devised to at least a first order level.

Span loaded airframes and twin boom airframes were considered for this contract. Conceptual UAV designs were created by integrating the different powertrain components with the two types of airframes. The PCS Solar Aircraft System Simulator (SAAC was developed by incorporating the standard characteristics profiles for the powertrain components along with the appropriate data for Liebeck, Wortman, and Clark Y airfoils into a previously devised solar electric UAV simulation code. One hundred twenty five solar electric UAV configurations and missions were simulated. In addition to those requirements listed in Table 1, the simulations were carried at latitudes of 0°, 25°, and 40° with mission start dates of March 15 and June 15. Since there was no time-of-day requirement for reaching the maximum altitude, all aircraft took off at dawn. The simulation results included the smallest wing area (for specified aspect ratio) needed to accomplish the specified mission. Those results were used to assess the potential advantages and disadvantages of the various energy source and drive system components.

Each task is described in detail in the following sections.

ENERGY SOURCE TECHNOLOGY SURVEY

Introduction

There is an extraordinarily large number of electrical power systems that can be considered for the solar-electric powered UAVs. Solar cells, non-rechargeable (primary) and rechargeable (secondary) batteries, fuel cells, semi-cells, flywheels, and capacitors are candidates for the UAV. Microwave and laser beamed power systems can also be considered. The best power system(s) cannot be determined a priori, but rather a total systems approach must be undertaken to determine the best power system configuration for specific mission requirements. For this contract, the mission requirements were defined up front (Table 1), but the energy storage requirements (if any) needed to satisfy the mission requirements were certainly not known before the required mission simulations were conducted. It was therefore necessary to rank and prioritize the candidate power systems and then to select several of those candidate power system technologies that would be characterized and included in the aircraft mission design/analysis and simulation tasks.

The energy source technology survey can be broken into six distinct parts:

1. Solar Cells
2. Non-Regenerative and Regenerative Fuel Cells
3. Primary and Secondary Batteries
4. Flywheels
5. Semi-cells
6. Capacitors

A qualitative ranking system was devised in order to compare and to prioritize the candidate power systems. The criteria that were applied for selecting the candidate power systems to be included in the analyses are listed in Table 4 and the relative rankings are shown in Table 5. The relative rankings that were assigned by PCS, Inc. accounted for input from the open literature, interviews with various experts, and direct experiences of PCS, Inc. personnel. Of all the candidate power systems listed in Table 5, only the semi-cells and capacitors were not selected for analysis for this study. For the power system technologies that were deemed suitable for the UAV, the standard performance characteristics profiles were devised for both the 1997 and 2001 timeframes. A general discussion of the candidate energy source technologies and the standard characteristics profiles for the most suitable technologies follows.

In addition to the above mentioned energy sources an investigation of microwave and laser beamed power aircraft was performed. While these aircraft may indeed be smaller because of the increased energy flux (when compared with the sun), the requirement of a transmission tower (or series of towers), ground infrastructure and support logistics necessary for such an operation made these systems impractical. Secondly, these systems were deemed unacceptable because of safety concerns of aircraft/wildlife passing through the energy transmission beam.

Solar Cells

Introduction

A solar cell or photovoltaic cell (PV) is a solid state semiconductor device which converts solar energy into electrical energy using the photovoltaic effect. When photons of sufficient energy strike the top surface of the cell they liberate electrons from the

semiconductor material (for example silicon). To take advantage of this liberation of electrons a solar cell separates the electrons from the semiconductor material before they have a chance to recombine to the material. This is accomplished by an internal electric field which is produced in the cell by a p-n junction. This junction is formed very near the front surface of the cell by diffusing n type dopant into the p type semiconductor to make a n/p junction. The net effect of the junction is to produce an electric field with a polarity which accelerates electrons toward the front surface and holes toward the rear surface of the cell. Electrical contacts are added to the front and back of the cell in order to utilize this flow of electrons.

Solar Cell Performance

There are three main types or classes of solar cells under production today, thin film, single junction and multiple junction. The theory behind the operation of each type of solar cell is the same, however the materials and manufacturing techniques used for each class differ. In addition to the types of solar cells just listed there are various solar energy concentrator devices which can enhance the performance of the PV's.

There have been significant advances in solar cell development over the last decade. Tables 6 through 13 summarize this development for thin film, single junction and multi-junction solar cells constructed of various materials. These tables represent the state of the art in single cell and submodule production of the cells and materials listed.

Solar Cell Module Performance

Obviously, single cell or small submodules do not represent how these solar cells would perform in a solar aircraft. The efficiencies given in the single cell modules are probably not attainable in mass production. However these tables do indicate which types of cells and materials hold the most promise. In order to get a more realistic estimate of the performance of various types of solar cells one has to look at the performance of full modules. Tables 14 though 19 list solar cell module performance for various solar cell types and these numbers are more indicative of the types of performance which could be achieved in the electric aircraft.

Thin Film Technology

Of all the cells studied, perhaps the most rapid development has come in the area of thin film solar cells. Over the past 20 years significant changes in efficiency have taken place. Figures 1.0 and 2.0 show the rapid increase in efficiency as a function of time over the last 20 years for both CdTe and CuInSe cells.

Cost

For solar aircraft applications both the cost and durability of the solar cell modules are of concern. Even though the multi-juntion and single junction crystalline cells have the highest performance, their applications toward solar powered aircraft have disadvantages. Except for basic Silicon cells, single and multi-junction solar cells can be very costly $500 per cell or more[i]. This cost would be prohibitive in using these cells to populate the wing surface of a fleet of Pathfinder sized solar aircraft. Also the majority of these cells are extremely brittle. This quality makes their use in an aircraft whose wings must flex and move under aerodynamic loading an engineering challenge not to mention ground handling.

Selection

If only cost and integration issues are used as the criteria for the selection of a solar cell type then the PVs which hold the most promise in solar powered aircraft are the thin film solar cells. The cost of these cells is low and they are fairly flexible. They have the potential to be used as the aerodynamic surface of the aircraft and conform to its curves. Although the efficiency of this type of cell is less than that of crystalline cells developments are still being made and the efficiency levels of these cells have increased significantly since their initial development. Figures 1 and 2 show major advancements in two types of thin film cells over the past two and a half decades.

Because each of the solar cell types has characteristics which may make it the most desirable for an electric aircraft, none were eliminated from consideration. Therefore, from this data, PCS estimated an overall characteristic efficiency, mass and cost of each type of solar cell on a per module basis which is an attempt to best represent and differentiate each type of solar cell. Table 20 shows this comparison.

Regenerative and Non-Regenerative Fuel Cell Systems

Introduction

Fuel cell systems are characterized by the energy conversion components. These include the fuel cell stacks, energy storage component, reactants and tankage, as well as the ancillary components such as piping, valves, heat exchangers, product water separators, and recirculation pumps. Electrolyzer stacks are also required for regenerative fuel cell systems. For this study, four different non-regenerative fuel cell system types were analyzed along with one type of regenerative fuel cell system. The non-regenerative fuel cell system types all included the same fuel cell stack(s) but differed in the reactant storage and/or reactant feed systems. Those four different system types were:

1. Gaseous hydrogen storage and gaseous oxygen storage,
2. Gaseous hydrogen storage and multiply turbocharged air feed system,
3. Cryogenic hydrogen storage and cryogenic oxygen storage, and
4. Cryogenic hydrogen storage and multiply turbocharged air feed system.

For the single type of regenerative fuel cell system that was analyzed, only gaseous hydrogen storage and gaseous oxygen storage were assumed.

Although several different fuel cell types may potentially be feasible for solar electric aircraft propulsion systems, only proton exchange membrane (PEM) fuel cells were analyzed for this study because:

1. PEM fuel cell systems are best suited for operation on pure hydrogen, which is the only fuel that was considered for this study,
2. For regenerative fuel cells, the only electrolyzer technology that can be considered for flight applications is PEM,
3. A tremendous amount of resources are being invested worldwide in PEM systems for light duty transportation applications, hence, small lightweight PEM hardware may be significantly advanced over the 1997 performance baseline.

H_2-Air and H_2-O_2 PEM Fuel Cell Technology

There are at least one dozen PEM fuel cell stack designs that could be selected as the baseline PEM hardware for this study. The main problem common to all but one of those designs is that each of those stacks was designed for H2-air operation for ground

transportation applications. The target lifetime of those stacks is only about 3,000 hrs. and the lifetime on pure oxygen, rather than air, would undoubtedly be significantly less than that. For all PEM applications using pure oxygen rather than air, some development will be required such as changing the gas flowfields to accommodate the pure oxygen. A PEM fuel cell previously developed for Unmanned Undersea Vehicle propulsion application under a NASA LeRC Contract was designed for operation on pure O_2 and may be best suited for the solar UAV. However, operating life of that system must still be substantiated for the UAV missions. The UUV PEM stack design was subsequently modified and is currently being developed for the light duty vehicle applications using H_2-Air, so both the H_2-O_2 and H_2-Air options can be considered for the basic UUV design. Without knowing apriori which type of fuel cell system configuration (H_2-O_2 or H_2-Air) would be best suited for the mission requirements, hardware currently being developed by Ballard Power Systems, Inc. was considered to be the baseline PEM fuel cell. Ballard was selected because they are the world leader in the transportation PEM fuel cell stack technology and they are the only company which has a semi-production facility for fabricating PEM fuel cell stacks. Furthermore, there has already been some development work for pure oxygen operation on Ballard hardware. Ballard hardware was also considered the PEM fuel cell stack baseline for the 2001 time frame since an enormous amount of development funding is being applied to commercializing the Ballard hardware for ground transportation applications where low stack volume and low stack weight are goals.

One significant note to consider is that NASA is pursuing improvements to the existing Space Shuttle Fuel Cell System and will soon decide if the existing alkaline fuel cell system should be replaced by a PEM fuel cell system[ii] . As part of that Shuttle Fuel Cell Upgrade Program, NASA has awarded two short-term (90 day) contracts (one to International Fuel Cells and one to AlliedSignal Aerospace) to devise conceptual PEM fuel cell system designs using their respective fuel cell technology baselines. In addition PCS Inc. was awarded a contract to develop ancillary component models for the shuttle fuel cell program[iii]. Some of these component models were used in this study. Both of the other contracts will be completed in 12/97 and NASA plans to pursue system hardware development efforts via competitive procurements open to all PEM fuel cell developers. Through this program, there may be significant advances in PEM fuel cell system development for H_2-O_2 operation and by 2001, PEM fuel cells for aerospace applications utilizing pure oxygen may be readily available.

Baseline PEM Fuel Cell Stack Technology

The Ballard Power Systems, Inc. Mk 7 hardware was considered state-of-the-art for the 1997 performance baseline. Pow, et al.[iv] reported that 17 full-sized Mk 7 stacks have been produced as of November 1996, therefore, the hardware is assumed to be available. Overall stack performance is acceptable at the high power density regime but the Mk 7 lifetime has not been fully verified. Full rated power for the Mk 7 is 32 kW and this value was used for the 2001 performance baseline. It was assumed for this study that since the Mk 7 hardware has not been fully verified for operating lifetime, the maximum rated power for the Mk 7 as reported by Pow et al. was decreased by 22% from full rated power for the 1997 performance baseline, or 25 kW. The rationale for this was that sufficient lifetime could be achieved with the present Mk 7 design if the stack was operated at power levels less than full rated power.

The PEM fuel cell stack characteristics assumed for this study are listed in Table 21 and the electrochemical performance baseline and projections are shown in Figures 3 and 4. The fuel cell stack current-voltage relationships for the 1997 performance baseline are shown in Figure 5 for H_2-Air and for H_2-O_2. For the 2001 performance projection, it was assumed that full rated power could be sustained while maintaining acceptable life endurance. Also, the projected improvements from the 1997 timeframe to 2001 would occur at the higher current density regimes since the ongoing development efforts are targeting the light duty transportation applications where high power density is required. This translates to an improvement in the current-voltage curves at higher current densities but not necessarily at the lower current densities as shown in Figures 3 and 4.

The operating point (current and voltage) for the fuel cell system must be selected and this choice will have an effect on the total system mass and volume. For example, if the fuel cell is operated in a low current density, high voltage efficiency regime, then a relatively large fuel cell stack is required but the amount of required reactants is relatively small. Conversely, if the fuel cell is operated in a high current density, low voltage efficiency regime, then a relatively small fuel cell stack is required but the amount of required reactants is relatively large. Since no overnight flight requirements were imposed for this study, it was estimated that the discharge period for a fuel cell would be small. For the small discharge time period, it is best to minimize the fuel cell stack mass and volume as opposed to the reactant mass and a volume, hence the performance characteristic profiles are based upon fuel cell operation in the high current density regime.

Ancillary Components for Non-Regenerative PEM Fuel Cell Systems

For each fuel cell system type, a hydrogen storage sub-system, an oxygen (or air) supply sub-system, a stack heat exchanger and a power conditioner were included for the mass and volume estimations. Pressurized gas, and cryogenic storage sub-systems were included for both the 1997 technology baseline and for the 2001 technology baseline for both hydrogen and for oxygen. For the hydrogen-air systems, a multi-staged turbocharging sub-system for air was analyzed in place of gaseous or cryogenic oxygen. For the non-regenerative PEM fuel cell systems, the hydrogen supply sub-system consisted of gaseous or liquid storage vessels, a resistance heater if cryogenic hydrogen storage was implemented, and a hydrogen recirculation pump (when needed). Similarly, the oxygen supply sub-system consisted of gaseous or liquid storage vessels, a resistance heater if cryogenic oxygen storage was implemented, and an oxygen recirculation pump. For air systems, a turbocompressor took the place of the oxygen storage vessels, the oxygen recirculation pump, and the cryogenic tank resistance heater.

PEM Fuel Cell Stack Mass and Volume

Fuel cell stack mass and volume were scaled to the Ballard Mk 7 specifications that were reported by Pow et al. As noted in Table 21, the mass correlations are valid for at least twenty single cells per stack. This was because the stack endplates and tierod masses were "distributed" among the overall single cell mass, that is, the stack mass is computed solely from the number of single cells per stack. (So the calculated mass of a two cell stack, for example, would be less than the actual stack mass because the estimated end plate and tierod masses would be lower than actual). The amount of reactants required for the entire mission was calculated from the operating current, the total number of single cells, and the operating time. For all cases, an extra 10 mole% of hydrogen was added to account for venting losses and tankage residuals. Likewise, for pure oxygen systems, an extra 10 mole% was assumed but for the air systems, 100 mole% excess air flow was assumed.

Fuel Cell Waste Heat and Heat Exchanger

High power density fuel cell operation requires some degree of cooling for operating times greater than fifteen to thirty minutes. For short peak power bursts, the fuel cell stack can most likely withstand the amounts of generated heat. The fuel cell waste heat was estimated to be:

Waste Heat per Stack (Watts) = I_{FC}*(1.25-V_{FC})*(number of cells/stack)

where: I_{FC} is the fuel cell stack current (Amps) and

V_{FC} is the average single cell operating voltage (Volts).

Based upon previously developed correlations for aerospace heat exchangers[v], the heat exchanger mass was simply estimated to be 4 kg/kW heat duty and the heat exchanger volume was estimated to be one liter per kW heat duty. For the 2001 timeframe, a 25% reduction in heat exchanger mass and volume was assumed.

Pressurized Gas Storage Sub-systems

Storage vessels for high pressure gas containment were characterized by the initial storage temperature and pressure, the tank efficiency factor, and the safety factor. The tank volume was set equal to the volume of the stored gas, ie., the tank thickness was ignored in the tank volume calculation. Ideal gas behavior was assumed for the stored reactants and a 10 mole% excess of stored reactant was assumed. The tank efficiency factor was defined as { P_b•V/W }where P_b is the tank burst pressure (psia), V is the internal tank volume ($in.^3$), and W is the tank weight (lbs.). The unit for tank efficiency is always quoted as "inches". Tank efficiency factors can vary from 50,000 to 3,000,000 in. depending upon several factors, including the materials of construction and the number of fill cycles that are needed. High efficiency factors translate into small, lightweight tanks. Standard off-the-shelf steel tanks have efficiency factors between 50,000 and 280,000 in. and store gases at around 2,200 psia for the larger tanks (5+ ft. cylinders, 1+ ft. diameter) and up to 6,000 psia for the smaller bottles (1 ft. cylinder, 4 in. diameter). Lightweight tanks are constructed of a thin metal liner which serves as a gas diffusion barrier wrapped with a composite material or fiber to provide strength. Tanks rated for 3,000 psia storage are commercially available today and have efficiency factors of 800,000 in. For the 1997 performance baseline, a pressure vessel efficiency factor of 800,000 in., representative of a Kevlar wrapped tank, was used. For the 2001 performance baseline, an efficiency factor of 1,000,000 in., representative of a carbon fiber wrapped tank, was used. From the known volume of reactant required, the tankage mass was calculated as:

W(lbs.) = (SF•P_bV) / (Tank eff. factor) (where SF is the safety factor)

The safety factor can be viewed as a factor for determining the tank wall thickness. A safety factor of 2 for example, can mean that the tank shall be constructed with wall thickness twice the theoretical value needed for a specified storage pressure. Typical safety factors for commercial applications are around 4 while most aerospace applications have

safety factors around 1.5 . For the 1997 performance baseline, a safety factor of 2 was assumed while a 1.5 factor of safety was assumed for the 2001 baseline. For both technology baselines, the storage pressure was assumed to be 3,000 psia.

Cryogenic and Supercritical Storage Sub-systems

For non-regenerative fuel cell systems, hydrogen and oxygen can be stored as cryogens or in their supercritical states. The lightest weight tankage option is that currently used on the Space Shuttle but that system is extremely costly. Another option is that which was originally designed for the fuel cell powered UUV which is heavier than the Space Shuttle tanks but less costly. The UUV system was considered for both the 1997 and the 2001 baselines.

Oxygen Recirculation Pump

For the Ballard Mk 7 fuel cell stack, it is necessary to use an excess amount of oxygen (or air) to carry the product water out of the fuel cell stack. This gas/liquid mixture must be separated under most operating regimes and the oxygen gas should be recycled back to the fuel cell stack inlet. The oxygen compressor which would accomplish the recirculation was assumed to consume about 10% of the gross stack output power and assumed to weigh about 0.5 kg for both the 1997 and 2001 technology baselines.

Turbochargers for Air Delivery Sub-systems

PCS, Inc. has previous experience in developing turbocharger performance and sizing models for high altitude internal combustion engine aircraft. Even at the 100 kft altitude, where three stages of turbocharging may be required for H_2-air fuel cell operation, this type of oxidant delivery sub-system may be smaller and lighter than the gaseous and cryogenic storage options. No detailed analyses were performed for this contract, but some conservative mass and volume values for a turbocharging system, including parasitic power requirements, were assigned for the turbocharger system. The reference design point was for a 6 kW (gross power) H_2-air fuel cell system using 100% excess air where the turbocompressor mass and volume was scaled from a three-stage turbocharged system currently being researched at NASA Lewis Research Center[vi].

H_2O Electrolyzer Technology for Regenerative Fuel Cell Systems

Hamilton Standard PEM electrolyzer hardware was considered state-of-the-art for 1997. The hardware design has been fully verified at various levels of single cell and stack

sizes[vii] so the 1997 and 2001 performance baselines that were developed for regenerative fuel cell systems in this study incorporated the Hamilton Standard electrolysis hardware.

The PEM electrolyzer stack characteristics that were assumed for this study are listed in Table 22. The electrolyzer performance curves are shown in Figure 6 for both the 1997 and 2001 technology baselines. Performance was assumed to be identical for both baselines since no known development efforts are underway to improve upon the 1997 baseline performance.

Unitized Regenerative Fuel Cell / Electrolyzer Technology

Hamilton Standard has previously conducted some development work for a unitized regenerative fuel cell/electrolyzer system. This technology was not available for the 1997 timeframe but it was assumed that such a system could be implemented in the 2001 timeframe. The mass and dimensional characteristics listed in Table 22 for the dedicated electrolyzer were assumed to also apply to the unitized design. The projected current-voltage characteristics of the unitized stack are shown in Figure 7.

Water Separator for Regenerative Fuel Cell Systems

For regenerative fuel cell systems it is necessary to remove the fuel cell product water from the fuel cell and separate the water from the excess oxygen (if any). The means by which the product water must be removed and separated from the excess oxygen is dependent upon the fuel cell stack design. For the Ballard Mk 7 fuel cell stack, which was considered to be the baseline fuel cell for this contract, the water must be carried out of the fuel cell stack by excess oxygen. (In contrast, the UUV fuel cell design, for example, includes a water transport plate which separates the water and excess oxygen internally and excess oxygen flow is not mandatory). Once the oxygen/water mixture exits the fuel cell stack, the oxygen and water must be separated. The oxygen can be recycled to the fuel cell stack inlet and the water can be stored for subsequent electrolysis. There are several types of water separators that can implemented. PCS, Inc. completed a conceptual design modeling effort for a space shuttle PEM fuel cell system where two types of water separators were modeled: a passive membrane separator, and a dual function water separator/oxygen recycle compressor unit.[viii] For this contract, a passive water separator was considered as the baseline where no direct parasitic power was required for separator operation but only a 3 psi maximum pressure drop would be imposed on the regenerative fuel cell system. (The recycle compressor was sized to overcome this pressure drop as well as the pressure drop in the fuel cell stack). Based upon the PCS, Inc. models and the

literature, the passive water separator mass was assumed to be 5 kg with a volume of 0.5 liters for both the 1997 and 2001 technology baselines.

Photovoltaic Energy Conversion for Electrolyzer Power Source

Normally, the solar-regenerative fuel cell system mass and volume must include those values for the solar cells. The power required by the electrolyzer is determined from the amount of water that needs to be electrolyzed and the time available to carry out the electrolysis process and both of those parameters are calculated in the solar electric aircraft mission analysis code. But since the photovoltaic cells are always assumed to be mounted upon the airframe, all of the photovoltaic mass and volume associated with the electrolyzer sub-subsystem are included in the airframe sizing algorithms and no photovoltaics are included in the regenerative fuel cell system sizing algorithms.

Power Conditioning for the Regenerative and Non-Regenerative Fuel Cell Systems

Fuel cell and electrolyzer stacks can be designed to minimize power management and distribution requirements by tailoring the single cell dimensions and total number of single cells. For this contract, the power management device was assumed to weigh 4.0 kg/kW gross power and occupy 0.5 liter/kW gross power for each fuel cell and electrolyzer.

Fuel Cell System Performance Estimates

The fuel cell system standard characteristic profiles for mass and volume estimates are summarized in Table 23. Mass and volume estimates for the non-regenerative fuel cell systems are shown in Figure 8 for a 5 kW (net power) fuel cell operating for 10 hours. The endpoints of each line represent the 1997 performance baseline (lower left point for each line) and the 2001 performance baseline (upper right point for each line). By definition, the slope of each line must be non-negative. Clearly, the energy density of the liquid hydrogen (LH_2) systems are best for both technology baselines but there was not much difference in specific energies for the 1997 baseline. For the 2001 baseline, the systems which utilize gaseous hydrogen storage exhibit the best specific energies but the liquid storage systems still have superior energy densities. The energy densities of the gaseous storage systems did not improve noticeably from the 1997 baseline to the 2001 baseline since the same storage pressure (3,000 psia) was assumed for both. But the specific energy increased dramatically for the cases with gaseous storage because the tank efficiency factors were

increased by 25% (from 800,000 in. to 1,000,000 in.) for the 2001 baseline and the storage tank safety factor was decreased by 25% (from 2 to 1.5) for the 2001 baseline. There were no such improvements projected for the supercritical storage tanks. Also, since the fuel cell stack performance for the 1997 baseline was assumed to be 22% less than the 2001 baseline, more reactants were required for the 1997 baseline than for the 2001 baseline. This allowed for noticeable energy density and specific energy improvements in the systems which utilized liquid reactant storage but only slight energy density improvements for those system with gaseous storage. It is especially interesting to note that the H_2-air systems with a turbocharger are comparable to the pure O_2 systems.

Batteries

Introduction

Batteries transform chemical potential energy into electrical energy. In general, batteries are broken into two distinct categories

1. Primary Batteries which can not be recharged, but have higher performance than
2. Secondary or Rechargeable Batteries which can be recharged.

Each category is discussed below.

Primary Batteries

A myriad of primary batteries are available today ranging from the low cost commercial alkaline batteries that are used in ordinary flashlights to the higher cost lithium batteries that are predominantly used by the military. Four primary battery types were selected for analysis in this study: the commercial off the shelf (COTS) D-size alkaline battery, the zinc-silver oxide (AgO-Zn) battery, the lithium-sulfur dioxide (Li-SO_2) battery, and the lithium thionyl chloride (Li-SOCl) battery. These four primary batteries span the range of inexpensive, low performing systems to the most expensive, best performing systems. For these primary battery systems, it was assumed that no heat exchanger would be needed, since the discharge time would be much smaller for a primary battery than for a secondary battery for the missions required in this study. It was also assumed that no discharge controller would be required since the battery would not be used for more than one mission, that is a 100% depth-of-discharge would be acceptable. Obviously, no charge controller is needed. Listed in Table 24 are the primary battery characteristics that were used. The standard characteristic profiles for both the 1997 and the 2001 performance baselines are identical for the primary batteries since no significant

development efforts are underway to improve the respective performance within the timeframe of interest.

Rechargeable Batteries

Many different types of secondary battery systems have been under development for terrestrial, space, and military applications. Even though most of the new development programs are targeting rechargeable nickel metal-hydride and rechargeable lithium batteries, there are still significant ongoing efforts worldwide which are focused upon improving the secondary lead-acid and secondary nickel cadmium batteries. Those are the four secondary battery types were included for analysis in this study.

Out of all of the ongoing battery development programs, the electric automobile battery development programs which are supported by the United States Advanced Battery Consortium (USABC) have most direct relevance to this effort. The UAV, like the electric automobile, requires power system components that are small, light, safe, durable, environmentally clean, easy to integrate and operate, and cost effective on a life cycle basis. The main differences between the UAV application and electric automobile application are the power profiles (the electric automobile battery will be designed to the Federal Urban Driving Cycle while the UAV may have drastically different charge/discharge profiles), battery recharging flexibility (the electric automobile can make use of ground based charging and controller stations that may be too large and heavy for on-board UAV battery chargers/controllers), ease of maintenance (the electric automobile will have more flexibility to design a battery system with maintenance requirements in mind), and possibly cost (electric automobile batteries will probably need to be less expensive than a UAV battery). Because advances in the USABC sponsored battery development programs would be beneficial to a battery powered UAV, the projected goals of the USABC were used for the 2001 performance characteristics for the UAV. In Table 25, the near-term and the long-term goals of the USABC are shown for comparison purposes.

There are several design variations for each of the four rechargeable battery types (lead-acid, nickel-cadmium, nickel-hydrogen, lithium) considered for this contract. As an example, there are sealed valve regulated lead-acid batteries and flooded lead-acid batteries. There are back-to back anode, 26% and 31% KOH electrolyte nickel-hydrogen batteries. There are also nickel-metal hydride batteries with different hydride formulations and there

are metallic lithium, intercalated lithium, lithium-ion, and lithium-ion polymer batteries. For this study, general performance characteristics were defined to represent each battery type for both the 1997 and 2001 performance baseline. Listed in Table 26 are generally accepted state-of-the-art characteristics for the rechargeable battery types included in this study. Published battery performance parameters were used for the 1997 performance baseline while the long-term goals of the USABC were assumed to be relevant for the 2001 performance baseline. The long-term USABC goals were planned to be met in 1998. At present, the long-term goals for most of those categories listed in Table 25 have still not been validated at multi-kilowatt power levels. It was assumed then, for this effort, that the 2001 performance baseline for the secondary batteries will be equivalent to the long-term goals of the USABC.

Present state-of-the-art and projected performance and cost characteristics varied somewhat among the battery experts that were consulted by PCS, Inc. for this effort. Most of the performance discrepancies were borne out by the challenges of scaling up the battery size (power and energy capacity) while most of the cost discrepancies were a result of differing marketing forecasts. The battery report published by the California Air Resources Board (CARB) was used as the guideline for assessing the technology readiness levels of various battery technologies.[ix] The comprehensive summary of the current state-of-the-art of rechargeable batteries published by Pellerin[x] provided a superb basis for assigning the 1997 performance baseline characteristics.

It should have been a simple matter to discard from this study those secondary batteries which have the lowest nominal specific energies and energy densities, however, this was not done because the mission requirements for this study required only 35 minutes at altitude with no flight time restrictions and synergistic effects may make the larger, heavier secondary battery systems feasible. Some of the factors which may allow for this include thermal conditions, charge/discharge limitations, cost, and synergistic effects with the aircraft itself (such as using the battery system as part of the airframe structure). Furthermore, since some of the electric vehicles on the road today utilize lead-acid batteries (General Motors EV1, for example) there is ample evidence that the nominally lower energy dense and specific energy batteries should be investigated as part of this study.

Secondary Battery System Ancillary Components

Similar to the fuel cell systems, the rechargeable battery systems require several ancillary components which include, charge/discharge controllers, heat exchangers, power

conditioners, and support structure. The assumptions which were discussed for fuel cell heat exchangers and power conditioners were also applied to the rechargeable battery systems, ie., 4 kg/kW heat exchanger and 4 kg/kW for power conditioning. A prime example of the importance of these battery system ancillary components can be illustrated by examining the nickel-hydrogen battery system which will be implemented for the International Space Station. The nominal energy density of about 50 Wh/kg for the Space Station nickel-hydrogen battery is much greater than the 6.5 Wh/kg energy density of the entire battery system (not even including the charge/discharge controller)[xi].

Standard Characteristic Profiles for Secondary Battery Systems

The standard characteristic profiles that were devised for the candidate secondary battery systems are shown in Table 26 with sample calculations for a 5 kW (net) power output with a 12 hour charge and 12 hour discharge period.

Aluminum and Lithium based semi-cells

The semi-cell systems can be described as hybrids between batteries and fuel cells. For these systems, there is one consumable (or sacrificial) electrode, usually the anode (or fuel electrode), and one gas diffusion electrode, usually the cathode. The aluminum-oxygen (and aluminum-air) and the lithium hydrogen-peroxide systems are examples of semi-cells. Both the lithium based and aluminum based semi-cell systems must be considered strictly as primary systems since the only means for system recharging involves direct mechanical replacement of the fuel electrodes (ie. lithium, aluminum) which are consumed during the energy conversion reactions. The most significant development efforts for the aluminum based semi-cells were conducted in the early-mid 1980's for electric automobiles and from 1991-1997 for the NAVY Unmanned Undersea Vehicle program. There has been no significant development work for lithium semi-cells since the late 1970's and little system level data exist at all for those systems. Since neither one of these systems was considered to be available in 1997 they were not selected as a candidate power system for this contract. Furthermore, there was no indication that any development efforts for the lithium based systems are being planned in the near future, therefore, no improvements to the current state-of-the-art were foreseen. There is some interest from the U.S. Navy in continuing the development of the Aluminum-oxygen semi-cell system (for submarines) but no programs are being conducted today.

In addition to the relatively low technology readiness levels for the aluminum and lithium semi-cells, there are system level issues that must be overcome for these semi-cell technologies to be practical. The main concern is that the reaction products dissolve in the electrolyte. This degrades the electrochemical performance, thus, the reaction products must be removed from the electrolyte solution to maintain high performance. This requirement dictates that extra components be added to the system and causes significant system level complexities. While it is possible to overcome the system level complexities, the semi-cells were not included for analysis for this contract due to the low ratings for all categories except specific energy and energy density.

Flywheels

Power Computing Solutions, Inc. has completed a survey of flywheel energy storage systems for use in an all electric airplane. Flywheel researchers at the NASA Lewis Research Center were contacted and participated in this overview of current state-of-the-art (SOA) flywheel systems and their predicted performance in four years.[xii] Currently, much work is underway to study, build and integrate flywheel energy storage systems. Terrestrially, flywheels are being integrated into hybrid vehicles under the Partnership for the Next Generation of Vehicles (PNGV) and are also being considered as a dual purpose energy storage/momentum wheel system for future satellites. A discussion of flywheel basics, their maximum energy storage potential, and potential synergistic effects are detailed in Appendix B.

Flywheel Components

A typical flywheel storage system consists of five distinct components:

1. An energy storage rotor
2. A reversible electric motor/generator
3. Bearings to support the rotating components, containment and vacuum housing
4. High/Low-power electronics to convert and condition electrical power as well as measure and control system functions
5. A structure to support the bearings.[xiii]

Electric Motor/Generators

Kinetic energy is transferred into and out of a flywheel system through its motor/generator set. When operating as a motor, electrical energy is converted to torque by

the motor and applied to the rotor causing it to spin more rapidly. In the generator mode, the stored kinetic energy is taken from the rotor and, and through the motors mechanical/electrical coupling adds electric energy to the system while slowing the rotor down. Each time the motor/generator is used, the inefficiencies of the pair will result in some power loss. Therefore high efficiency motor/generator sets are required.(see Electric Motor Section)

Power and Control Electronics

In order to improve the efficiency of power transfer between the flywheel's motor/generator and the vehicle's other systems, most flywheel systems incorporate high-power electronics. For several of these types of motor/generator sets, such as permanent-magnet types that employ pulse-width modulation to vary their power input and output, power electronics are required. Once again, because all of the power going into and out of the flywheel system must go through the power electronics, efficiency is very important. Low-power or control electronics are also necessary to control the addition or removal of power to the flywheel system. Some autonomous means for up/down loading of power must be developed and are usually included in a single power/control electronics subsystem "box".

Bearings

Bearings are required to support the rotating parts of the flywheel system. In addition to supporting the static weight of these parts, they must also resist the dynamic loads that are encountered during operation. In addition, the bearing system must provide for very low drag so that the rotors do not slow down significantly because of friction. Two types of bearings are used in flywheel systems: ball bearings that support the rotor mechanically, and magnetic bearings that support the rotor with magnetic attraction and/or repulsion forces. In all of the applications considered for the electric aircraft, magnetic bearings were used as the baseline.

Vacuum/Containment

A flywheel rotor spinning rapidly in the air would experience two very undesirable effects. The first is that large aerodynamic drags would result from the high speed of the rotors and secondly is that these high speed aerodynamic drags would produce great amounts of heating of the rotor to the point of potential mechanical failure or combustion. All flywheels must therefore be encased in an evacuated airtight housing. In addition to

maintaining a vacuum, the high energies contained by the flywheel rotor must be contained in the event of a failure of one of the flywheel components. If a carbon fiber rotor is used and a failure occurs, the very hot carbon dust, which would be created by the disintegrating rotor, when exposed to oxygen has the potential to cause an explosion (This has actually occurred).

Flywheel Energy Storage System Options on the All Electric Aircraft

Flywheels are considered for two types of energy storage systems. The first is for load leveling, and the second is for the replacement of a battery system. Load leveling systems store relatively small amounts of energy and cycle frequently during their operation and in general have high specific power. Flywheel batteries store much greater amounts of energy and are designed to fully substitute for chemical batteries in electric vehicles.

Load-Leveling Systems

The majority of work in flywheels for load-leveling comes from the work on hybrid automobiles. During the short periods when extra power is needed (such as hill climb, passing, etc.) the stored energy in a flywheel is used to provide these peak power requirements. As will be shown later by looking at current flywheel systems, flywheels are particularly well suited to this task with their very high specific power and moderate specific energy. After the excess required power period is over, the remaining energy system would then speed up the flywheel to its' previous state with some form of regenerative braking in the case of the hybrid vehicle or though some other energy source. In this analysis it was assumed that rapid transients in aircraft power output would not be required, therefore, flywheels which provide high specific power were not considered as candidates.

Flywheel Batteries

Performance

Flywheels used as the sole source of energy storage on the vehicle would have to, in essence, perform just as a chemical battery would. Therefore, flywheel batteries should be compared directly with chemical batteries. Compared to load-leveling flywheel systems, the higher ratio of energy to power needed for these "battery" applications are a greater challenge for flywheels. One distinct advantage that flywheels should have over battery systems is their cycle life. Table 25 below shows the various USABC goals for battery development. The battery goals are, in general much better than those shown by flywheels

to date in terms of specific energy. Table 28 shows a list of candidate flywheel materials which have been proposed along with their maximum energy storage density. Some of the materials have been integrated into flywheel systems and these are indicated by a √. The maximum theoretical specific energy for a flywheel is a little over 400 W-hr/kg. Carbon fiber composites possess the highest strength to weight ratio for the candidate flywheel rotor materials. This allows them to store the same amount of energy in a lighter rotor than is possible with other materials. Remember, the numbers given above are only for the rotor and do not include the motor/generator, bearings, containment vessel and power conditioning and control. Practical rotors, those designed to operate in the real world with all of their ancillary equipment, could perhaps achieve 1/2 of the theoretical maximum specific energy. [xiv]

Flywheel Evaluation

Efficiency

Round trip efficiencies of over 90% have been demonstrated in tests at Oak Ridge National Laboratory for flywheel systems.[xv] In comparison most batteries are well below 80%. Several different components lead to the high overall efficiency of the flywheel system.

The first is high motor/generator efficiencies. Because of the effect for a rechargeable system the motor efficiency is essentially used for both power input and power output the efficiency of the set is especially important. Secondly, lowering the efficiency of the motor/generator set leads to additional heat build up in a vacuum enclosure which has the potential to reduce life and degrade the components.

A second component of the power loss comes from the aerodynamic drag associated with the spinning rotor. To reduce this drag, a near vacuum is pulled (10^{-5} torr) to obtain run-down times on the order of 200 days. This level of vacuum is achievable with today's technologies. Another obvious loss mechanism is the bearings used to support the spinning rotor. However, test of a fully magnetic bearing indicated losses of less than one percent per day.

Cycle and Calendar Life

Flywheels should have long service lives, especially if magnetic bearings are used. The bearings and power electronics should provide adequate life for the flywheel system. The principal life limiting factor is fatigue of the flywheel rotor. Each time the flywheel is

accelerated/decelerated to extract power, the rotor is fatigued. Enough of these cycles near the burst speed of the rotor will cause a failure. The solution is to derate the flywheel speed. This causes some decrease in the performance of the system but it is usually minimal. Most of the performance predictions in the flywheel literature are based on a life of at least 100,000 deep cycles.

Cost

Because of the limited number of high performance flywheel systems, cost numbers high specific energy flywheels are difficult to obtain. The best current estimate according to NASA is a system from American Flyweel Systems (AFS) with a composite fiber rotor. AFS estimates that a production run of 20 flywheel battery modules at 40 kWh each would cost approximately $6,000.00. Given 500 discharge cycles as the target discharge (corresponding to a 2 or 3 year driving cycle) for a total of 1.5 cents/kW-hr-cycle. Comparatively a lead-acid battery would be about 22 cents/kW-hr-cycle. Obviously, flywheel systems cannot be currently produced at these price points but they do have that potential.

Safety

The primary risks associated with energy storage in flywheel systems arise from a failure of the rotor. A failure of a fiber composite flywheel cause a vaporization of the epoxy matrix and the resulting vapor can explode.[xvi] However, most fiber composite wheels show a less alarming failure mode by increasing the temperature of the surrounding materials without explosion and turning the fibers into a "fluffy ball". Of more importance to the aircraft could be the momentum transfer to the aircraft. Concerns in automotive applications of a vehicle roll over or spin would most likely be exacerbated for aircraft applications. One solution to the problem is to reduce the total energy stored in each flywheel thereby reducing the effects of a failure. This however leads to higher system mass.

Environmental Interactions

Flywheels should pose little adverse affects on the environment. Especially when compared with chemical batteries, flywheel systems have few direct wastes and have no emissions for the life of the unit.

Flywheel Choice

Figure 9 presents all of the known companies currently working on flywheel systems and their projected specific energy and power. The most promising of the flywheel systems shown above for solar aircraft appears to be that by U.S. Flywheel Systems (USFS). This company is entirely privately funded and so most of its' research is kept proprietary. The USFS flywheel projects a system-level specific power of 600 W/kg and a specific energy of 132 W-hr/kg, both of which are better than most chemical batteries. The USFS flywheel uses a fiber composite rotor spinning at 90,000 RPM. The Energy Density for the system is 109 W-hr/L and a Power density of 489 W/L. These masses and volumes do not include power electronics.

Flywheel Scaling

The following Algorithms were used to scale the flywheel system with the USFS flywheel system used as a baseline:

Rotor Mass = Energy Storage/ Rotor Specific Energy

Motor Mass = Peak Motor Power * Motor Specific Mass (See Motor Correlation)

Bearing Mass = Bearing Specific Mass * Peak Motor Power

Web Mass = 4% * Rotor Mass

Power Conditioning Mass = Power Conditioning Specific Mass * Peak Power

Structure = 100% * Sub total Weight (1997)

= 50% * Sub total Weight (2001)

DRIVE SYSTEM TECHNOLOGY SURVEY

Table 30 shows the results of the drive train qualitative survey. Each of the components listed in this table is discussed in more detail.

Propellers

The use of a propeller in order to generate thrust for subsonic flight dates to the beginning of powered flight. The design and use of propellers under most flight conditions is well understood due to its long history of use and development. However, in certain

areas of flight, such as high altitude (over 70 kft) applications, the history of propellers is sparse if not entirely absent. There has been very little work done in the design and construction of propellers that are capable of operating within the regime of interest for this contract, ie. 90-100 kft. This regime is unique because it requires the propeller to operate within a low Reynolds Number, High Mach Number flow field. Also, if the same propeller is used for takeoff and climb then it must be capable of operating over an extremely large change in atmospheric density. These two concerns are the main obstacles to designing and constructing a propeller for high altitude, low speed applications. Table 28 shows the relative advantages and disadvantages of the two most commonly used propeller control systems. Ducted propellers and ducted fans were investigated for this contract but, in the end because of the large size of the propellers and extreme weight sensitivity of electric aircraft were considered unsuitable for this application.

History

There is not a lot of history related to the design of high altitude propellers. None to date have been developed and tested to altitudes higher than 71,000 ft (Pathfinder). Although there is no direct historical reference to the use of propellers at altitudes between 24.4 km (80,000 ft) and 30.5 km (100,000 ft), the examination of those designed for lower altitudes will still provide trends that should be applicable to high altitude propellers.

Condor

The Condor aircraft was a high altitude unmanned military demonstration aircraft constructed in the 1980's as a reconnaissance aircraft. It presently holds the record for piston driven high altitude aircraft with a flight at 20.4 km (67,000 ft). The propeller used in the condor was designed by Hartzell Propeller Co. of Piqua OH. It's a variable pitch three bladed propeller. The propeller blades are of kevlar composite construction. Each blade weighs approximately 8.2 kg (18 lbs) and the whole propeller system including the pitch control mechanism weights approximately 74 kg (163 lb).

Perseus A

The Perseus A was designed as an unpiloted atmospheric science vehicle capable of flight up to 24.4 km (80,000 ft). To date it has reached an altitude of 15.2 km (50,000 ft). The flight to 15.2 km (50,000 ft) used a 2.8 m (9.2 ft) diameter propeller. This is not the

same propeller which was designed for use at 24.4 km (80,000 ft). To date the high altitude propeller has been used to altitudes up to 12.2 km (40,000 ft). The high altitude propeller has 2 blades and is 4.4 m (14.4 ft) in diameter. It is constructed of a tubular spar with a light weight composite shell and is designed to absorb 50 kw (67 hp) of power at altitude. The propeller pitch is actuated by an electric motor. When this motor is inactive a break locks the blades at their current pitch. This breaking system enables the electric motor to be shut down when not in use. The propeller blades weigh approximately 7 kg (15.5 lb) and the pitch control mechanism weighs approximately 3 kg (6.5 lb). The Perseus propeller was designed using the Xrotor propeller code developed at MIT.

Strato 2C

The Strato 2C is a high altitude manned aircraft used for environmental research. It uses two 5 bladed variable pitch propellers with a diameter of 6 m (19.7 ft). The propellers are constructed with a wooden spar and a composite shell. The propeller pitch is controlled by a hydraulic governor which is driven by the propeller gearbox and integrated into the gearbox oil system. Due to the fairly low cruise RPM (approximately 640) a conventional feathering system with counter weights was not used. Instead an all hydraulic system is used. This system has a separate emergency feathering pump supplied with oil out of a separate volume in the gearbox oil sump. The propeller is designed to absorb 300 kw (400 hp) or shaft power from the engine.

Pathfinder

The Pathfinder aircraft constructed by Aerovironment Inc. holds the present altitude record of 71,000 ft. This aircraft is powered by 6 electric motors and propellers. The propellers are fixed pitch with a composite construction.

Grob EGRETT

The Grob EGRETT is an atmospheric science aircraft built by the Grob company of Germany. It is a twin engine propeller driven aircraft. The maximum altitude it has reached was 16.5 km (54,000 ft) in 1988.

Propeller Concepts and Operation

The ability to transfer power to the air stream is directly proportional to the atmospheric density of the air. For a given rpm the horsepower absorbed by the propeller and transferred to the air stream at 24.4 km (80,000 ft) will be about 1/30 th that absorbed at sea level. Due to this dramatic reduction in performance between sea level and the cursing altitude a number of concepts have been proposed that can increase the performance of the propeller through the altitude range. Aside from the airfoil selection and twist of the propeller blade there are two main factors which will significantly effect the performance of the propeller at a given altitude. These are the diameter and RPM of the propeller. RPM is limited by propeller tip Mach number constraints. Typically the propeller tip Mach number limit is around 0.75 Mach. This is done to avoid the formation of shock waves on the propeller blade. Shock waves can have a number of adverse effects on the performance of the propeller. Due to the pressure gradient through the shock wave the drag of the propeller blade can increase significantly. Also since most propeller blades are fairly flexible once a shock wave forms the change in the pressure field on the surface of the blade can cause the blade to twist thereby allowing the shock travel along the blade section. This motion of the shock wave over the surface of the blade can initiate a flutter in the blade which can severely reduce its performance if not destroy the propeller. This relationship between the allowable RPM and diameter is shown in Figure 10. Because of the restrictions on RPM the most effective way of increasing the output power of a propeller is by increasing its diameter.

Dual Propeller Concept

The dual propeller concept is based on the premise that if you use two separate propellers, one designed for low altitude operation and one designed for high altitude operation, then the overall propulsion efficiency will increase throughout the complete altitude range of the aircraft. By reducing the altitude range the propeller has to operate within the propeller design can be tailored to give higher efficiency. A side benefit to this concept is that it allows for easier takeoff since only the smaller low altitude propeller needs to be used thereby reducing the necessary ground clearance needed. This concept is particularly applicable to an aircraft that has only one or two engines / propellers. The greater the number of engine / propellers that are used the smaller the required propeller diameter. So as the number of engine / propellers increases the advantage of using a dual propeller system decreases. Figure 11 shows how the number of engines / propellers effect the required propeller diameter necessary to produce a given thrust level.

A dual propeller system would operate by having the large propeller fixed in a horizontal position during takeoff and landing. The smaller propeller would be used for takeoff and climb to some predetermined design altitude. After takeoff the large propeller would be released and left to freely rotate with the blades in the feathered configuration in order to minimize drag. Once the initial design altitude for the larger propeller was reached it would be locked to the drive shaft and the pitch angle adjusted to its proper setting. The smaller propeller would be left to rotate with the larger propeller although its contribution to the thrust generate would decrease significantly as the aircraft continued to climb in altitude.

One of the main drawbacks to the dual propeller concept is the extra weight and complexity of the dual propeller system. A dual shaft is needed which would allow the large propeller to rotate independently of the smaller propeller. The large propeller must also be capable of rotating freely of the drive shaft and therefore must have a clutch mechanism to engage and disengage it from the drive shaft. Both the large and small propeller would also need its own pitch control mechanism. And finally the control system needed to operate the dual propeller system would be much more complicated then that used for a single propeller system.

Variable Diameter Propeller

Sikorsky Aircraft has recently done work on developing a variable diameter propeller for a tiltrotor aircraft. The ability to vary the diameter of the propeller throughout the flight would have significant benefits for a high altitude aircraft. As the air density decreases the diameter could increase in order to keep the thrust generated constant. It would also aid in takeoff and landing by reducing the ground clearance needed by the aircraft. However, the present state of the art of this type of propeller does not lend itself toward use on a light weight high altitude aircraft. The propeller presently under development is for a vertical takeoff and landing aircraft. The requirements for this aircraft are much different then those of a high altitude aircraft therefore the weight and power absorption capability of this propeller would not be applicable. Also the present propeller is capable of extending its diameter approximately 30%, for high altitude aircraft applications the percentage increase would need to be greater, on the order of 50% or more. It is possible to continue development of the concept toward a propeller which would be usable by a high altitude aircraft however the cost and timeframe associated makes this development prohibitive. Although this concept is interesting, due to its present state of early development and lack of synergy with present development programs this concept

cannot be considered as a viable alternative to a conventional propeller system.

Application of Propellers

For a solar powered aircraft there are some unique requirements that may influence the type of propeller selected. As with Pathfinder, solar powered aircraft will have a very low wing loading. In order to achieve this it is beneficial to distribute the weight of the aircraft over the length of the wingspan as much as possible. The power generation is also unique in the respect that it is not centralized at one location in the aircraft but rather distributed over the entire wing surface. Because of these two issues it can be seen how a multiple engine aircraft with the engines spaced evenly along the wing span would have its advantages. From Figure 12 it can be seen how the diameter of a propeller will decrease with the addition of multiple engine / propeller systems. There are however some positive and negative effects of reducing the propeller diameter. The maximum RPM the propeller will be capable of operating at will increase as the diameter is decreased, as shown in Figure 11. This has a positive effect on the propeller performance since the propeller can now run at a higher Reynolds number. However the efficiency of the propeller and its output thrust will decrease as the diameter is decreased. This is shown in Figure 13. For this analysis an efficiency of 85% was used over the entire range of operation.

Electric Motors

It must be recognized that all electric motors are AC (alternating current) motors. Direct current (DC) motors must have some mechanism provided to form the inversion function. In the case of brush type machines, for example, the brushes acting upon the commutator switch the motor windings to invert the currents. As the speed of any AC motor is a function of it's source frequency, variable speed operation of a motor requires supplying a variable frequency drive synchronous with its rotation. Establishing rotor speed and/or position necessitates that some form of rotor sensing be provided. Depending upon the type of motor used, rotor sensing could consist of speed, and perhaps position. Electronically controlled motor drives have reached a high level of sophistication, with the power voltage ratings of the electronic switches being the principle present limitation. An understanding of the differences between fixed bus operation from a utility source, and operation from an electronically controlled source having both variable voltage and variable frequency has allowed motors to be designed specifically for electronic control. One major systematic difference with electronically controlled motors is that when they are operated as constant power devices they exhibit a negative input impedance. This impedance is a

consequence of maintaining constant power. For example, if the supply voltage drops, the motor controller will draw increased current to maintain the power. The effects of negative input impedance may vary from increased voltage cross coupling to total system instability when several such loads share a common bus. In order to identify such system interactions a complete high fidelity system model of the source, the controller, the motor, and the load dynamics must be implemented.

Other Systematic Interactions of Electric Motors

One item of particular importance is that when motors are being driven, energy may flow in either direction. In addition to the "forward" energy supplied to the load, reverse energy may result from overhauling or pulsating loads such as aerodynamic forces acting upon a control surface, or a propeller being shadowed by a fuselage (this may be more prevalent in a "pusher" aircraft configuration). Reverse energy also results from uncoupled energy being returned to the source. This is often considered as a power factor effect but it actually represents over-excitation of the motor for its particular operating point, caused by improper design. The power system must be capable of accepting this reverse energy if serious voltage transients and system interactions are to be avoided. In particular, diodes must be avoided in the input. These dynamic load effects are not defined by either the vendor of the motor, or that of the controller. Also, the dynamics of a motor/controller combination are not easily measured during static testing conditions such as those provided by dynamometers. As a result, system interactions such as reverse currents, crosstalk, and electromagnetic interference (EMI) have been greatly underestimated during the system design stage and surprises have occurred during operation. Today, dynamic test loads are available for lower powered machines, and adequate computer models are available to define system interactions once a total system design is complete. In as much as many of these effects are based upon currents that do not create useable torque, proper operation of the motors can do much to avoid their creation.

Electromagnetic Interference (EMI)

As electronically controlled motors will be operating with high transient currents, the various motors operating simultaneously are potential sources for mutual interference. To achieve electromagnetic control while minimizing system mass will require recognition of the peculiarities of each motor with its driver and their systematic interactions and impacts. In particular, any circulating energy must be contained within the smallest

possible volume, the motor drive system must be lineal in all four quadrants, and inductive current effects must be controlled by exploiting cancellation effects such as that experienced with strip line conductors. High frequency transients associated with "Hard Switching" of the power electronics should be avoided through design. EMI testing during dynamic operation of the motors will require an elaborate test facility, and ultimately will rely upon system simulation of the dynamic effects. Electromagnetic control (EMC) is vital, many system failures previously attributed to external interference have been in fact self-induced system interactions.

Brush Motors

Brush motors are the most highly developed and the least expensive. The short life of the brushes at high altitude, maintenance in general, and electrical noise are major technical problems. These motors may be either voltage controlled, or have their back emf varied by field control. For most aeronautical applications, these motors have been replaced by the so-called brushless motors.

Brushless DC Motors

A brushless DC motor is one in which the field excitation is provided by permanent magnets, and the brush (switching) function is performed by semi-conductor switches. It is classes as a fixed excitation synchronous machine. Control of the switching semiconductors requires establishing the actual position of the rotor. These motors were developed in order to avoid the problems experienced with brush type motors and have found wide application in lower powered machines. Control of this type of motor is generally achieved by varying the supply voltage. Field weakening to deliver more torque at higher speeds is achieved only at the expense of reduced power factor. These motors have been developed for terrestrial applications including electric vehicle traction drives, but due to cost considerations, systems with high power densities and high multiple horsepower ratings at present seem to be largely limited to military applications. With these motors, maximum power and maximum efficiency occur at different operating points which makes careful analysis of the vendor data mandatory.

Induction Motors

Induction motors are potentially the least expensive and certainly the most rugged of the available motor types. Optimum control of an induction motor is possible when both frequency and voltage are independently controlled (Field Orientation). Due to their asynchronous operation, induction motors are more easily designed to avoid torque conflicts than synchronous machines when operated in situations requiring torque summation. These motors have simple rugged construction and are torque controllable over a wide range of speed, easily over a 3:1 RPM range. Their characteristic rotor loss may be minimized through design, but remain a concern to be addressed for high power or high altitude operation. The many advantages of induction motors have made them the most popular machine for present day electric vehicle propulsion for applications up to several hundred horsepower. NASA LeRC has spent several years in the development of induction motors and the associated field oriented controllers to a high state of development. Detailed dynamic system models devised by Krauss and Associates of induction motors and controllers are available and readily adaptable. For application to the main propulsion system, high speed induction motors would be prime candidates. Other motor requirements would have to be evaluated on actual systematic trades. One possible concern would be the cooling of the rotor, particularly at altitude.

Switched Reluctance Synchronous Motors

Switched reluctance synchronous motors have highly salient poles having minimum mutual coupling. They are simple rugged machines which display low rotor loss. Due to the lack of coupling between phases, they may continue to operate under some failure modes. These machines have been developed in large sizes most noticeably as military aircraft starter generators, but few civilian applications have been made to date. As a result of their limited application, their system costs are still high. The control of these motors in four quadrants is complex, and characterized by high transient currents returning back into the power system. The power factor of these machines is generally lower than that of competing machines, and their output torque is subject to pulsation, nevertheless, the switched reluctance motor remains a viable option for propulsion.

Permanent Magnet Induction Motors

The University of Wisconsin at Madison has been developing a motor that combines some of the characteristics of induction and permanent magnet machines.

Although results are promising, no industrial base exists for either of these motors, or for their controls.

Axial Flux Motors

These machines are generally most suitable for very high speed applications. Their rotors are typically comprised only of magnetic material with all windings located externally. One variation would be the conventional automobile alternator which uses a combination of axial and radial flux paths with the rotor winding consisting of a solenoid. Several types of these machines exist: The Lundell such as that used in NASA LeRC's Brayton Cycle Generator, The Rice and more recently the "Electric Turbine" (American Motor Systems). As a group, these high speed machines display poorer performance than more conventional types. As a result of the increased air gaps and the resulting higher leakage reactance, as a group, they are longer, heavier, and less efficient.

Variable Speed Operation

Every motor develops a generated back emf proportional to its excitation and rotational speed. In any system, physical limits such as source voltage, component limitations, arc over, etc. limit the maximum voltage available. Similar limits apply to the maximum available current to avoid power quality problems. Figure 14 qualitatively depicts a typical motor torque vs. speed characteristic with limits upon current and voltage. Maximum current (Point 1) may be drawn until limited by the back emf (point 2). Field weakening allows higher speed at reduced torque, resulting in constant power operation (point 2 to point 3). Square law loads such as those from variable pitched propellers would appear as shown in the figure. Efficiency characteristics of a typical induction motor appear as shown in Figure 15. By varying the voltage to frequency ratio, high efficiency may be realized over a wide range of speed. Relatively complex controls are used with induction motors in high power servo applications. However, propulsion systems do not require servo type bandwidths which are typically several hertz. The reduced torque rate requirements will simplify the control and optimization of efficiency or torque per amp rather than torque response. Such control schemes are under development at Paul Krauss and Associates (West Lafayette, IN) and at Motive Power Development (San Diego, CA). Once maximum efficiency is obtained over a wide operating range, a fixed gear reduction could represent the minimum mass system if the propeller characteristics would

accommodate this. If a variable pitch propeller is required, controlling the motor torque during pitch changes would reduce the gear loading experienced during both pitch change and operation.

Power Densities of Electric Motors

The torque developed by a motor is a function of the magnetic flux density and the area of the air-gap (rotor surface). This leads to the concept of "Magnetic Shear" which may be on the order of 10 psi at the available flux density and the resulting torque is, in turn, more dependent upon the magnetic material being applied than the particular machine type. For equally sophisticated machines, the power densities realized are subject to the same physical laws and limitations. The "soft" magnetic materials presently applied to high power density electric motors may be placed into two categories: Silicon Iron materials, typified by flux densities of 1.5 to 1.9 Tesla with material costs of dollars per pound and materials containing Cobalt exhibiting flux densities of 2.2 to 2.5 Tesla and costing over fifty times more. This increased performance at the expense of greatly increased cost has tended to group high performance motors into two groups. In military/aerospace applications, the systematic advantage of lower weight is a good trade against system performance. For civilian applications, particularly those which anticipate eventual volume production, the high fixed cost of the high flux density materials is prohibitive.

If the flux density of a motor is maintained constant, its torque is constant and the shaft power will vary directly with its rotational speed. There are limitations to motor shaft speed, rotor critical speed, rotor surface speed, the gearing required to match the rotor to the load.

Scaling Laws

If the speed and magnetic flux density of a machine is held constant, the current rating of its windings will increase as the square of dimensional change due to the increased cross section of the conductors. The total flux in the magnetic path will increase as the square of the dimensional change, as will the voltage rating. As a result, the power capability of the motor increases as the fourth power of dimension. The machine volume and weight will vary as the cube of the dimension. As a result, power density of a motor will increase as the 4/3 power. In actual experience, this is somewhat optimistic. The California Department of Energy scales electric vehicle traction motors as:

Weight(lbs.)=5000x(horsepower)/RPM

with additional factors of 3 for induction motors and 5 for permanent magnet motors. As this ratio ignores the advantage of scale, it is suspect for application over a wide power level range but should provide adequate scaling for our power range.

Some qualitative motor characteristics are shown in Table 29. For this effort, both a DC brushless machine and an induction machine were selected as baseline motors because of they appear to be the most adaptable for civilian motive applications. The baseline induction motor selected for this study is one that was developed by Sundstrand under a contract to NASA LeRC. That contract did not require that the motor be optimized for any particular configuration or application. Its dimensions are 4.25" diameter. x 10" length (including the resolver) for a volume of 142 $in.^3$ (2.33 l), single or dual stator, and it weighs about 9.1 kg (20 lb.). Half of that weight is comprised of the electronics and the other half of the weight is comprised of the housing. Peak RPM is 14,600 with 300 in.lb. torque with a constant operational efficiency of over 95% at a nominal power of just over 8 kW. For the brushless DC motor, the baseline mass was 7.4 kg (16.3 lbs.), the baseline volume was 86 $in.^3$ (1.41 l) with nominal power of 5 kW at 95% efficiency. For the 1997 performance baseline, the scaling laws described previously (i.e., power density changes with 4/3 power of dimension and volume and mass each change with 3rd power of dimension) were applied to the baseline motor characteristics listed above. For the 2001 performance baseline, a 1/3 reduction in volume and mass from the 1997 baseline was assumed. It was determined that the 1/3 reduction in both mass and volume could be achieved through reductions primarily in the motor housing. While the option for the brushless DC motor was available, there was no significant difference in calculated motor performance between the induction motor and the brushless DC motor. Hence, since the actual data were available for the induction motor, the simulation cases reported later incorporated the induction motor.

Electric Aircraft Gear Train and Transmission

Shaft power leaving the electric motor in the all electric aircraft is connected to a propeller through either a simple shaft rotating at the same speed as the propeller or is coupled through a transmission of some type which provides either fixed or variable multiplication of the motors speed. When used, a transmission(single/multiple ratios or

continuously variable) provides some amount of decoupling between the electric motor and the propeller so that aircraft performance will be enhanced.

To find best aircraft performance, a trade is performed by coupling different motors with a propeller with and without speed reductions and transmissions and studying aircraft performance variations. Most of the motors considered candidates for this class of aircraft (Brushless DC, and Induction Motors) when coupled with modern control systems can operate efficiently over a wide range of speeds (about 3:1) without suffering a major reduction in efficiency. Figure 16 shows a typical DC Brushless motor efficiency plot as a function of speed and torque output.[xvii]

Aerovironments Pathfinder aircraft uses Brushless DC electric motors directly coupled with each propeller. These propellers turn from 600 RPM at sea-level to 1,800 RPMS at 100 kft when operating at full power and have a fixed pitch.[xviii] The motors electronic controller limits the motor to 2,000 RPM.

Small high speed motors produce the highest power output per unit weight but, when coupled with the entire aircraft may not provide for the lowest aircraft weight. Several of the potential motor candidates can operate at high speeds (>2,000 rpm). In addition, these high speed motors will need the addition of a speed reduction transmission which adds weight to the to the aircraft. This may not provide the best overall aircraft performance unless a transmission is used. For this study, several types of transmissions were considered. They were: the single speed reduction gear box, the multi-speed gear box, and the Continuously Variable Transmission (CVT). Each of these will be discussed in greater detail below.

Single/Multi-Speed Gear Box

The single speed gearbox offers the ability to couple a high speed motor with a low speed propeller with the simplest transmission system (excluding straight shaft coupling). While providing a light weight solution, the single speed gearbox may require that the motor have a relatively wide operating range (high efficiency over a wide speed range) and/or that the propeller have a variable pitch mechanism.

A multi-speed transmission offers the ability to operate the motor/propeller combination at higher combined efficiency points over its operating range and/or may eliminate the need for a variable pitch propeller. The single/multi-speed gear box algorithms are based on data received from NASA Lewis Research Center.[xix] NASA Lewis provided the following guidelines for the analysis.

A typical well engineered spur gearbox efficiency has a .5% loss per gear mesh including four bearings. For spiral bevel gears each mesh loss would be about .75%. A satisfactory method of estimating weight for a transmission can be found using about .050 lbs/ft-lb of output torque plus 5 lbs for each clutch and 5 lbs for each break.

For this analysis it was assumed that Epicyclic Gearing would be used. Epicyclic gearing is a family of gear arrangements which includes two of the most common gear types: planetary parallel shaft drives and the bevel gear differential. For a Planetary gear arrangement the range of ratios normally used is from 3:1 to 12:1.[xx] For this analysis if the required gear ratio is greater than 12:1, two Planetary gear sets are used and the .050 lbs/ft-lb of output torque is doubled.

Continuously Variable Transmissions (CVT)

The CVT, invented in 1886 can achieve infinitely many gear ratios over it's operating range. This allows the motor/propeller combination to operate at its highest efficiency points over its entire range of operation. Many types of CVT's have been designed for the conventional automobile. In addition, considerable development has taken place to integrate flywheel/CVT systems into hybrid vehicles.[xxi] Currently Volvo and Honda offer CVT's on passenger cars. Honda offers the Civic CVT which can be purchased in the U.S.

Four types of CVT's were compared for this study. The Steel V-belt, Flat belt, Toroidal traction, and the Cone-roller traction. Figure 17 shows an overview of the V-belt Van Doorne CVT.

Transmission Analysis

For this analysis each of the transmission candidates were modeled to the same criteria so that a comparison could be made. For the four CVT candidates, an earlier NASA study[xxii] was used as the guide, while for the single/multi-speed gear box systems the previously discussed algorithms were used.

In order that each system was compared at the same power/torque throughput, the NASA design study for the CVT's is used as the baseline. Each of the transmission candidates were required to have a maximum output torque of 330 ft-lb, a maximum Transient Power of 75 kW, and a RPMin/RPMout of 21,000/3000. Reliability for the CVT's was set at 90% for 2,600 hrs at 16 kW (the same as current automatic transmissions).

Figure 18 shows a weight comparison for the various transmission candidates. This shows the Single/multi-speed reduction gear box weight less than 1/2 that of the lightest CVT the Cone-roller Traction System. Figure 19 shows specific power as a function of transmission type.

Figure 20 and figure 21 shows peak efficiency as a transmission type and transmission efficiency as a function of speed for the CVT candidates. Efficiency for the single/multispeed gear box is assumed constant over it's operating range. While all the CVT's have relatively flat efficiency curves, none compare with the efficiency of single/multi-speed gear box system. While these transmission comparisons were done, at significantly higher through torque than the final aircraft candidate motors required, the relative sizes and efficiencies should hold over the entire range.

Final Selection

With the only remaining candidates being the single/multi-speed gear boxes, a comparison between the weight of a high speed motor coupled with a gear reduction vs. a heavier, slower motor needs to be made. This was done using the correlations for transmissions and electric motors discussed earlier in the report. Assuming a high speed motor (50,000 rpm) coupled with a single speed reduction transmission, which allows the propeller to operate at up to 2000 RPM, yields a total weight of 1 pound. The reduction in mass for a 1 kWe motor when going from a high speed motor to a low speed motor increases motor weight by over a pound (see speed-power relationship in electric motor section). Due to the added complexity of a single speed transmission and after consultation with NASA Ames it was decided that the no transmission would be used.

SOLAR ELECTRIC AIRCRAFT MISSION SIMULATION RESULTS

The original intent of using the 12 design missions chosen by NASA was to evaluate electric propulsion systems' feasibility on missions of scientific interest. It was originally anticipated that different combinations of equipment would be needed to meet the different requirements and that some missions would be just too demanding to meet with any combination. Neither case proved true. Table 31 shows that for all twelve missions considered, the multi-junction cells would provide an aircraft which could meet every mission. Indeed, all of the solar cell candidates would provide, without energy storage an aircraft capable of meeting the mission requirements (shown in Table 1) except for

amorphous silicon cells which would could not meet the 1000 km ROA mission at either 90 or 100 kft for the 150 kg and 225 kg payloads. While the size of the UAV changed to meet the varying requirements, all missions could be satisfied by the same mix of technologies. This was an important and surprising conclusion; however, it left many questions unanswered. Therefore, a strategy of identifying key questions of interest and test cases designed to address those questions was devised in consultation with NASA Ames. In order to limit the vast array of permutations possible, a significant down select of missions was required. To this end, one of the most demanding missions was selected as a baseline, to which individual missions and technological changes were compared.

Baseline

A Baseline Case was selected in order to make relative aircraft comparisons between the various energy storage candidates, drivetrain components, and mission options. This Baseline case was then used to make decisions about the relative advantages and disadvantages of various technologies and missions and to help reduce the size of the trade space. This baseline case is used as the comparison point unless a particular trade would better be highlighted through a different mission or airframe choice. All variations from the baseline are listed in the text below.

The baseline mission parameters selected are as follows:

- 25 degree latitude:
- 1000 km radius of action(ROA)
- 100 kft maximum altitude
- 1997 Technology Components
- Silicon Solar Cells
- Aspect Ratio of 20
- 150 kg Payload
- June 15 Mission Start Date
- Span Loaded Airframe.

Using Power Computing Solutions, Inc. Solar Aircraft Analysis Code (SAAC) any combination of mission and energy source/energy storage technologies can be simulated. This however does not ensure that the required missions will be successful with the aircraft components and time of year/latitude selected. SAAC was used to provide all the results shown below.

Figure 22 shows a plot of cruise power(level flight), available power from the solar arrays, and altitude as a function of time. The aircraft takes off when the available power and the cruise power are equal and, when excess power is generated it is translated into lift. Table 1 shows a SAAC summary output for an aircraft which will fly this required mission profile.

Figure 23 shows true and indicated velocity as a function of altitude. Clearly the indicated velocity is almost constant over the entire climb to altitude but true velocity is changing as a function of the square root of the relative density ratio. Figure 24 shows aircraft range and altitude as a function of mission time. From Figures 23 and 24 it is clear that for those missions where range determines the wing size, an aircraft which can quickly climb to altitude and cruise at high velocities is preferred.

Figure 25 shows the induced and profile drag coefficients for both the tail and the wing on a span loaded aircraft. The tail, in this case is the airfoil used for trim drag. Notice that Wing induced drag drops with increasing altitude but profile drag increases for both the wing and the tail. This drop in induced drag is a direct result of the falloff of the lift coefficient (Cl) with Reynolds number in the thin air of the upper atmosphere for the Liebeck airfoil. (See Appendix A) The Tail induced drag is very small because the size of tail chosen and the low trim forces required. Figure 26 shows the Reynolds number fall off of both the wing and the tail as a function of altitude. The much lower Reynolds number of the tail is due to the smaller cord length.

Figure 27 shows the aircraft total drag and its' constituent components as a function of altitude. Clearly the wing makes up the vast majority of the drag because of its large size. The other components are all less than an order of magnitude lower with the fuselage drag being the smallest.

Size Figure of Merit

It is general practice in the aviation community to use gross weight as an indication of overall aircraft size. While this works well for more conventional designs, it has less utility for solar powered UAVs. The reason is that important comparisons can be inferred from gross weight, like overall cost and relative size. With solar powered UAVs, these values cannot be reduced, and therefore inferred from weight. Since the cost of these machines is dominated by the solar cells and the physical size of the vehicle is very much larger per pound than one is generally used to, a better figure of merit to use is wing area. This is true because solar power is bought by the square meter. Also, for a fixed aspect

ratio (which dominates this study), both wing span and chord can be easily inferred. Weight will still tend to track with wing area as long as solar cell class and aspect ratio are held constant, but will not otherwise. As an example, results to be presented later show that while the synergistic amorphous silicon and multi-junction solar cells yield essentially the same wing area (and are therefore physically the same size vehicles) , the multi-junction solar cell design has twice the wing loading. This implies that the gross weight is twice as large. However, payload and range are unchanged, so the lighter design should be more attractive. Or is it? Very low wing loading introduces many operational recovery issues and generally lower flight speeds. This could mean that the heavier, higher wing loading design would be more operationally flexible. At the very least, it is obvious that using weight as a figure of merit is inadequate, and that using wing area is better for this class of air vehicles.

Span Loading vs. Twin-Boom Aircraft

Because of the unusual flight regime in which this aircraft will be required to fly, a fundamental question arises as to how the aircraft should be configured. There are two distinct categories of aircraft which this contract delved into, the span loaded airframe and the Twin-Boom. The first is a "flying wing or span loaded" airframe which utilizes a low pitching moment airfoil which has this pitching moment compensated by a tail integrated under the trailing edge of the primary airfoil. The second is a Twin-Boom airframe which uses a primary airfoil with better low Reynolds number characteristics (when compared to the span loaded wing) with a higher pitching moment, which requires a boom cantilevered tail be used to counteract this large pitching force.

Because of the low Reynolds number, effects on the primary airfoil should be seen most clearly for the highest flying aircraft, where this low Reynolds number is experienced for the longest time (See Figure 26 above). The baseline case for this comparison is as follows:

- 0 degree latitude
- 1000 km radius of action(ROA)
- 100 kft maximum altitude
- 1997 Technology Components
- Single Junction Solar Cells
- Aspect Ratio of 20

- June 15 Mission Start Date.

Figure 28 shows a bar chart of wing area as a function of payload for both Twin-Boom and Span Loaded airframes. This figure shows that a wing area reduction can be achieved by selecting a span loaded airframe over a twin-boom configured aircraft for all payload masses at these mission selected parameters. Figures 29 and 30 show total aircraft drag as a function of altitude for an aircraft with a 75 kg and 225 kg payload respectively. With the larger payloads and wings the twin-boom aircraft begins to realize some of the potential of the better performing airfoil, but still overall produces a larger aircraft.

Because selected aspect ratio has a direct effect on chord length and therefore Reynolds number, the choice of an aspect ratio of 20 needs to be evaluated in the context of selecting an airframe type. To more fully explore the effect of aspect ratios on aircraft performance (both twin boom and span loaded airframes) additional runs were made at aspect ratios of 10 and 30. Figure 31 shows the effect of aspect ratio on aircraft wing size. Clearly, for low aspect ratio wings (relatively high Reynolds numbers) there is a significant advantage to the span loaded airframe. As aspect ratios increase, the advantages of the superior low Reynolds number behavior of the Wortman airfoil appears and, at an aspect ratio of 30 provides the twin boom aircraft has a smaller overall wing area than the span loaded airframe. Figure 32 shows wing span as a function of wing aspect ratio. While the overall wing area does indeed go down as the aspect ratio is increased the wing span has a minimum at around a aspect ratio of 20. Because wing span is an important operational constraint in aircraft of these sizes the aspect ratio for this study was selected at 20. The span loaded airframe is used for comparing the remaining energy sources, drive train components, and missions. The Aerovironment Pathfinder aircraft has a aspect ratio of 12.3.

Latitude Variations

Mission flexibility is a key for almost any aircraft. In the case of the all electric aircraft, the ability to operate over a wide range of latitudes greatly increases its value to the user. Figure 33 shows a plot of aircraft wing area as a function of latitude for four different solar cell types for aircraft with the following characteristics:

- 0 degree latitude
- 0 km radius of action(ROA)
- 100 kft maximum altitude

- 1997 Technology Components
- 150 kg Payload
- Aspect Ratio of 20
- June 15 Mission Start Date
- Span Loaded Airframe.

The largest aircraft by a significant fraction is the amorphous silicon aircraft where the integration of the aircraft skin and the amorphous solar cells is not possible. Multi-Junction silicon cells provide the best performing aircraft at all latitudes, while single junction silicon cells make an airframe about double the size of the multi-junction system. While currently considered 2001 technology, amorphous silicon cells integrated into a mylar covering of the wing provides significant performance enhancements over both the plain amorphous and the single junction silicon cells. In addition, Figure 33 clearly shows that either a multi-junction aircraft or the synergistic amorphous both provide better "wide latitude" mission capability with little change in overall aircraft size. Also notice that during missions with a 6/15 start date, the minimum aircraft size is not found when operating the aircraft at the equator but rather when operated from about 20 to 30 degrees. This is due to the increased length of the day at these mid latitudes at that time of year while still providing a high enough sun angle to not greatly affect the performance of the cells. At higher latitudes, while the daylight is longer at this date the low sun angles produce aircraft of increasing size.

A second factor which impacts directly on operational capability of an aircraft is wing loading. Figure 34 shows wing loading as a function of latitude for these four solar cell types. Interestingly, while the synergistic amorphous and the multi-junction aircraft both provided similar airframe wing areas, the multi-junction system provides significantly higher wing loading than the amorphous aircraft, leading to a selection of a multi-junction airframe as the preferred candidate if these are the only parameters considered. Multi-junction cell issues arise when compared with amorphous silicon on the basis of cost, aircraft installation, and fragility.

Figure 35 shows wing area as a function of latitude for the same mission parameters as given above except that a 1000 km ROA is required. Aircraft with non-synergistic amorphous silicon cells did not provide a solution at any latitude so they are not included in this chart. Once again, multi-junction and synergistic amorphous cells provide the smallest airframes while single junction silicon cells produce about a doubling of the multi-junction wing area. Figure 36 shows wing loading as a function of latitude for this

mission and increases the wing loading differential between amorphous and multi-junction aircraft.

Time-of-Year Variations

Along with the ability to operate over a wide latitude, the ability to operate at all times of the year improves aircraft capability. Figure 37 shows wing area as a function of time of year for an aircraft with the following characteristics:

- 25 degree latitude
- 1000 km radius of action(ROA)
- 100 kft maximum altitude
- 1997 Technology Components
- 150 kg Payload
- Aspect Ratio of 20
- Span Loaded Airframe
- Single Junction Silicon Cells.

Between a March 15 start and June 15 start a difference in wing area of about 50% is found. Between March 1 and March 15 an increase in wing area of over 100% occurs. No solutions were found for January or February mission start times. The dramatic increase in plane size required to accomplish the mission is the result of the lower sun angles and limited daylight. This combination make solar aircraft operations earlier than mid March or after late October highly unlikely for this mission.

General Solar Cell Parametrics

While not a requirement of the study, it is useful to look at aircraft size trends as a function of solar cell parameters. While it is obvious that higher efficiency solar cells in combination with lighter weight solar cells provide better aircraft performance, how much and at what cost remains the key issue. Should great expense be placed in obtaining the highest performing, lightest weight cells or could nearly the same performance be realized by less costly, lower performing cells?

Figure 38 shows wing area as a function of solar cell efficiency for an aircraft with the following characteristics:

- 0 degree latitude

- 100 kft maximum altitude
- 150 kg Payload
- Aspect Ratio of 20
- Span Loaded Airframe
- 6/15 Mission Start
- Solar Cell Specific Mass of 1.0 kg/m2.

The range of solar cell efficiencies was chosen to span the range from low efficiency amorphous to high efficiency multi-junction cells. Clearly, when choosing between low and high solar cell efficiencies, both the 0 km ROA and the 1000 km ROA benefit from higher efficiency cells. Using a constant specific mass cell (1 kg/m^2) dramatic increases in wing area occur below solar cell efficiencies of 20%. Above about 20 % however, the slope is quickly flattening out. For the 1000 km ROA a greater benefit can be achieved by going to higher efficiency cells. Going from 20% efficiency cells to 25% efficiency cells, a reduction in area of about 30% occurs for the 1000 km ROA while for the 0 km ROA a reduction in wing area of about 20% occurs.

Figure 39 shows wing loading as a function of solar cell efficiency, and as expected shows increases in wing loading as a function of increasing solar cell efficiency. Wing loading is increased by 38% for the 1000 km ROA and by 36% for the 0 km ROA.

Figure 40 shows wing area as a function of solar cell specific mass with the range representing the range of mass from the amorphous silicon cells to SOA multi-junction cells. For these cases, solar cell efficiency was held constant at 15%. Once again significant reductions in wing area can be found by reducing solar cell specific mass. Reductions in wing area from 225 m^2 to 150 m^2 (33 % reduction) occurred when reducing solar cell specific mass from 1. kg/m^2 to .2 kg/m^2 for the 0 km ROA case while reductions from 325 m^2 to 175 m^2 (53% reduction) occurred when going over the same range of solar cell specific masses for the 1000 km ROA case. Figure 41 shows wing loading as a function of solar cell specific mass for these same two cases. A reduction in wing loading of about only about 3.5 % occurs for the 0 km ROA case while for the 1000 km ROA a reduction of 5% occurred. Obviously, the only way to significantly improve wing loading is to increase the solar cell efficiency.

Performance Baseline Effects on Aircraft

Figure 42 shows the effects of 1997 technology and 2001 technology on the all electric aircraft. Comparisons are made on predictions of solar cell performance for the single junction, multi-junction, and the synergistic amorphous silicon cells. Plain amorphous was not looked at further based on the discussion earlier in this report. The following describes the common parameters for this comparison:

- 25 degree latitude
- 100 kft maximum altitude
- 150 kg Payload
- Aspect Ratio of 20
- Span Loaded Airframe
- 6/15 Mission Start
- 0 km Radius of Action.

The worst performer is the 1997 single junction cell type. A reduction in area of nearly 50 % can be achieved by the projected improvements in the SOA single junction solar cells in 2001. Current multi-junction cells produce aircraft similar to the 2001 timeframe single junction cells, while multi-junction Year 2001 cells provide the smallest aircraft. Figure 43 shows the same basic comparison except with a 1000 km ROA.

Altitude Effects on Aircraft Size

As the required altitude of the aircraft increases, significant reductions in the atmospheric density drive up aircraft size. Figure 44 and 45 shows wing area and % Change in Wing area from the base case as a function of altitude for single and multi-junction cells as well as synergistic amorphous. The baseline case is the single junction silicon cells at an altitude of 90 kft while all aircraft have the following characteristics:

- 25 degree latitude
- 150 kg Payload
- Aspect Ratio of 20
- Span Loaded Airframe
- 6/15 Mission Start
- 0 km Radius of Action.

Notice that going from 90 kft to 100 kft for the single junction aircraft produces over a 50% in required wing area, yet for multi-junction cells produces a change of only about 25%. The synergistic amorphous aircraft changes wing area by 20%.

Figures 46 and 47 show the same aircraft mission except with a ROA of 1000 km. The same basic relative trends hold except that the high power per wing area multi-junction solar cell aircraft shows greater reductions in wing area with increasing range requirements.

Payload Mass

Of great interest to the user of any aircraft is its ability to carry useful amounts of payload. This contract called for mission simulations with 75 kg, 150 kg and 225 kg payloads. The baseline aircraft mission was used with the various payloads.

Figure 48 shows a comparison with these three payloads in combination with the various solar cell types on a 0 km ROA mission. The single junction cells provide a 70% increase in wing area when changing from a 75 kg payload to a 225 kg payload. The multi-junction cells provide a 71% increase in wing area and the synergistic amorphous provide a 110% increase in area. The amorphous system offers less growth potential than either the single or multi-junction celled airframes.

Figure 49 shows this same except with a ROA of 1000 km. For the single junction aircraft an increase in wing area of 67% occurs when changing from a payload of 75 kgs to 225 kgs. For the Multi-junction solar cell aircraft a change in area of 78% occurred while for the synergistic amorphous cells a change in area of 80% occurred.

Comparing the differences in missions for the 225 kg, single junction cells we find that an increase in wing areas from 230 m^2 to 260 m^2 occurs. For the multi-junction cells no increase in area is required because the same aircraft which made a 0 km ROA can make a 1000 km ROA. For the synergistic amorphous cells an increase in area from 175 m^2 to 195 m^2 occurs.

Energy Storage

This studies original intent was to look at the influences of various energy source and drive train technologies on the all electric aircraft. Unfortunately, because of the missions considered it was not possible to find which energy storage technologies provide true enabling capability for the all electric aircraft. As was shown in the results section,

every one of the missions studied could be performed with at least three solar-only aircraft with current technologies. Now the question turns to: can energy storage technologies provide benefits to the aircraft studied? Because each of the missions considered was possible without stored energy, the mission selected to compare energy storage systems needed to be as challenging as possible for the all electric aircraft. The mission parameters chosen to show the benefits of energy storage most clearly are as follows:

- 40 degree latitude
- 225 kg Payload
- 90 kft maximum altitude
- Aspect Ratio of 20
- Span Loaded Airframe
- 6/15 Mission Start
- 1000 km Radius of Action.

A note about the mission selection. In general, most of the airframes are most challenged by the ROA requirements. The aircraft are driven to obtain their altitude quickly and then race at maximum altitude to their final range and altitude requirements. As was shown earlier, the higher the altitude the faster the aircraft travels. Because of this, selecting 90 kft as the maximum aircraft altitude reduced forward velocity, thereby, making the mission more challenging than the 100 kft aircraft.

In addition to the mission selection, several of the energy storage candidates were not simulated. This reduction in the candidate energy storage systems was possible because of the fact that all of the missions could be performed in a single day and therefore no recharge system was needed. All of the rechargeable systems have poorer specific energies and specific masses than their primary counter parts. For example a regenerative fuel cell requires either a unitized fuel cell or a separate electrolyzer to separate the collected water. Both regenerative systems included additional mass which would not be used. For the batteries, all primary systems can operate at higher Depth-of-Discharge (DOD) and have higher specific energies than their rechargeable counterparts. For these reasons only primary systems were considered.

Figure 50 shows a bar chart of wing area as a function of energy storage option. Significant reductions in wing area can be achieved by the addition of a small amount of energy storage. Wing area is reduced from 182 m^2 to 167 m^2 (8% reduction) by the addition of 2000 W-hr of Alkaline D-cells and is reduced to 157 m^2 (15% reduction) by the

addition of 2000 W-hr of Lithium cells. Greater and less amounts of energy storage produced larger aircraft. Notice that fuel cells are not included on the chart. Because the fuel cell itself is sized for its peak power requirement and the energy storage requirement is low, the specific energy of the fuel cell with a relatively high power output / low energy storage ratio produces a system with very poor specific energy. For a 2000 W-hr case with a peak power output of about 15 kW a specific energy of about 30 W-hr/kg occurs. The off-the-grocery store shelf D-cells have a specific energy of about 60 W-hr/kg. The flywheel system produces a specific energy of about 50 W-hr/kg. It was found that this mission required at least a 55 W-hr/kg energy storage system to find any benefits to energy storage. Table 33 shows the output from the SAAC for the Lithium battery energy storage case.

With this reduction in wing area, some increase in wing loading should be experienced. Figure 51 shows wing loading for the three systems studied. Wing loading improvements of about 8% occurred for both energy storage options occurred over the solar-only choice.

Figure 52 shows both Altitude and Lithium Battery level as a function of mission time. Notice that the benefit the lithium battery gives to the aircraft is additional time at altitude which allows the aircraft to increase its range most effectively.

Aircraft Mass Fraction

One characteristic of interest is the relative mass fraction of each subsystem which makes up the entire aircraft. Figures 53, 54 and 55 show percent Weight Breakdown for the single junction, multi-junction, and synergistic amorphous aircraft flow under the baseline conditions. Payload mass fractions vary from about 17% for the single junction, 26% for the multi-junction cells, to 36% of the payload mass for the synergistic amorphous cells. These are all quite high payload mass fractions. When both payload and solar cell mass fractions are combined the totals are 40% of the aircraft weight for the single junction aircraft, 41% for the multi-junction aircraft, to 37% for the synergistic amorphous aircraft. This indicates a direct tradeoff of solar cell for payload mass fraction in the aircraft while the sum of the other mass fractions remaining almost constant.

Cost

While it is difficult to calculate the cost of any unbuilt or unique aircraft, one method to estimate the relative cost is to look at component costs and thereby speculate on

relative aircraft costs. Figure 56 shows a bar chart of aircraft solar cell uninstalled cost for the baseline mission. Great differences in the cost/m^2 of the solar array occur when looking at each aircraft. It does, however, take a significantly smaller airframe to perform the same mission with better performing solar cells. Capital costs for the single junction cells needed to meet the mission requirements are about $4 million while a reduced size multi-junction aircraft needs almost $18 million to perform the same mission. Amorphous cells require only about $2 million. One factor which does not show up in these numbers is the aircraft integration costs. Both single junction and multi-junction cells require significant time and resources to integrate the cells into a airframe. The amorphous cells offer the potential to greatly reduce integration costs by doing double duty of providing the aerodynamic cover for the wing with cells because of the flexible mylar substrate sheet on which the amorphous cells sit. This "double duty" has the potential to make these aircraft significantly less expensive to build.

CONCLUSIONS

This analysis suggests that there is some potential for the all electric aircraft to find a niche in high altitude reconisance or atmospheric research. The combination of advances in energy storage and drive train technologies as well as modern construction methods and materials may lead to a practical (while still very large) aircraft which can meet a significant amount of the ERAST mission requirements. Questions of recurring costs for each aircraft and operational limitations have been addressed and, if acceptable could provide a viable platform for atmospheric research. Further work needs to address the potential for the aircraft to be able to perform all of the ERAST mission altitude requirements at any time of day or night. This will lead to considerably different aircraft because of the large requirements expected for these missions.

Acknowledgments

Special thanks to Andy Hahn of Ames Research Center for all his help in the completion of this contract.

Required Altitudes	27.44 km (90,000 ft .) 30.49 km (100,000 ft .)
Required Payload Masses	75 kg (34 lbs.) 150 kg (68 lbs.) 225 kg (102 lbs.)
Required Radius of Action	0 km 1000 km (621 miles)
Time Required at Altitude	35 minutes continuos

Table 1 Aircraft Mission Requirements

Solar Cells Primary Battery Systems Secondary Battery Systems Non-Regenerative PEM Fuel Cell Systems Regenerative PEM Fuel Cell Systems Flywheel Systems Electric Motors Propellers Transmissions

Table 2 Electric Powertrain Components Analyzed for the High Altitude UAV

	Sunrise I	Sunrise II	Solar Riser	Solar One	Solar I	Gossamer Penguin	Solar Challenger	Raptor Pathfinder
Gross Weight (lb)	27.5	22.5	290	400	440	165	340	380
Wing Area (ft^2)	90	90	260	260	237	313	266	800
Wing Span (ft)	32	32	30	68	52	72	47	100
Solar Cell Power (W)	450	578	400	864	1800	541	2500	11,400
Average Airspeed (ft/s)	25	35	29	42	65	22	36	52
Gross Weight per Cell Power (lb/W)	61	39	725	463	244	305	136	33
Gross Weight per Wing Area (lb/ft^2)	0.31	0.25	1.12	1.54	1.86	0.53	1.28	0.48
Propulsion Energy Source	Solar	Solar	Battery	Battery	Battery	Solar	Solar	Solar
Recharging Subsystem	None	None	Solar Array Charging while on Ground	Solar Array Charging while on Ground	Solar Array Charging while on Ground	None	None	None
Date of First Flight	1974	1975	1979	1979	1980	1980	1980	1993

Table 3 History of Solar Power Aircraft

Criteria	Comments
Availability	The hardware must be procurable within the relevant timeframe (ie., 1997 or 2001) or it was not considered. Higher priority was given to those systems which are presently undergoing advanced development to improve the performance characteristics in the 2001 timeframe.
Reliability	Hardware with proven reliability received higher priorities. Those systems with smaller numbers of components received higher priorities.
Energy Density and Specific Energy	The smallest, lightest systems received higher priorities. All ancillary components and operating constraints were included in the system. Power mass and volume estimates, including temperature requirements and heat rejection requirements.
Safety	Hardware that could be safely handled, installed, recovered, and operated received higher priorities.
Emissions/Environmental Impact	The systems with lowest emissions and the least hazardous disposal protocols received higher priorities.
Life Cycle Cost	The least expensive systems received higher priority. Relative installation and maintenance costs were estimated.

Table 4 Selection Criteria for Candidate Power Systems to be Considered

	Availability		Reliability		Energy Density and Specific Energy		Safety		Emissions/ Environmental Impact		Cost	
	1997	2001	1997	2001	1997	2001	1997	2001	1997	2001	1997	2001
Non-Regenerative Fuel Cells	G	VG	G	VG	VG	E	VG	VG	E	E	P	VG
Regen. Fuel Cells	P	VG	P	VG	VG	VG	VG	VG	E	E	P	G
Unitized Regen. Fuel Cells	P	G	P	G	VG	VG	VG	VG	E	E	P	G
Rechargeable Lead-Acid Batteries	E	E	E	E	G	G	VG	VG	E	E	E	E
Rechargeable Ni-Cd Batteries	E	E	E	E	G	G	VG	VG	G	G	VG	VG
Rechargeable Ni-H_2 Batteries	VG	E	VG	VG	VG	VG	VG	VG	G	G	G	G
Rechargeable Ni-Metal Hydride Batteries	VG	E	VG	VG	VG	VG	VG	VG	G	G	G	G
Rechargeable Li-Polymer Batteries	P	VG	P	VG	G	E	G	G	G	G	G	G
Primary Alkaline Batteries	E	E	E	E	P	P	VG	VG	G	G	E	E
Primary AgO-Zn Batteries	E	E	E	E	G	G	VG	VG	G	G	VG	VG
Primary Li-SO_2 Batteries	E	E	E	E	VG	VG	VG	VG	G	G	G	G
Primary Li-SOCl Batteries	E	E	E	E	E	E	VG	VG	G	G	P	P
Flywheels	P	E	G	G	G	G	P	P	E	E	P	VG
Al-O_2 Semi-cells	P	P	P	P	G	G	G	G	P	P	P	P
Li-H_2O_2 Semi-cells	P	P	P	P	G	G	G	G	P	P	P	P

Table 5 Qualitative Rankings of Candidate UAV Power Systems

P=Poor; G=Good; VG=Very Good; E=Excellent

Classification	Efficiency %	Area cm^2	V_{oc}	I_{cc} mA / cm^2	Fill Factor %	Test Center & Date	Description
GaAs Crystalline	25.1	3.91	1.022	28.2	87.1	NREL 3/90	Kopia AlGaAs window
GaAs Ge Substrate	24.3	4.00	1.035	27.6	85.3	NREL 3/89	ASEC AlGaAs window
GaAs Thin Film	23.3	4.00	1.011	27.6	83.8	NREL 4/90	Kopia 5 mm CLEFT
GaAs Submodule	21.0	16	4.04	6.6	80	NREL 4/90	Kopia 4 CLEFT cells
InP Crystalline	21.9	4.02	0.878	29.3	85.4	NREL 4/90	Sp Spire Epitaxal

Icc - Closed Circuit Current
Voc - Open Circuit Voltage
AM 1.5 - Air Mass 1.5

Table 6 III-V Cell Developments at AM 1.5 & 25°C

Classification	Efficiency %	Area cm^2	V_{oc}	I_{cc} mA / cm^2	Fill Factor %	Test Center & Date	Description
crystalline	24.0	4.00	0.709	40.9	82.7	Sandia 9/94	UNSW Perl
moderate area	21.6	45.7	0.694	39.4	78.1	Sandia 4/93	UNSW Perl
multi-crystalline	17.8	1.0	0.628	36.2	78.5	Sandia 3/94	Georgia Tech
large mult-crystalline	17.2	100	0.610	36.4	77.7	JQA 3/93	Sharp (mech. Textured)
thin crystalline	17.0	4.02	0.651	32.6	80.3	Sandia 9/94	ANU 20 mm thick
supported film	14.9	1.02	0.600	31.4	79.2	Sandia 12/88	Astro Power
large thin film	14.2	100	0.608	30.0	78.1	JQA 3/93	Mitsubishi 60 mm thick

Table 7 Silicon Solar Cell Developments at AM 1.5 & 25°C

Classification	Efficiency %	Area cm^2	V_{oc}	I_{cc} mA / cm^2	Fill Factor %	Test Center & Date	Description
Cd Te Cell	15.8	1.05	0.843	25.1	74.5	NREL 6/92	South Florida CSVT
CdTe Submodule	9.8	63.6	6.62	2.2	69	NREL 5/93	Solar Cells Inc.
CIGS Cell	13.9	6.636	0.644	29.9	72.2	NREL 8/93	NREL CIGS on Glass
CIGSES Submodule	12.7	69.1	7.49	2.49	68	NREL 4/94	Semens Prism Cover

Table 8 Polycrystalline Thin Film Cell Developments at AM 1.5 & 25°C

Classification	Efficiency %	Area cm^2	V_{oc}	I_{cc} mA / cm^2	Fill Factor %	Test Center & Date	Description
Cell	12.7	1.0	0.887	19.4	74.1	JQA 4/92	Sanyo
Submodule	12.0	100	12.5	1.3	73.5	JQA 12/92	Sanyo

Table 9 Amorphous Silicon Cell Developments at AM 1.5 & 25°C

Classification	Efficiency %	Area cm^2	V_{oc}	I_{cc} mA / cm^2	Fill Factor %	Test Center & Date	Description
GaInP / GaAs	29.5	0.25	2.385	14.0	88.5	NREL 6/93	NREL monolithic
GaAlAs / GaAs	27.6	0.50	2.403	14.0	83.4	NREL 3/89	Variam monolithic
GaAs / CIS Thin Film	25.8	4.00	____	____	____	NREL 11/89	Kopia / Boeing 4 terminal
a-Si / CIGS Thin Film	14.6	2.40	____	____	____	NREL 6/88	ARCO 4 terminal
a-Si / a-SiGe	12.5	0.26	1.621	11.7	65.8	NREL 12/92	USSCUssaUSSC / Cannon monolithic
a-Si / a-Si / a-SiGe	12.4	0.27	2.541	7.0	70.0	NREL 2/88	ECD monolithic
a-Si / a-SiGe / a-SiGe	12.4	1.00	2.289	7.9	68.5	JAQ 12/92	Sharp monolithic

Table 10 Multi-junction Cell Developments at AM 1.5 & 25°C

Classification	Efficiency %	Area cm^2	V_{oc}	I_{cc} mA / cm^2	Fill Factor %	Test Center & Date	Description
Si Crystalline	21.6	862	32.6	0.703	81.3	Sandia 2/94	Honda / Sun Power
Si Multi Crystalline	15.3	1017	14.6	1.360	78.6	Sandia 10/94	Sandia / HEM
Si Large Spherical	10.3	3931	20.1	2.720	73.6	NREL 9/94	Texas Instruments
CIGS	11.1	938	25.9	0.637	64.0	NREL(6/88)	ARCO
CIGS large	9.7	3883	37.8	2.440	64.0	NREL 5/91	Semans Solar
CdTe	8.1	838	21.0	0.573	55.0	NREL 9/91	Photon Energy
CdTe large	7.8	6838	92.0	0.969	60.0	NREL 10/93	Solar Cells Inc.
a-Si / a-SiGe / a-SiGe, Tandem	10.2	903	2.32	6.470	61.2	JAQ 12/93	USSC

Table 11 Planar Module Developments at AM 1.5 & 25°C

Classification	Efficiency %	Area cm^2	Concentration (suns)	Test Center & Date	Description
GaAs	27.6	0.126	255	Sandia 5/91	Spire
Si	26.5	0.150	140	Sandia 5/87	Stanford point contact
Si (Moderate Area)	25.7	1.21	74	Sandia 7/93	Sun Power rear contact
Si (Large)	21.6	20.0	11	Sandia 9/90	UNSW laser - grooved
GaAs (Si substrate)	21.3	0.126	237	Sandia 5/91	Spire

Table 12 Concentrator Single Cell Developments at AM 1.5 & 25°C

Classification	Efficiency %	Area cm^2	Concentration (suns)	Test Center & Date	Description
GaAs / GaSb	32.6	0.053	100	Sandia 10/89	Boeing mechanical stack
InP / GaInAs	31.8	0.063	50	NREL 8/90	NREL monolithic 3 terminal
GaAs / GainAsP	30.2	0.053	40	NREL 10/90	NREL stacked 4 terminal
GainP / GaAs	30.2	0.103	180	Sandia 3/94	NREL monolithic 2 terminal
GaAs / Si	29.6	0.317	350	Sandia 9/88	Varian / Stanford / Sandia mechanical stack

Table 13 Concentrator Multijunction Single Cell Developments at AM 1.5 & 25°C

Classification	Efficiency %	Area cm^2	Concentration (suns)	Test Center & Date	Description
GaAs / GaSb Submodule	25.1	41.4	57	Sandia 3/93	Boeing 3 mechanical stack units
Si Module	20.3	1875	80	NREL 4/89	Sandia / UNSW / ENTECH (12 cells)

Table 14 Concentrator Module Developments at AM 1.5 & 25°C

Concentration - Concentration Ratio of Concentrator Lens (Solar Flux at Cell / Solar Flux with No Concentration)

Company	Material	Area (cm^2)	Efficiency %	Power (W)
Solar Cells Inc.	CdTe	7,200	8.4	60.3
Solar Cells Inc.	CdTe	6,693	8.6	57.7
APS	a-Si / a-Si	11,522	4.6	53.0
Semans Solar	CIS	3,832	11.2	43.1
Semans Solar	CIS	3,859	10.2	39.3
BP Solar	CdTe	4,540	8.4	38.2
ECD	a-Si / a-Si / a-SiGe	3,906	7.8	30.6
Golden Photon	CdTc	3,528	7.7	27.5
Solarx	a-Si / a-SiGe	3,432	7.8	26.9
USSC	a-Si / a-Si	3,676	6.2	22.8
Fuji	a-Si / a-Si	1,200	8.9	10.7
Semans Solar	CIS	938	11.1	10.4
Matsushita Battery	CdTe	1,200	8.7	10.0
USSC	a-Si / a-SiGe / a-SiGe	903	10.2	9.2
BP Solar	CdTe	706	10.1	7.1

Table 15 Thin film Solar Array Module at AM 1.5

Classification	Efficiency %	Thickness mm	Specific Mass kg / m^2	Module Specific Mass kg / m^2
MJ a-SI	8	< 50 with KAPTON	0.100	0.375
CIGS	10	< 50 with KAPTON	0.100	0.375
CIGS	10	< 50 with KAPTON	0.100	0.286
CdTe	8	——	——	——

Table 16 Thin Film Solar Cell Module Performance at 25° C

Classification	Efficiency %	Thickness mm	Specific Mass kg / m^2	Module Specific Mass kg / m^2
Si (K6) (Spectrolab)	15	110	0.253	0.508
Si (K6) (Spectrolab)	15	150	0.345	0.591
Si (Semans)	15	350	0.805	1.005
GaAs/Ge (Spectrolab / ASEC)	18	125	0.663	0.877

Table 17 Single Junction / Single Crystal Solar Cell Module Performance at 25° C

Classification	Efficiency %	Thickness mm	Specific Mass kg / m^2	Module Specific Mass kg / m^2
GaAs (Spire)	18	5 (~ 105 with 3 mil coverglass)	0.228	0.485
GaAs (Spire)	18	5 (~ 70 with TEDLAR)	0.116	0.295
GaAs (Astropower)	18	3 (~ 103 with 3 mil coverglass	0.217	0.475

Table 18 Ultra Thin GaAs Solar Cell Module Performance at 25° C

Classification	Efficiency %	Thickness mm	Specific Mass kg / m^2	Module Specific Mass kg / m^2
GainP2 / GaAs	24	125 (standard 5 1/2 mil)	0.663	0.877
GainP2 / GaAs	24	5 (~ 105 with 3 mill coverglass)	0.228	0.485
GainP2 / GaAs	24	5 (~ 70 with TEDLAR)	0.116	0.295

Table 19 Multi-Junction Solar Cell Module Performance at 25° C

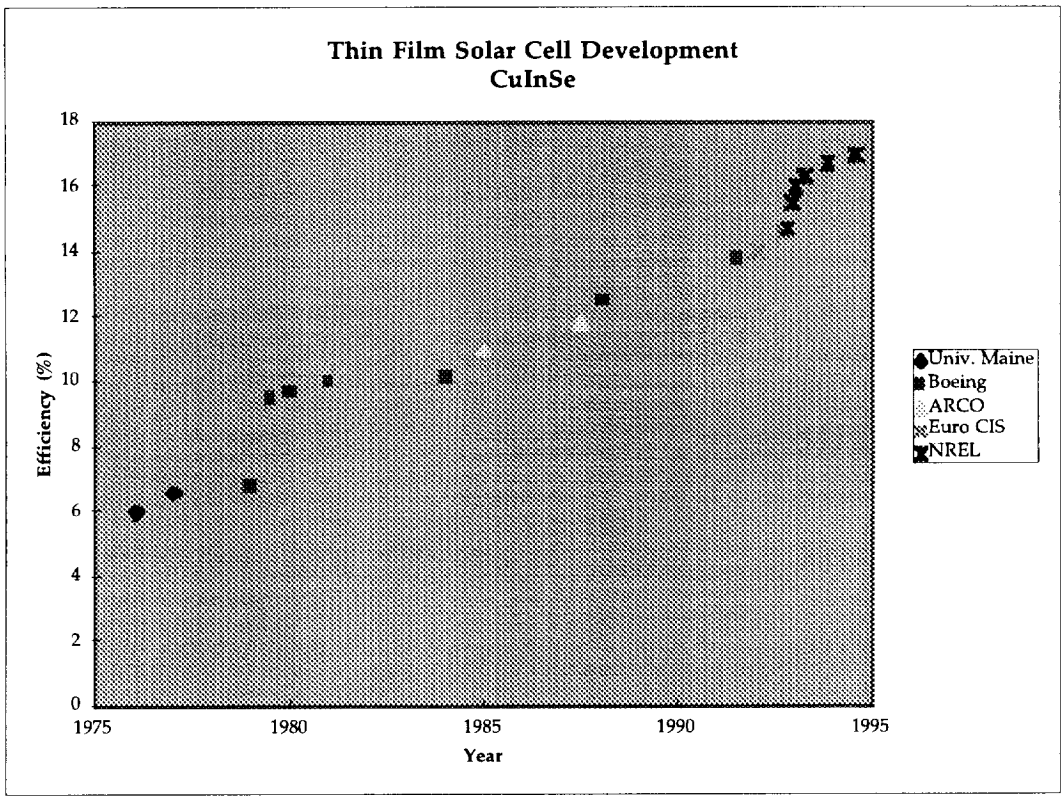

Figure 1 CuInSe Thin Film Solar Cell Development

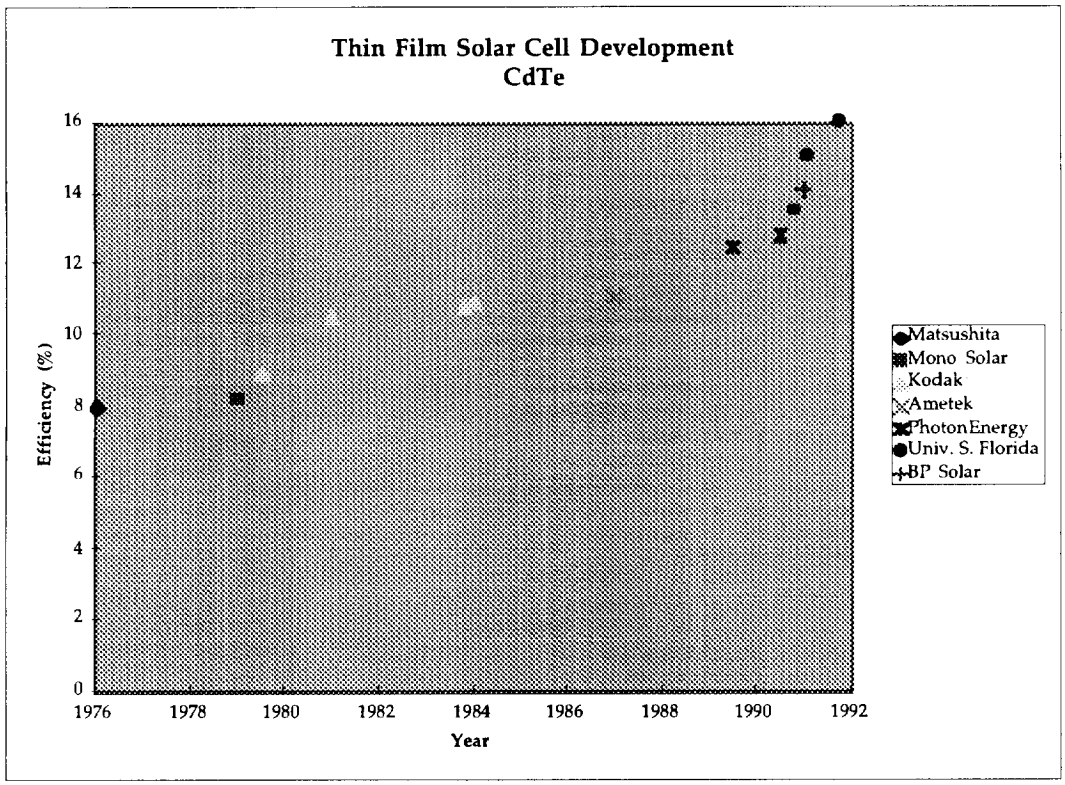

Figure 2 CdTe Thin Film Solar Cell Development

	Efficiency at AM0 (Air Mass 0)		Module Mass (kg / m^2)		Cost (Dollars per Watt)	
	1997	2001	1997	2001	1997	2001
Thin Film	8%	10 %	0.286	0.375	100	5 to 1.5 (projected)
Single Junction	15 %	20 %	0.295	1.005	5 to 3.5 (for 10 to 13% Si) 100 (for 15% Si K6)	500 (for 18% GaAs/Ge)
Multiple Junction	23 %	28 %	0.485	0.877	When Mature	Estimated to be 3 to 5 Times the Cost of Si

Table 20 Solar Cell Classifications

Cell Dimensions: 25 cm Height; 25 cm Width; cell pitch*: 2.15 cells/cm
Cell Active Area: 400 cm^2/cell (80% of cell envelope)
Cell Mass: 285 g/cell (includes estimate for endplates, tie rods, etc.)
(intended for at least 20 cells/stack)

Current Density - Voltage Relationship (Figure 1)* : V = m*cd + b
(V = voltage, volts/cell; cd = current density mA/cm^2)

For 1997 H_2-Air : m = -0.000248; b = 0.887
For 1997 H_2-O_2 : m = -0.000248; b = 0.927
For 2001 H_2-Air : m = -0.000155; b = 0.887
For 2001 H_2-O_2 : m = -0.000155; b = 0.927

Table 21 Reported and Assumed Mk 7 Stack Characteristics

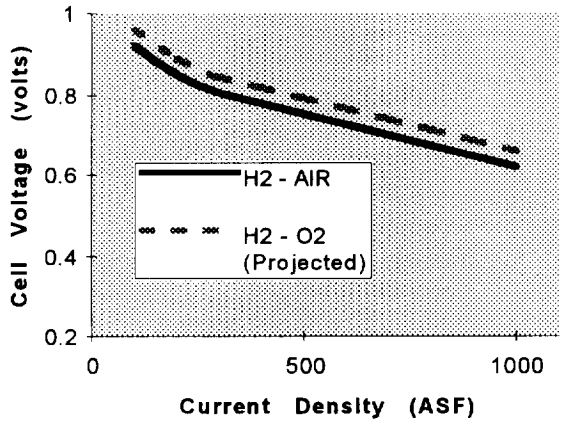

Figure 3 1997 State-of-the-Art PEM Fuel Cell Performance

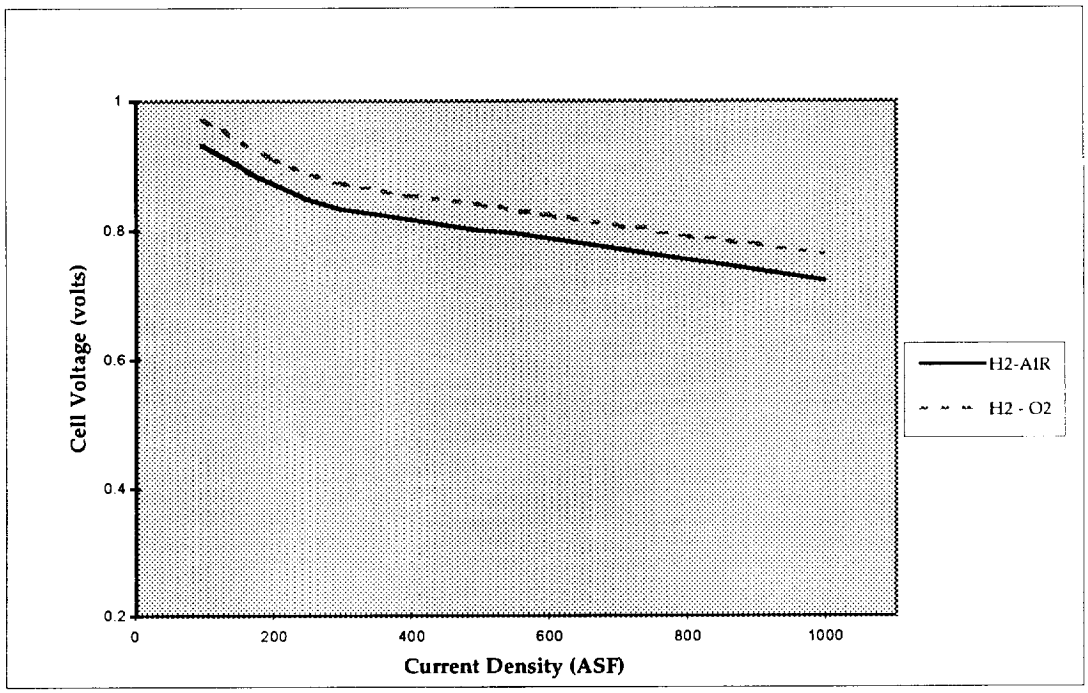

Figure 4 H2-O2 and H2-Air Fuel Cell Stack Performance Projections for 2001

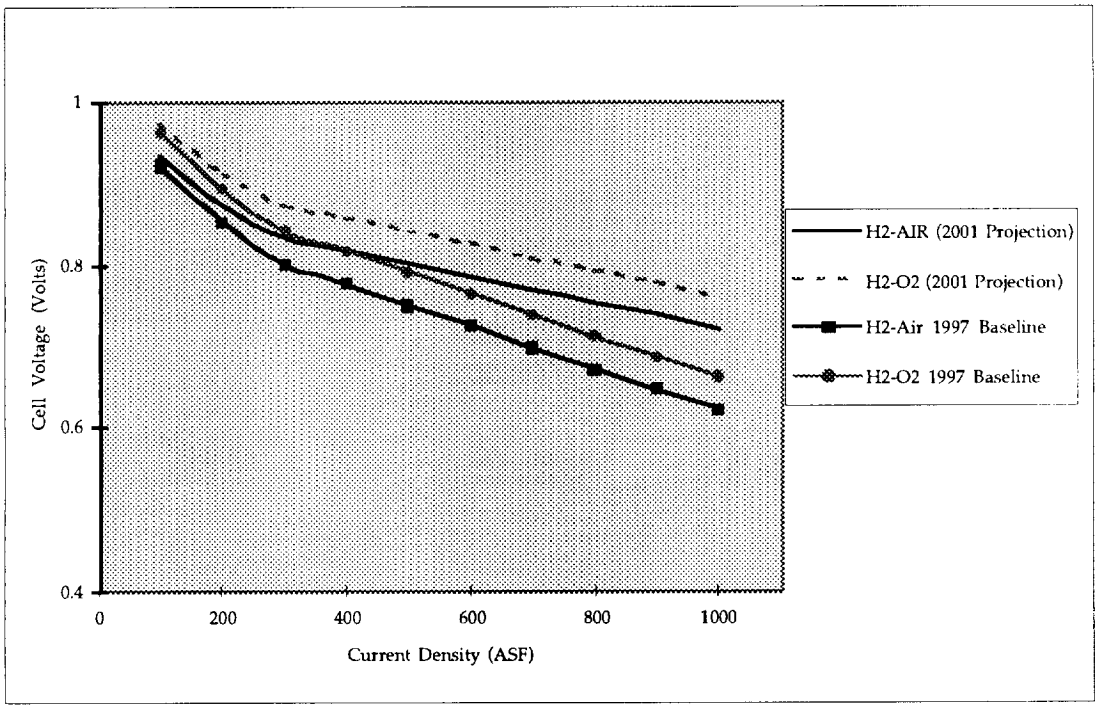

Figure 5 Comparison of PEM Fuel Cell Current-Voltage Relationships for 1997 Technology Baseline with Performance Projections for 2001

Cell Dimension: 18 cm diameter; 214 cm^2 active cell area, cell pitch : 3 cells/cm Cell Mass: 150 g/cell (includes estimate for endplates, tie rods, etc.) (intended for at least 10 cells/stack)
Current Density - Voltage Relationship (Figure 1)* : V = m*cd + b (V = voltage, volts/cell; cd = current density mA/cm^2) For 1997 : m = 0.0001704; b = 1.497 For 2001 : m = 0.0001704; b = 1.497 (Same as for 1997)

Table 22 Reported and Assumed Electrolyzer Stack Characteristics

(Asterisk denotes assumed or estimated characteristic)

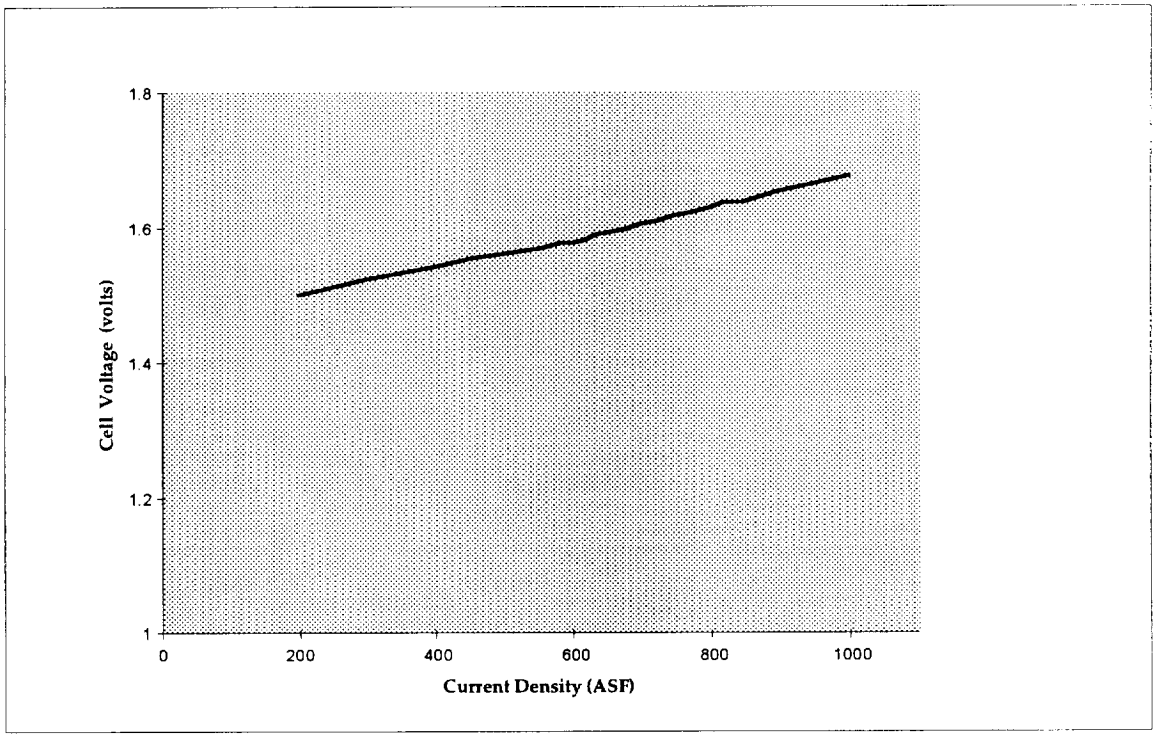

Figure 6 1997 State-of-the-Art Performance for PEM H2O Electrolyzer Stacks

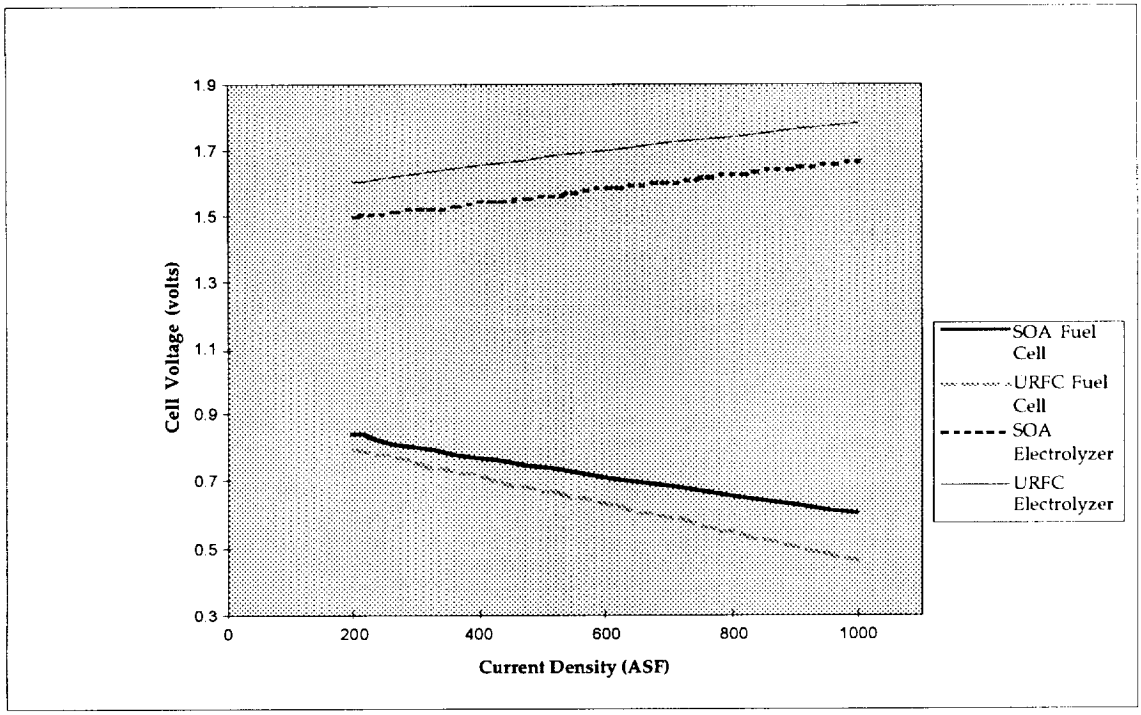

Figure 7 H2-O2 Unitized Fuel Cell/Electrolyzer Performance Projection for 2001

Type	System Wh/kg[1]	System Wh/l[1]	Scaling Laws Fuel Cell System[2]; Electrolyzer[3]
Primary $H_2(g)$-$O_2(g)$ 1997	390	156	A_m= 135; B_m=1241; C_m=1230; D_m=∞ A_v= 222; B_v=276; C_v=550; D_v=∞
Primary $H_2(g)$-$O_2(g)$ 2001	531	167	A_m= 163; B_m=2055; C_m=1554; D_m=∞ A_v= 357; B_v=288; C_v=577; D_v=∞
Primary $H_2(g)$-Air 1997	385	215	A_m= 163; B_m=1149; C_m=∞; D_m=100 A_v= 260; B_v=256; C_v=∞; D_v=260
Primary $H_2(g)$-Air 2001	531	212	A_m= 189; B_m=1881; C_m=∞; D_m=125 A_v= 329; B_v=264; C_v=∞; D_v=329
Primary LOH-Air 1997	423	594	A_m= 163; B_m=1401; C_m=∞; D_m=100 A_v= 260; B_v=1126; C_v=∞; D_v=260
Primary LOH-Air 2001	484	665	A_m= 189; B_m=1441; C_m=∞; D_m=125 A_v= 329; B_v=1158; C_v=∞; D_v=329
Primary LOH-LOX 1997	370	566	A_m= 135; B_m=1505; C_m=933; D_m=∞ A_v= 222; B_v=1210; C_v=2488; D_v=∞
Primary LOH-LOX 2001	400	645	A_m= 163; B_m=1576; C_m=977; D_m=∞ A_v= 357; B_v=1260; C_v=2604; D_v=∞
H_2O Elelctrolyzer 1997 Baseline[4,6]	NA (117 kg)	NA (52 l)	E = 3.871 $F^{(1)}$ = 30.2
H_2O Elelctrolyzer 2001 Baseline[5,6]	NA (77 kg)	NA (37.4 l)	E = 2.68 $F^{(1)}$ = 28.8
$H_2(g)$-$O_2(g)$ RFC[6] 1997	222	137	Additive for $H_2(g)$-$O_2(g)$ 1997 Baseline
$H_2(g)$-$O_2(g)$ RFC[6] 2001	316	151	Additive for $H_2(g)$-$O_2(g)$ 2001 Baseline

Table 23 Standard Characteristic Profile Correlations for Fuel Cell Systems

(1) Example Results for 12 Hour Fuel Cell Operation and 12 Hour Electrolyzer Operation

(2) System Mass (kg) = $1.15*FCP*\{1/A_m+FCOT*[1/B_m+1/C_m]+1/D_m\}$
System Volume (l) = $1.10*FCP*\{1/A_v+FCOT*[1/B_v+1/C_v]+1/D_v\}$

(3) System Mass (kg) = $3.871*E*(FCOT/EZOT)$
System Volume (l) = $1.1*E*\{0.571*[FCOT/EZOT]+1\}$

FCP = Net Fuel Cell System Power (Watts). Range is 750 - 40,000 Watts

FCOT = Fuel Cell System Operating Time (hrs.)

EZOT = Electrolyzer System Operating Time (hrs.)

E = constant ; F = kg water required to be electrolyzed.

(4) For PV assumed 64 W/m^2 and 0.4 kg/m^2 (considered as part of airframe)

(5) For PV assumed 80 W/m^2 and 0.3 kg/m^2 (considered as part of airframe)

(6) PV volume not included

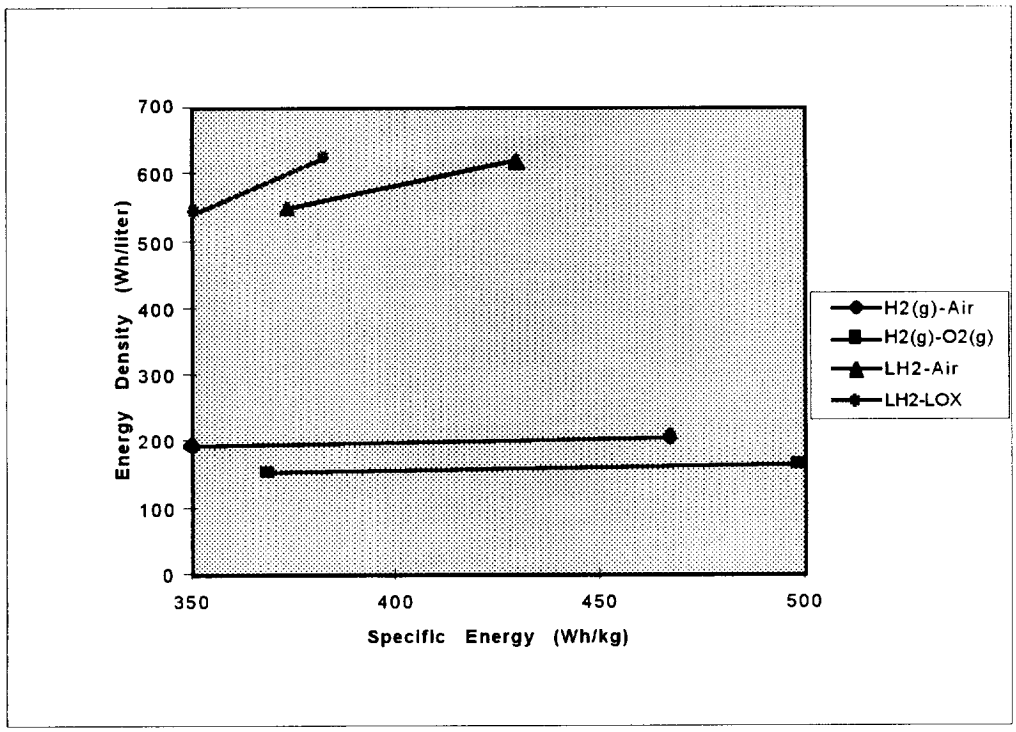

Figure 8 Comparison of Energy Densities and Specific Energy of Non-Regenerative Fuel Cell Systems for 1997 and 2001 Technology Baselines

Type	System Wh/kg[1]	System Wh/l[1]	Scaling Laws[2,3,4]
LiSOCl 1997	360	900	A_m= 400; A_v= 1000
LiSOCl 2001	360	900	A_m= 400; A_v= 1000
Li-SO_2 1997	248	405	A_m= 275; A_v= 450
Li-SO_2 2001	248	405	A_m= 275; A_v= 450
AgO-Zn 1997	144	612	A_m= 160; A_v= 680
AgO-Zn 1/101	144	612	A_m= 160; A_v= 680
COTS Alkaline 1997	68	176	A_m= 76; A_v= 196
COTS Alkaline 2001	68	176	A_m= 76; A_v= 196

Table 24 Primary Battery System Performance Characteristic Profile Estimates

(1) For 0.5 Hour Battery Operation, 1 kW net , 100% DOD
(2) System Mass (kg) = BP*{ BOT/[(Eff/100)*A_m] }
System Volume (l) = BP*{ BOT/[(Eff/100)*A_v] }
A_m = Nominal Wh/kg of the Battery;
A_v = Nominal Wh/l of the Battery;
DOD = Depth of Discharge always assumed to 100%; Eff=Percent Efficiency
BP = Net Battery System Power (Watts). Range is 10 - 5,000 Watts
BOT = Battery System Operating Time (hrs.);

	Mid-Term (1995)	Long-Term (1998)
Specific Energy (Wh/kg)	> 80	200
Energy Density (Wh/l)	> 135	> 300
Peak Specific Power (W/kg)	150	400
Power Density (W/l)	250	600
Cycle Life (cycles)	600	1000
Calendar Life (yrs.)	5	10
Efficiency (%)	75	75
Recharge Time (hrs.)	< 6	3-6
Fast Recharge Time (hrs.)	0.25	0.25
Continuous Discharge in 1 hr.	75	75
Power and Capacity Degradation (%)	20	20
Operating Environment (°C)	-30 to 60	-40 to85
Cost (US$/kW-hr)	< 150	< 100

Table 25 United States Advanced Battery Consortium Battery Goals

Type	System Wh/kg[1]	System Wh/l[1,5]	Scaling Laws[2,3,4]
Lead-Acid 1997	33	50	A_m= 38; B_m=250; C_m=250; D_m=160 A_v= 90; B_v=15; C_v=15
Lead-Acid 2001	40	62	A_m= 45; B_m=350; C_m=350; D_m=267 A_v= 120; B_v=30; C_v=30
Nickel-Cadmium 1997	40	54	A_m= 45; B_m=250; C_m=250; D_m=160 A_v= 100; B_v=15; C_v=15
Nickel-Cadmium 2001	44	72	A_m= 50; B_m=350; C_m=350; D_m=267 A_v= 110; B_v=30; C_v=30
Nickel-MH 1997	55	71	A_m= 65; B_m=250; C_m=250; D_m=160 A_v= 170; B_v=15; C_v=15
Nickel-MH 2001	77	107	A_m= 90; B_m=350; C_m=350; D_m=267 A_v= 200; B_v=30; C_v=30
Lithium-Ion 1997 [6]	82	83	A_m= 100; B_m=250; C_m=250; D_m=160 A_v= 250; B_v=15; C_v=15
Lithium-Ion 2001 [6]	108	122	A_m= 130; B_m=350; C_m=350; D_m=267 A_v= 250; B_v=30; C_v=30
Lithium-Ion Polymer 1997 [6]	82	71	A_m= 100; B_m=250; C_m=250; D_m=160 A_v= 170; B_v=15; C_v=15
Lithium-Ion Polymer 2001 [6]	104	122	A_m= 125; B_m=350; C_m=350; D_m=267 A_v= 250; B_v=30; C_v=30

Table 26 Secondary Battery System Performance Characteristic Profile Estimates

(1) For 12 Hour Battery Operation, 5 kW net , 100% DOD, and 12 Hour Recharge Time

(2) System Mass (kg) = $1.10*BP*\{ BOT/[(DOD/100)*A_m] + (1/B_m) + (1-Eff/100)/C_m) + BOT/(Eff/100)/RT/D_m \}$

System Volume (l) = $1.10*BP*\{ BOT/[(DOD/100)*A_v] + (1/B_v) + (1-Eff/100)/C_v) \}$

A_m = Nominal Wh/kg of the Battery; B_m=W/kg of the Charge/Discharge Controller;
C_m=W/kg of the Heat Exchanger; D_m(PV Mass) = 160 for 1997 and D_m=267 for 2001
A_v = Nominal Wh/l of the Battery; B_v=W/l of the Charge/Discharge Controller;
C_v=W/l of the Heat Exchanger; B_v and C_v= 25% of A_v for 1997 and 15% of A_v for

2001.
(For lithium technology, both B_v and C_v may be reduced).
DOD = Depth of Discharge (%); Eff=Percent Round Trip Efficiency
(Wh_{out}/Wh_{in}*100%)
BP = Net Battery System Power (Watts). Range is 100 - 40,000 Watts
BOT = Battery System Operating Time (hrs.); RT = Recharge Time (hrs.)
(3) For PV assumed 64 W/m^2 and 0.4 kg/m^2
(4) For PV assumed 80 W/m^2 and 0.3 kg/m^2
(5) PV volume not included
(6) Lithium Technology not Available in 1997 for >1 kW, Probably Available for 2001

Material	Composite Strength (GPa)*	Composite Density (kg/m3)	Theoretical Maximum Specific Energy (W-hr/kg)
Graphite (fiber) 1995 √	4.8	1609	414
Graphite (fiber) 1989 √	3.4	1609	293
Spectra ® (fiber)	1.4	1039	187
Kevlar ® (fiber)	1.8	1375	182
S-glass (fiber) √	2.1	2190	133
E-glass(fiber) √	1.8	2205	113
Silicon-nitride ceramic	.92	3250	39
Maraging steel	2.1	7860	37
Titanium alloy	1.2	4500	37
Magnesium alloy	.28	1790	22

Table 27 Flywheel Theoretical Maximum Specific Energy

*** Ultimate Strength for fibers, yield strength for metals, modulus of rupture for ceramics**

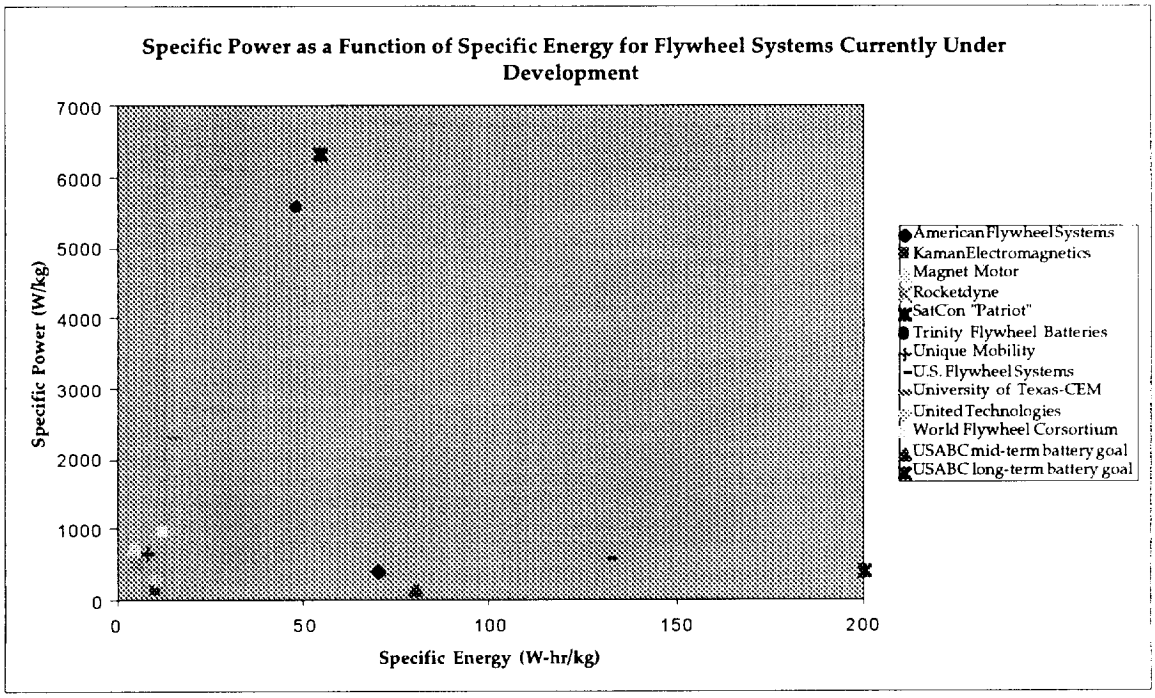

Figure 9 Specific Power as a Function of Specific Energy for Various Flywheel Systems

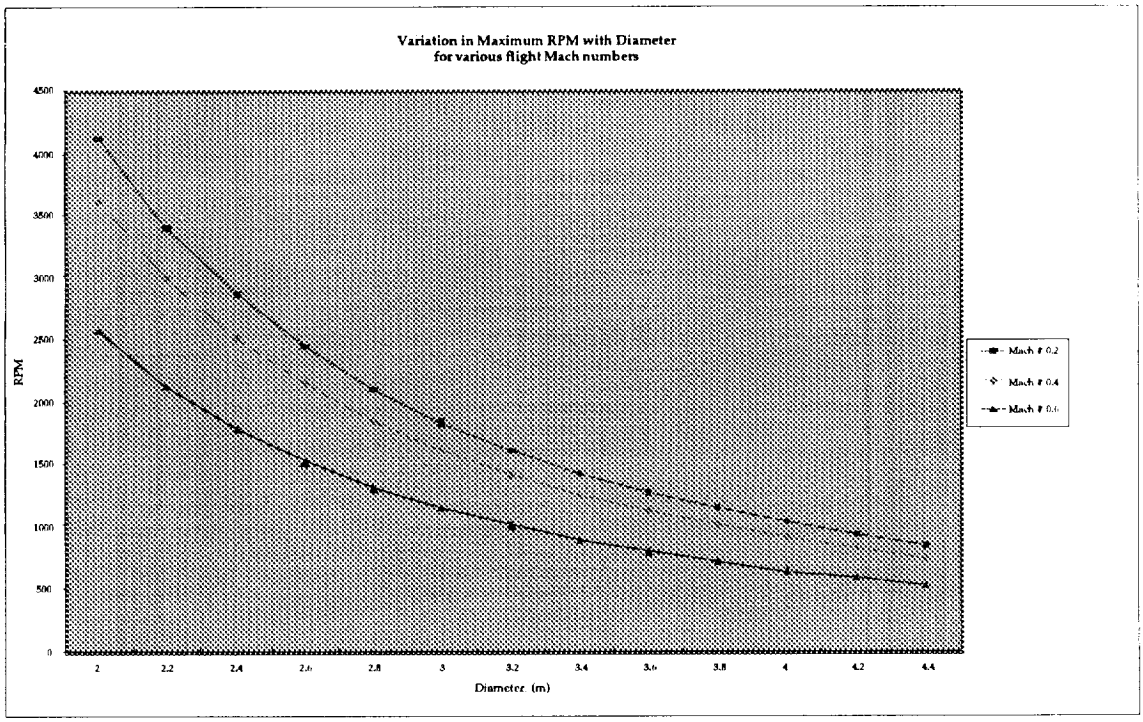

Figure 10 The Effect of Propeller Diameter on RPM

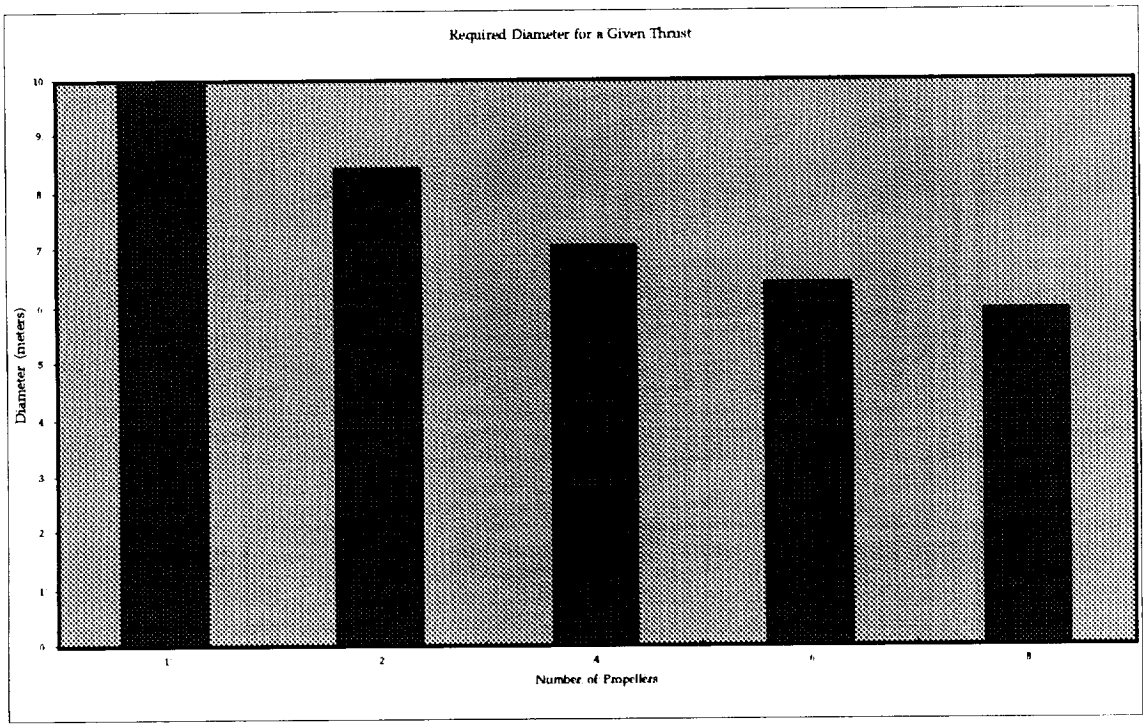

Figure 11 Propeller Diameter Versus Number of Propellers

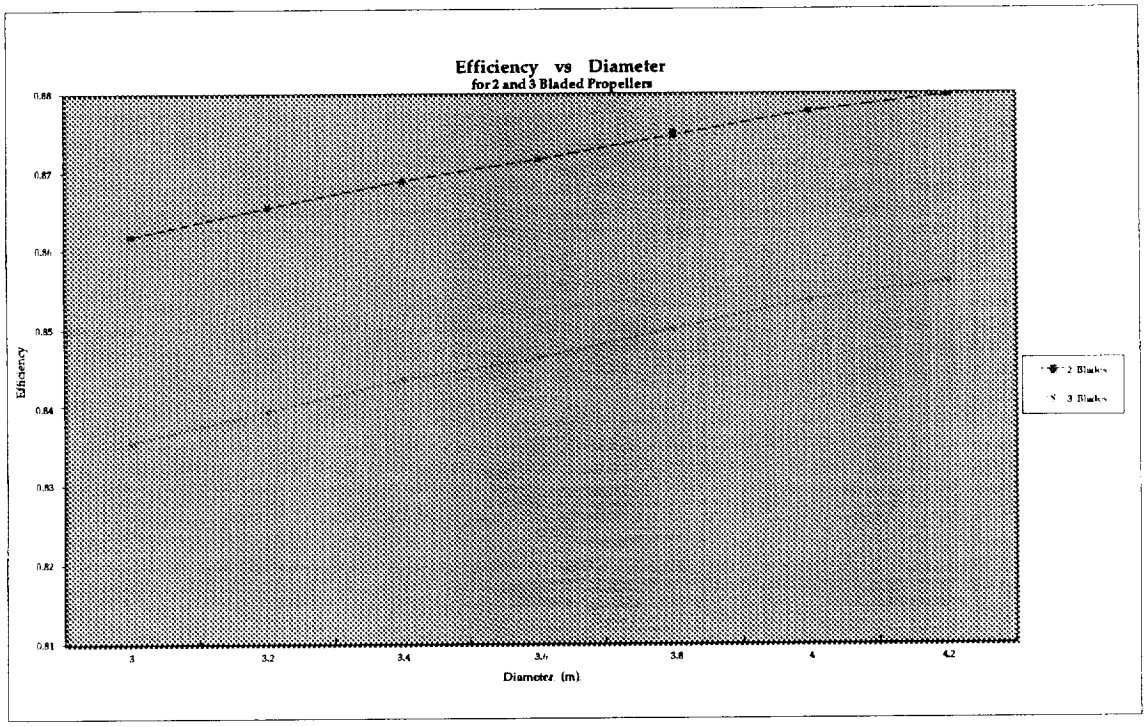

Figure 12 Effect of Propeller Diameter on Propeller Efficiency

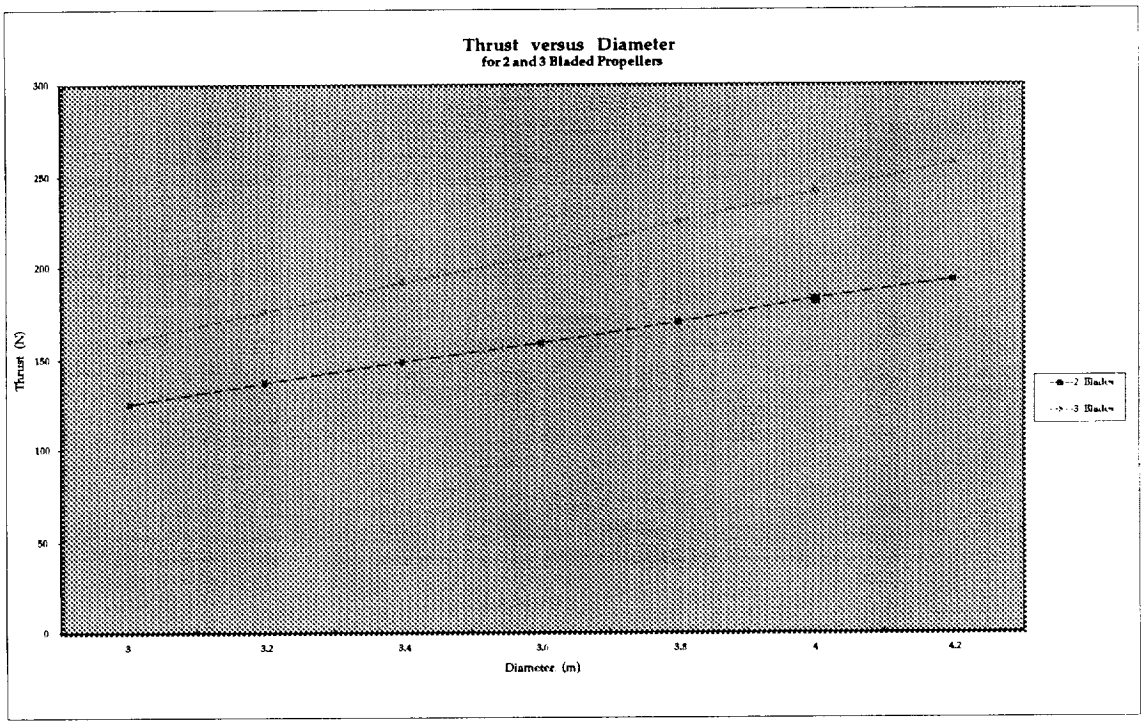

Figure 13 Effect of Propeller Diameter on Output Thrust

	Advantages	Disadvantages
Fixed Pitch	Light Weight Simple Controls	Less Performance May Constrain Mission Altitude
Variable Pitch	Heavier Needs Control System	Higher Performance May be Mission Enabling

Table 28 Fixed vs. Variable Pitch Propellers

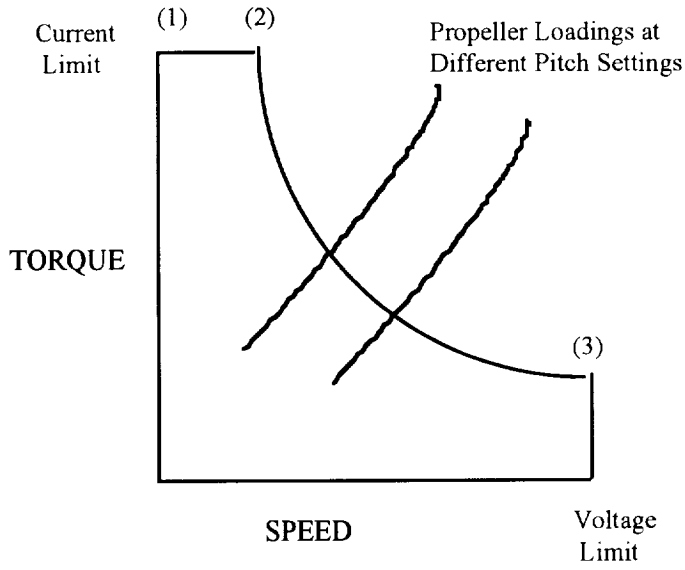

Figure 14 Qualitative Torque-Speed Motor Characteristics

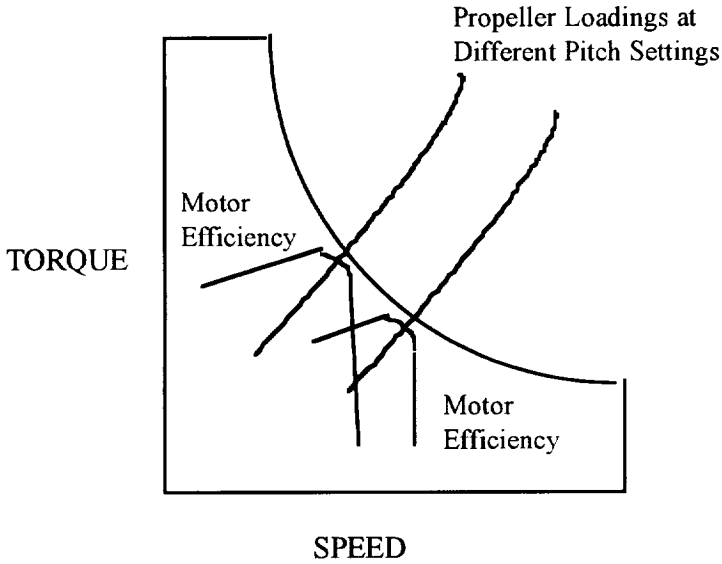

Figure 15 Qualitative Efficiency Characteristics of an Induction Motor

	Advantages	Disadvantages
Brush Motors	• Most Highly Developed • Least Expensive	• Short Life at High Altitude • General Maintenance Concern • Electrical Noise Concern • (Replaced by Brushless Motors for Most Aeronautical Applications)
Brushless DC Motors	• In General, Overcomes Problems with the Brush Motors • Used for Many Electric Vehicle Drives	• Max.Power and Max.Efficiency Occur at Different Operating Points • High cost for High Power Density and High Multiple Horsepower Ratings (ie., Limited to Military Applications)
Induction Motors	• Most rugged • Potentially Least Expensive • Most Popular Electric Vehicle Motor for Applications up to Several Hundred H.P.	• Rotor Loss is a Concern for High Power, High Altitude Operation (considered a Design Issue)
Switched Reluctance Synchronous Motors	• Simple and Rugged • Low Rotor Loss • Can Continue to Operate Under Some Failure Modes • Rotor Cooling Constraints Reduced (Relative to other Motor Types)	• Few Civilian Applications To Date Because of High Cost • Complex Control • Relatively Low Power Factor • Output Torque Subject to Pulsation
Permanent Magnet Induction Motors	• Potential to Combine Beneficial Characteristics of Induction and Permanent Magnet Machines	• No Industrial base Exists for These Motors or Their Controllers
Axial Flux Motors	• Generally Most Suitable for Very High Speed Applications	• Relatively Poor Performance • Longer and Heavier than Conventional Types

Table 29 Qualitative Characteristics of Candidate Motors

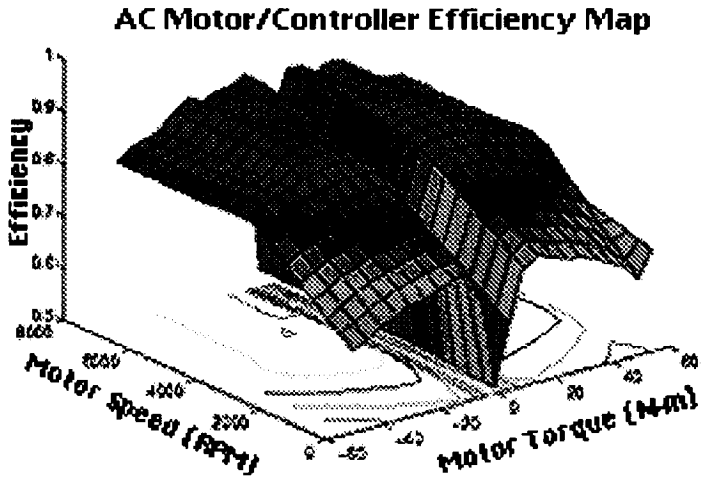

Figure 16 AC Motor/Controller Efficiency Map

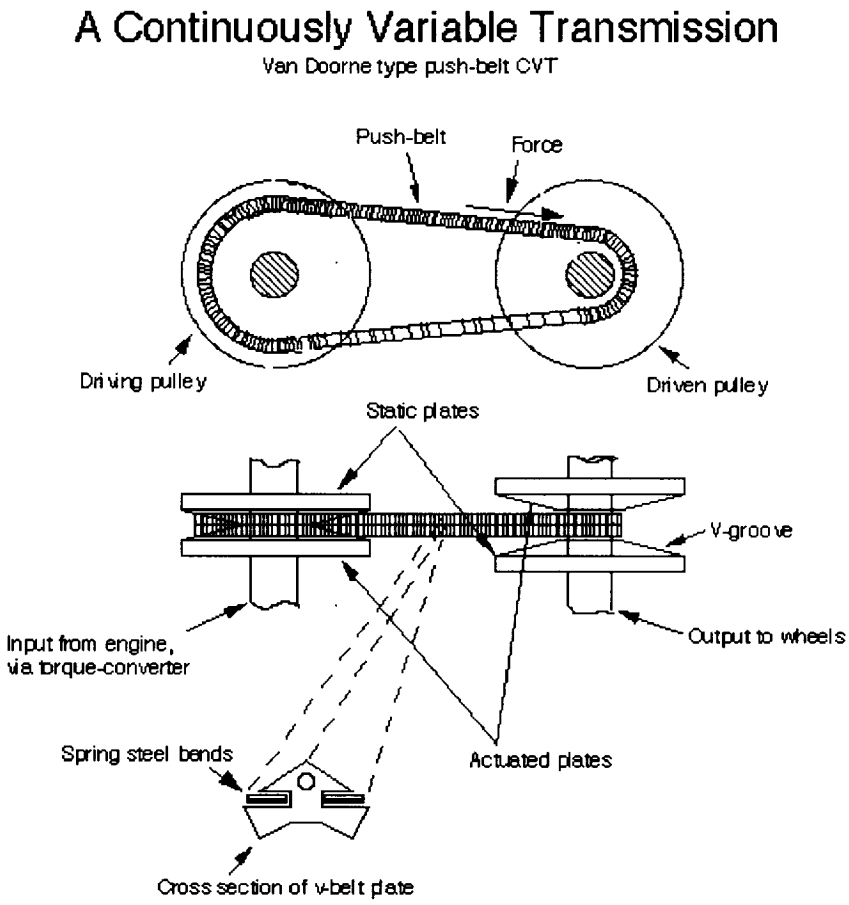

Figure 17 Continuously Variable Transmission

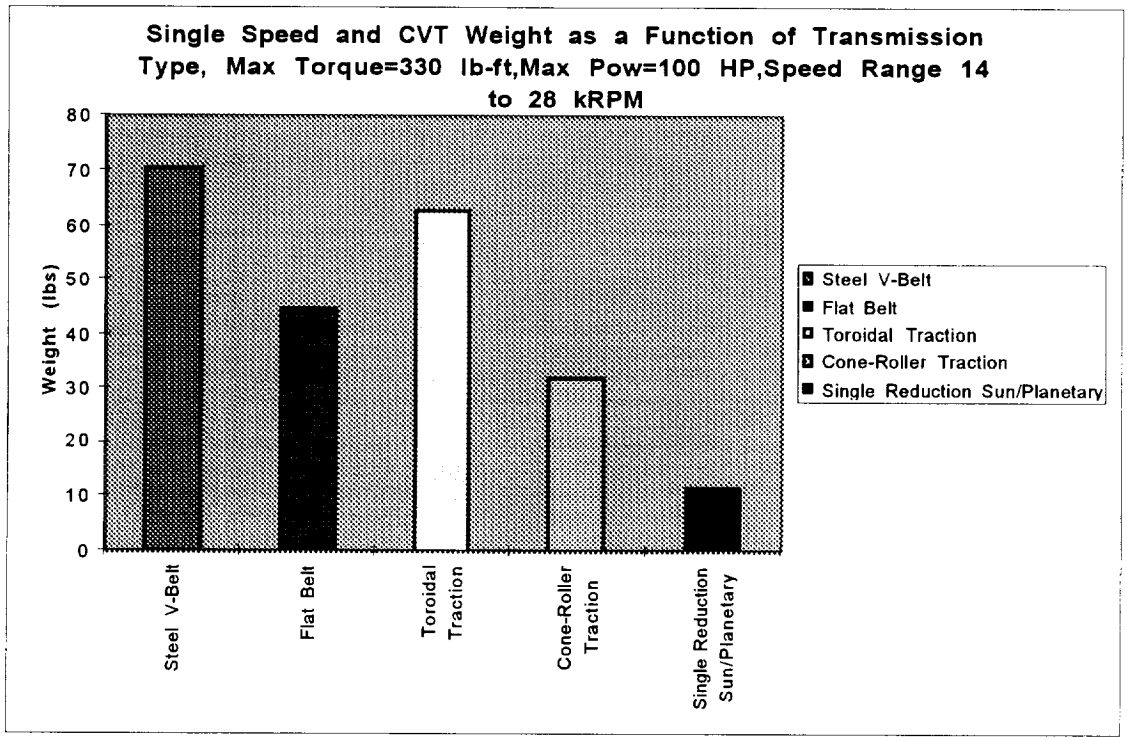

Figure 18 Weight as a Function of Transmission Type

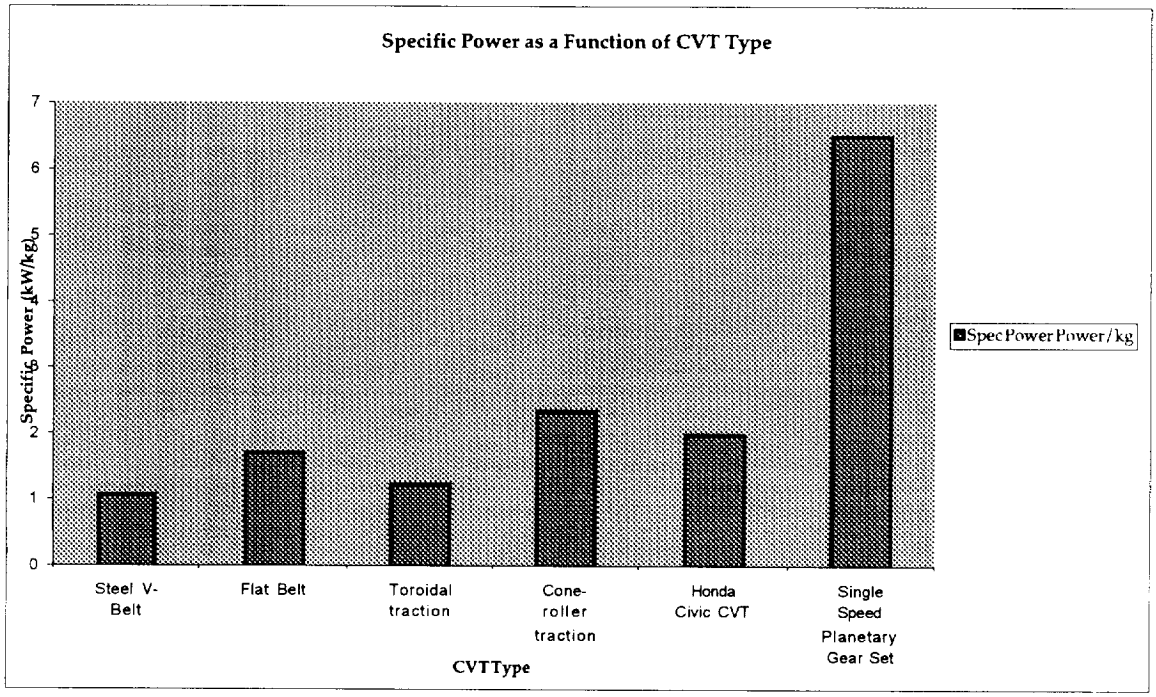

Figure 19 Specific Power as a Function of Transmission Type

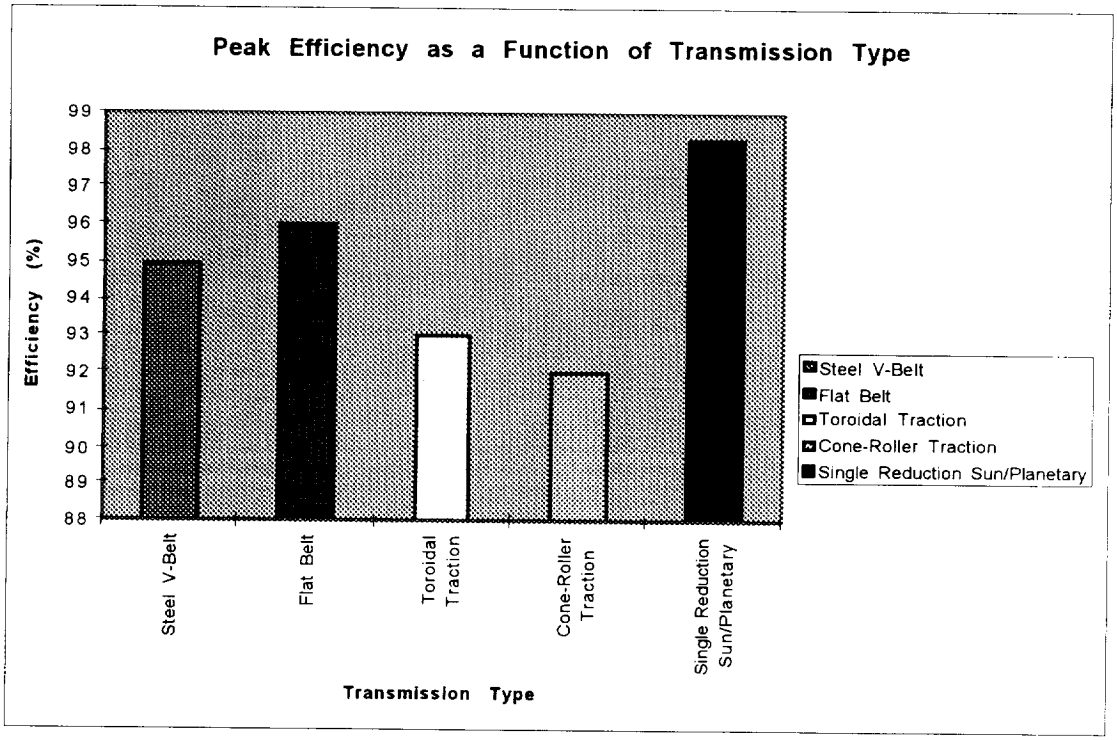

Figure 20 Weight as a Function of Transmission Type

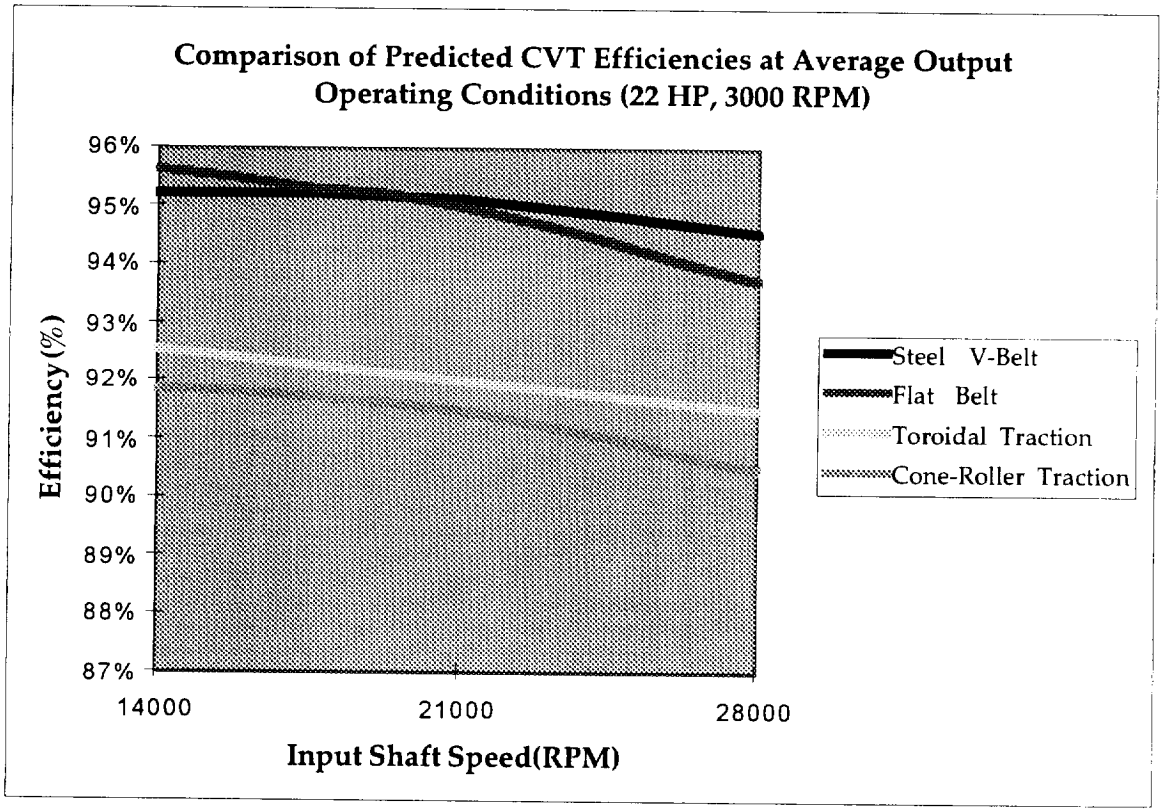

Figure 21 Efficiency as a Function of Input Shaft Speed and Transmission Type

	Availability		Reliability		Relative Performance		Safety		Emissions/ Environmental Impact		Cost	
	1997	2001	1997	2001	1997	2001	1997	2001	1997	2001	1997	2001
Motors												
Brush Motors	E	E	P	P	G	G	VG	VG	P	P	E	E
Brushless DC Motors	E	E	VG	VG	VG	VG	VG	VG	VG	VG	VG	VG
Induction Motors	E	E	E	E	VG	VG	VG	VG	VG	VG	VG	VG
Switched Reluctance Synchronous Motors	E	E	VG	VG	G	G	VG	VG	VG	VG	G	G
Permanent Magnet Induction Motors	P	P	G	G	E	E	VG	VG	VG	VG	P	P
Axial Flux Motors	G	G	G	G	P	P	VG	VG	VG	VG	G	G
Transmissions												
Single Speed	E	E	E	E	G	G	VG	VG	G	G	E	E
Multi-Speed	VG	VG	VG	VG	G	G	VG	VG	G	G	VG	VG
Continuously Variable Transmissions	P	G	G	G	P	P	VG	VG	G	G	P	P
Propellers												
Fixed Pitch	E	E	E	E	G	G	E	E	E	E	E	E
Variable Pitch	VG	VG	VG	VG	VG	VG	E	E	E	E	VG	VG
Variable Diameter	P	P	G	G	VG	VG	E	E	E	E	P	P
Dual Propellor	P	P	G	G	VG	VG	E	E	E	E	P	P

Table 30 Qualitative Rankings of Candidate Drivetrain

P=Poor; G=Good; VG=Very Good; E=Excellent

	0 km ROA			1000 km ROA		
	75 kg	150 kg	225 kg	75 kg	150 kg	225 kg
90,000 ft	Yes	Yes	Yes	Yes	Yes	Yes
100,000 ft	Yes	Yes	Yes	Yes	Yes	Yes

Table 31 Twelve Original Missions, Multi-Junction Cells 1997 Baseline

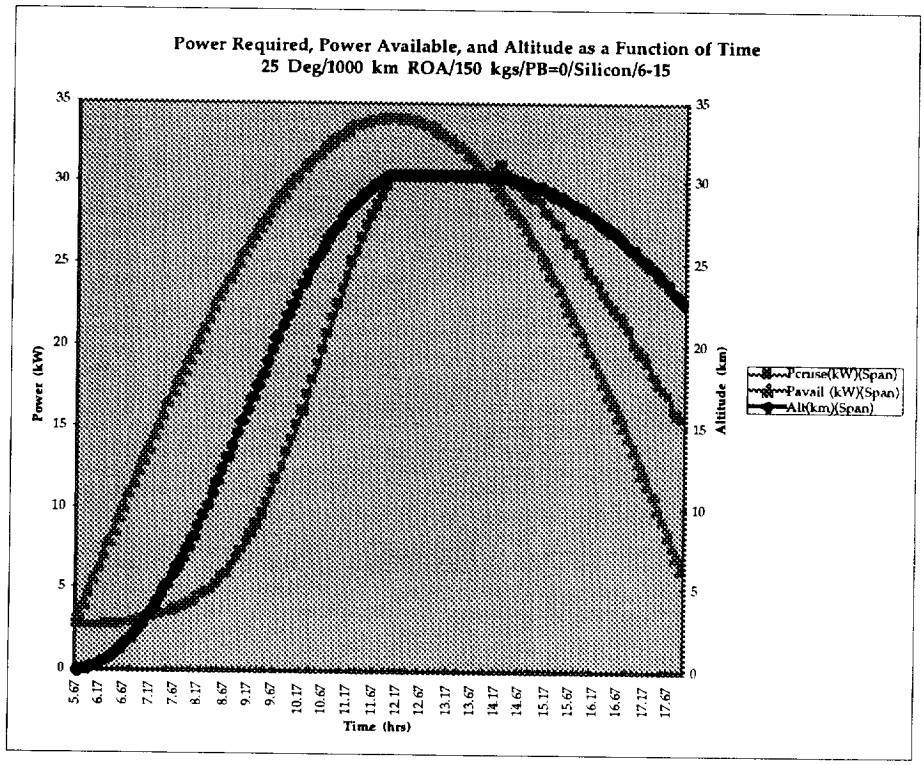

Figure 22 Cruise, Available, and Altitude as a Function of Mission Time

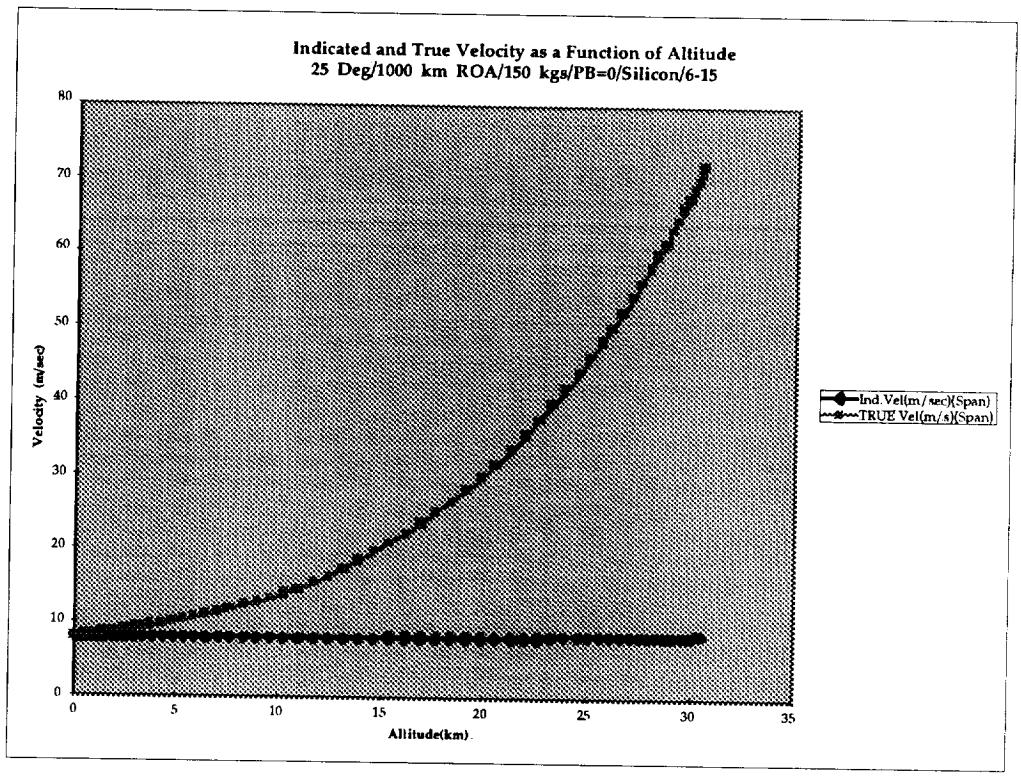

Figure 23 Indicated and True Velocity as a Function of Altitude

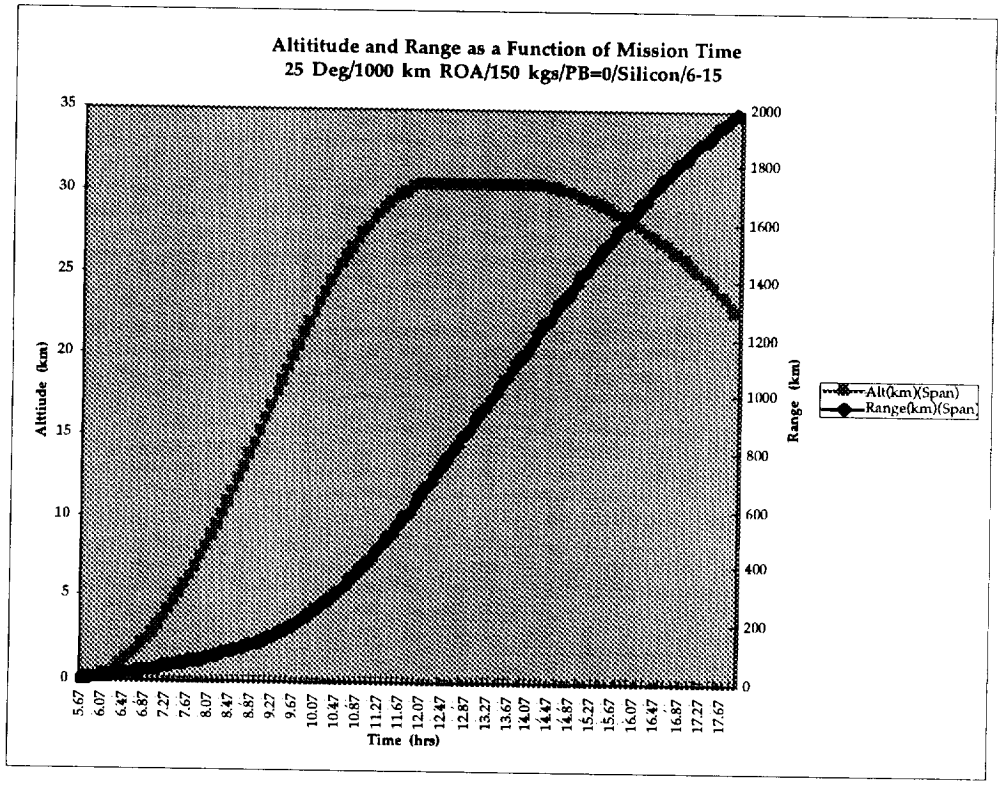

Figure 24 Altitude and Range as a Function of Mission Time

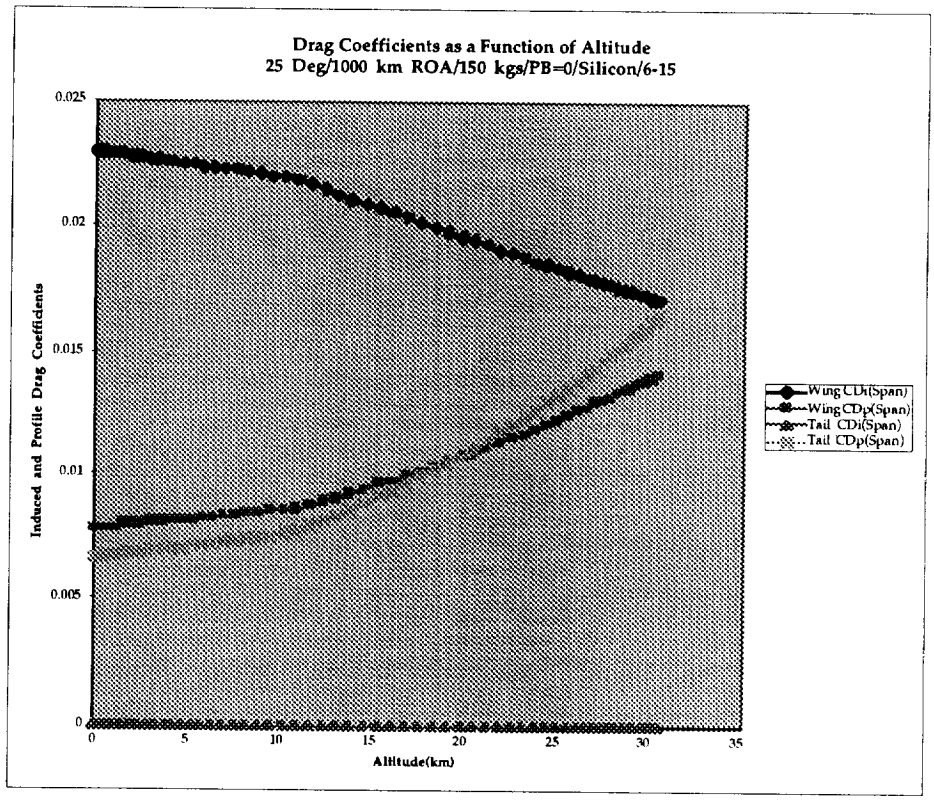

Figure 25 Drag Coefficients as a Function of Altitude

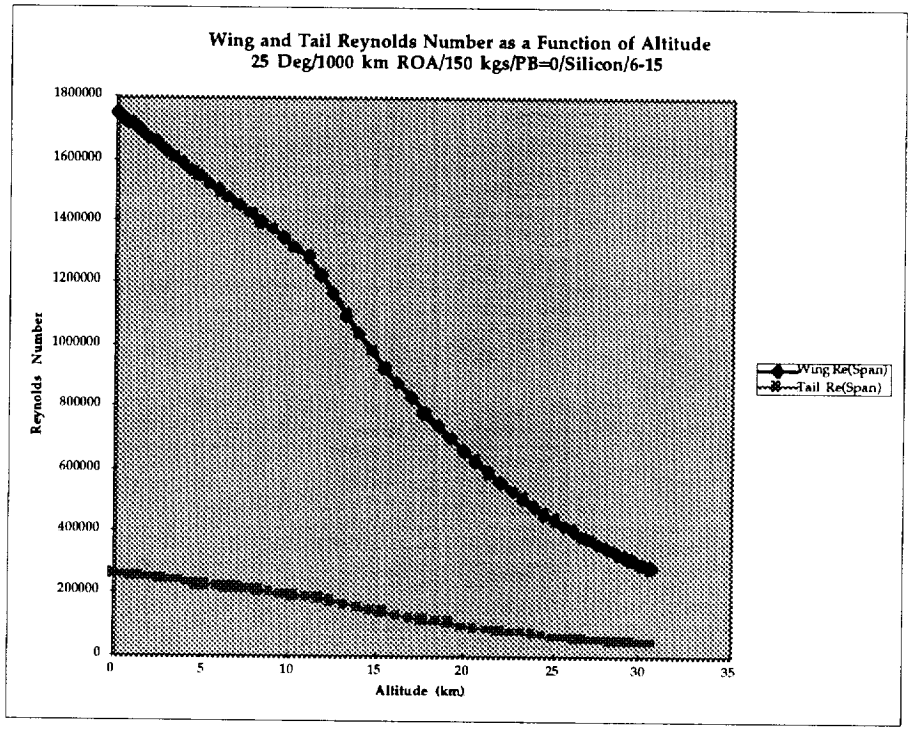

Figure 26 Reynolds Number as a Function of Altitude

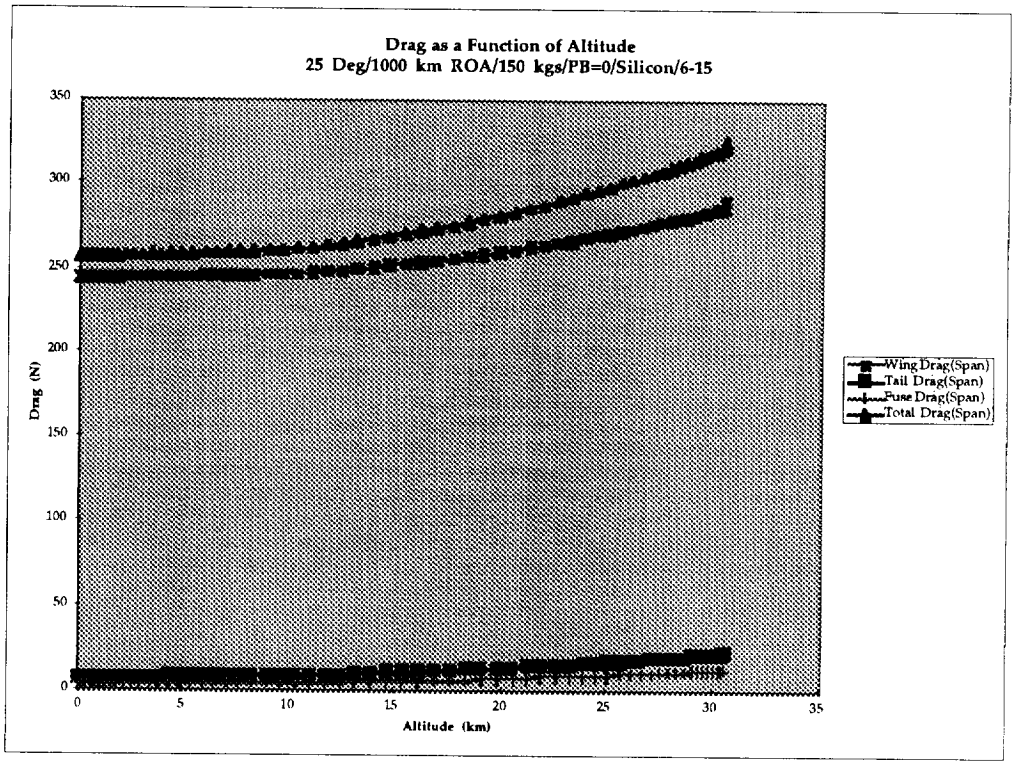

Figure 27 Drag as a Function of Altitude

**********Solar Aircraft Analysis Code (SAAC)**********

Mission Date at Take-off	6\15
Mission Duration (days)	0.00
Latitude (deg)	25.00
Maximum Altitude (km)	30.49
Minimum Time Duration at Max. Altitude (hrs)	0.58
Minimum Radius of Action (km)	1000.00
Payload Mass (kg)	150.00
Payload Power (W)	0.00

XXXXXXXXXXXXXX Airframe Output Data XXXXXXXXXXXXXX

Airframe Type:	Span Loaded	
Wing Area		204.00 m^2
Wing Span		63.87 meters
Wing Aspect Ratio		20.00
Wing Loading		0.90 lb/ft^2
Propeller Type :	Fixed Pitch	
Propeller Efficiency (%)		85.000
Propeller Diameter (m)		4.40
Propeller Blade Aspect Ratio		14.00

XXXXXXXXXXXXXX Power Subsystem XXXXXXXXXXXXXX

Drivetrain Performance Baseline:		1997
Solar Cell Type :	Single Junction	
Solar Cell Efficiency (%)		15.000
Solar Cell Specific Mass (kg/sq m)		1.005
Solar Cell Approximate Cost (1997 $)		$ 5.1 Million
Type of Energy Storage System :	None	
Motor Type :	Induction Motor	
Motor Efficiency (%)		95.000
Power Conditioning Efficiency (%)		95.000
Electrical Power Generated at Mid-Day(watts)		30898.18

Engine Mass (kg)		64.13 kg
Propeller Mass (kg)		41.56 kg
Solar Cell Mass (kg)		205.02 kg
Fuselage Mass (kg)		51.62 kg
Spar Mass	92.13 kg	
Rib Mass	14.97 kg	
Leading Edge Mass	83.84 kg	
Trailing Edge Mass	14.37 kg	
Control Mass	13.71 kg	
Covering Mass	116.26 kg	
Total Wing Mass	335.29 kg	
Boom Mass		0.00 kg
Tail Mass (kg)		49.20 kg
Payload Mass		150.00 kg
Energy Storage System Mass (kg)		0.00 kg
	Total Mass	896.00 kg
TakeOff Time	5.57 hours	

Table 32 Base Case SAAC Output

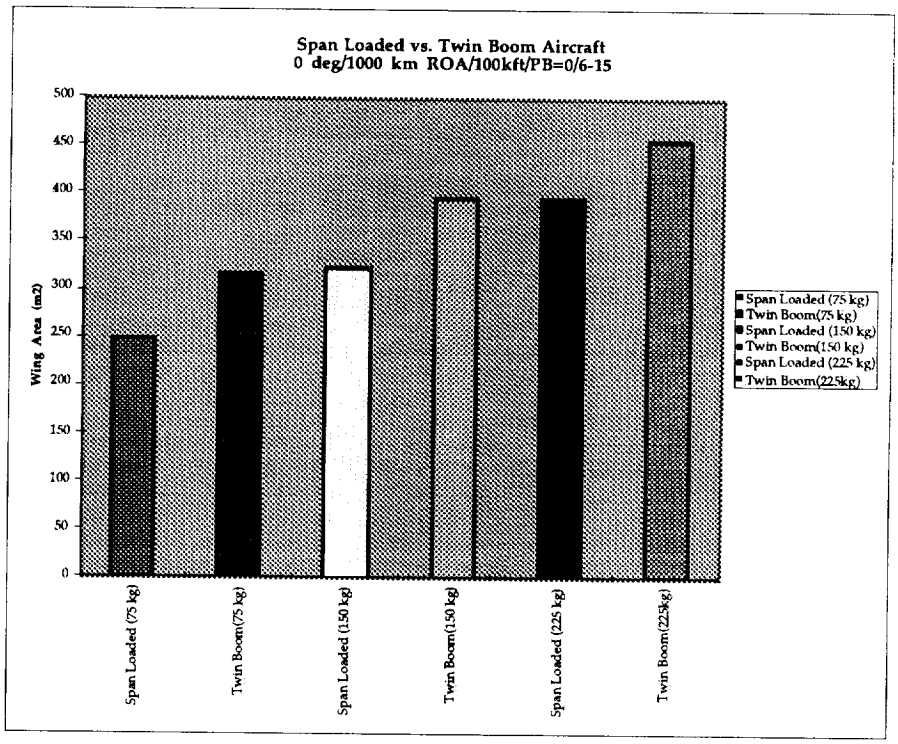

Figure 28 Comparison of Span and Twin Boom Aircraft

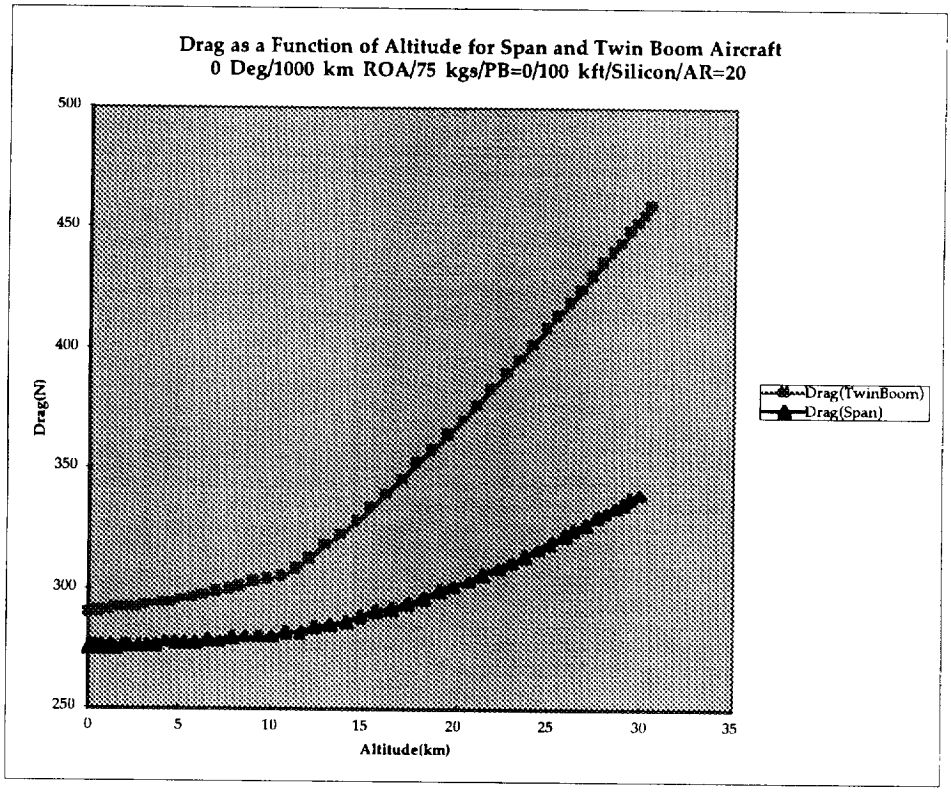

Figure 29 Comparison of Span and Twin Boom Aircraft Drags(75 kg Payload)

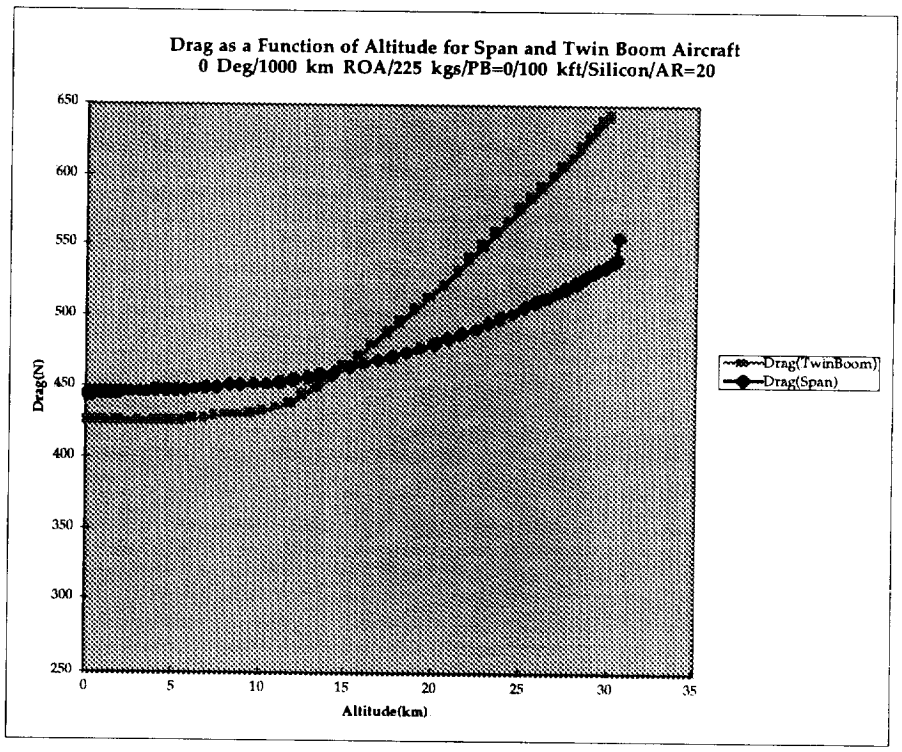

Figure 30 Comparison of Span and Twin Boom Aircraft Drags(225 kg Payload)

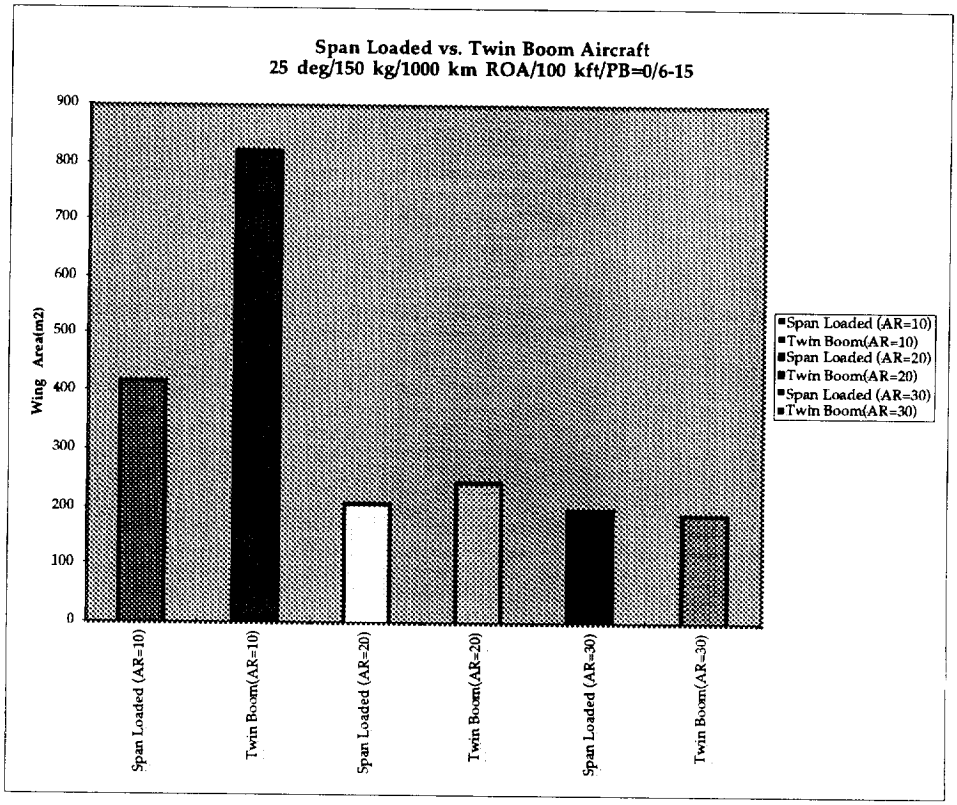

Figure 31 Effects of Aspect Ratio on Span and Twin Boom Aircraft Wing Area

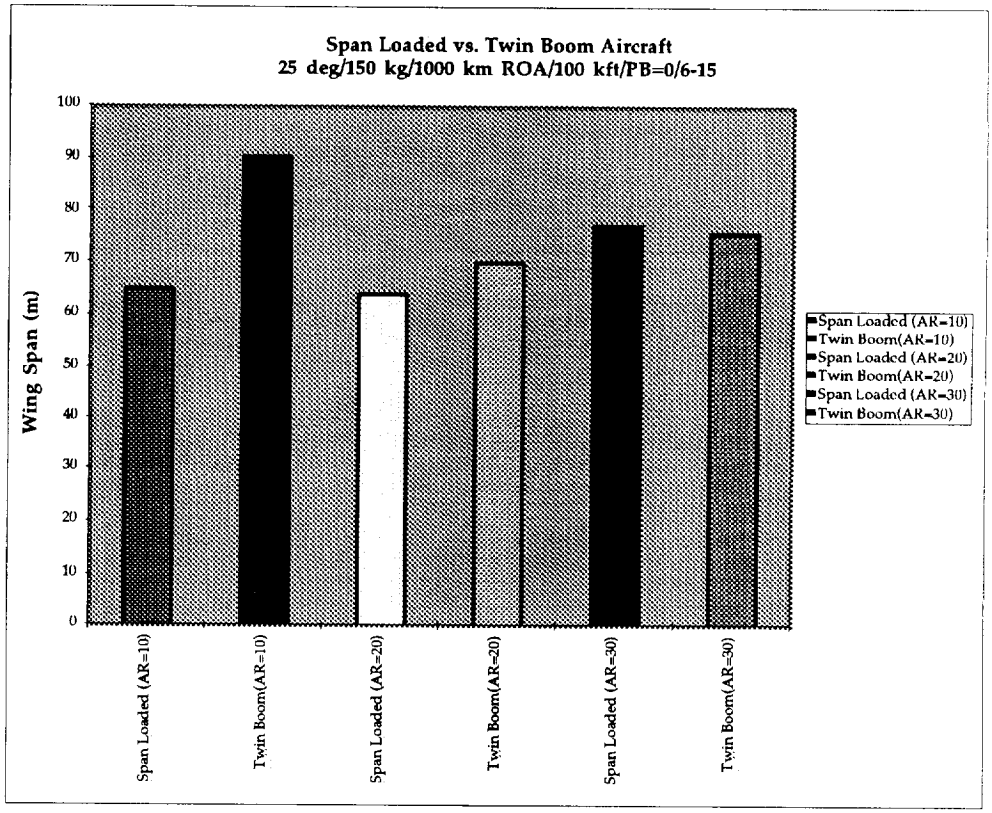

Figure 32 Effects of Aspect Ratio on Span and Twin Boom Aircraft Wing Span

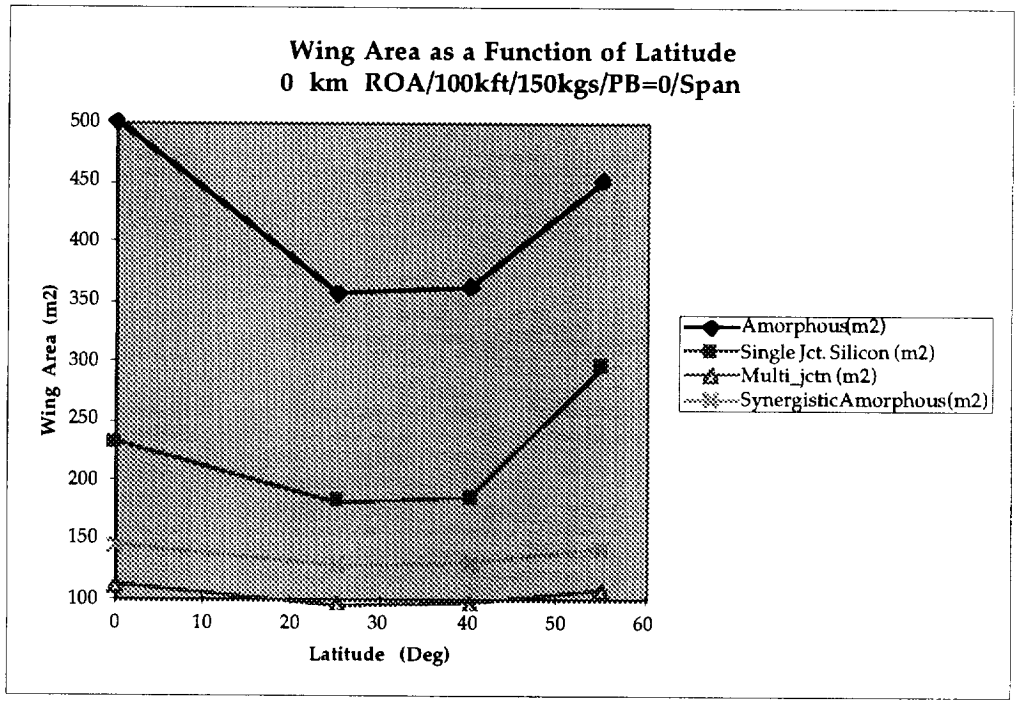

Figure 33 Effects of Latitude on Wing Area (0 km ROA)

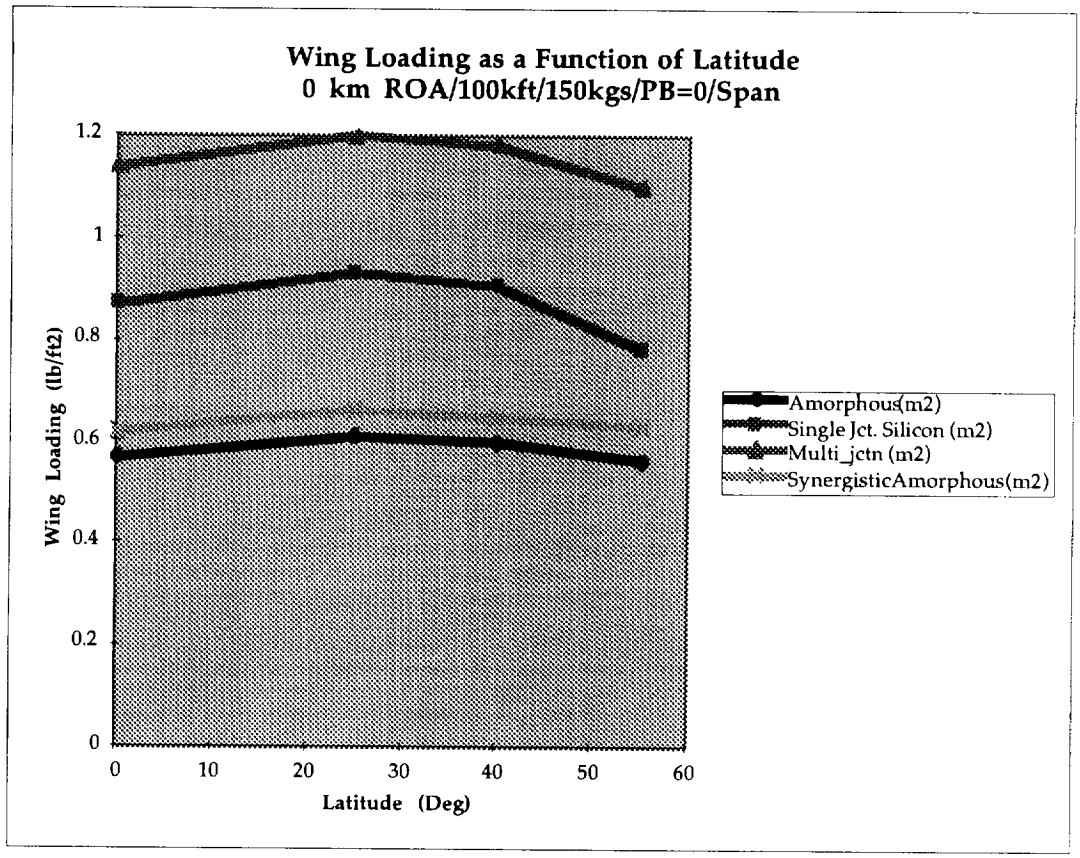

Figure 34 Effects of Latitude on Wing Loading (0 km ROA)

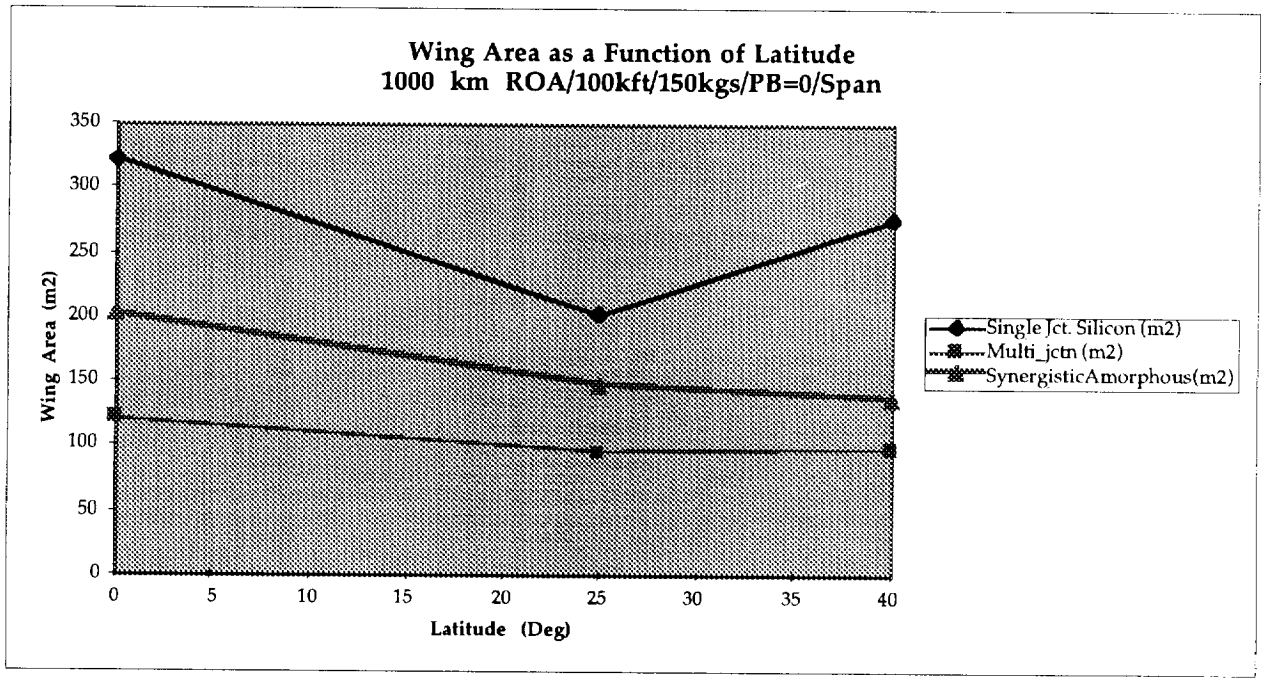

Figure 35 Effects of Latitude on Wing Area (1000 km ROA)

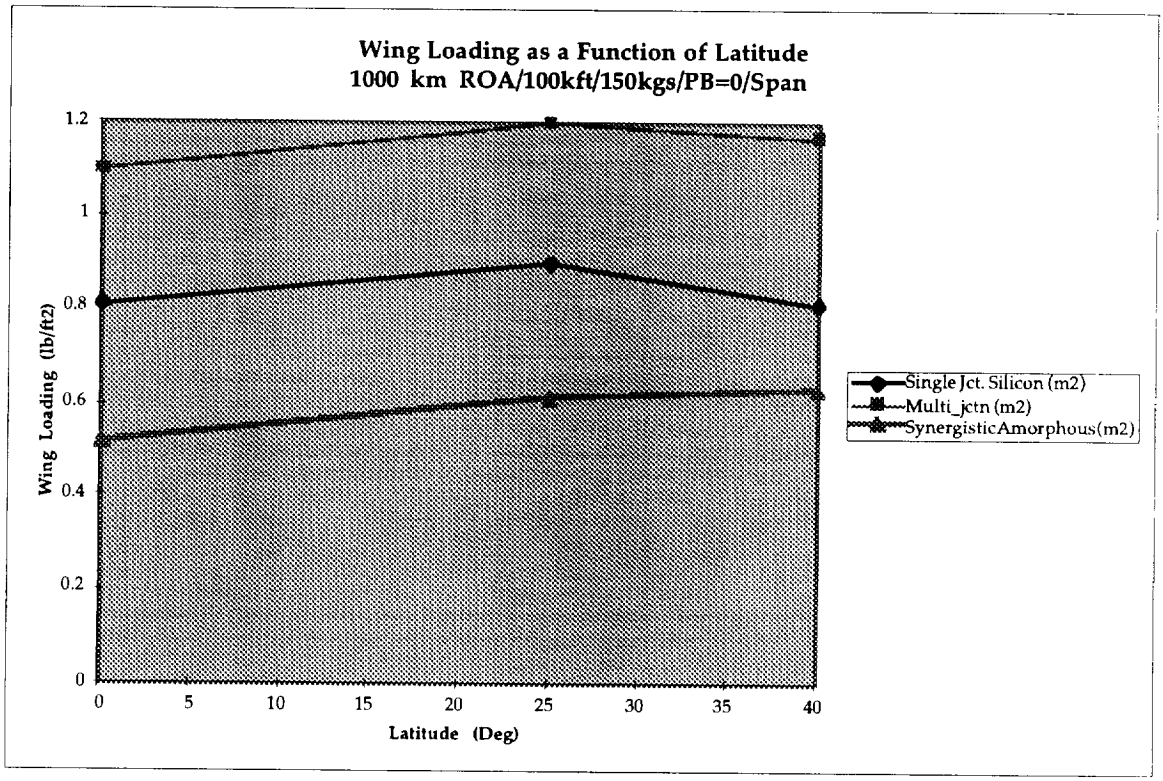

Figure 36 Effects of Latitude on Wing Loading (1000 km ROA)

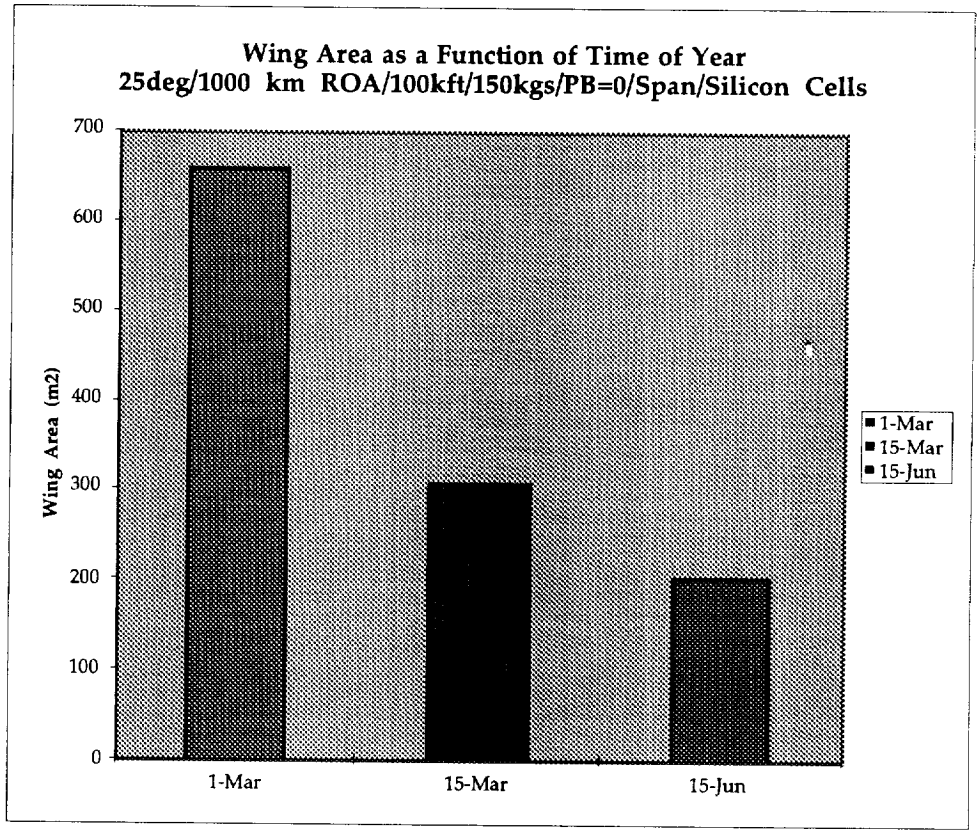

Figure 37 Effects of Time of Year on Wing Area (1000 km ROA)

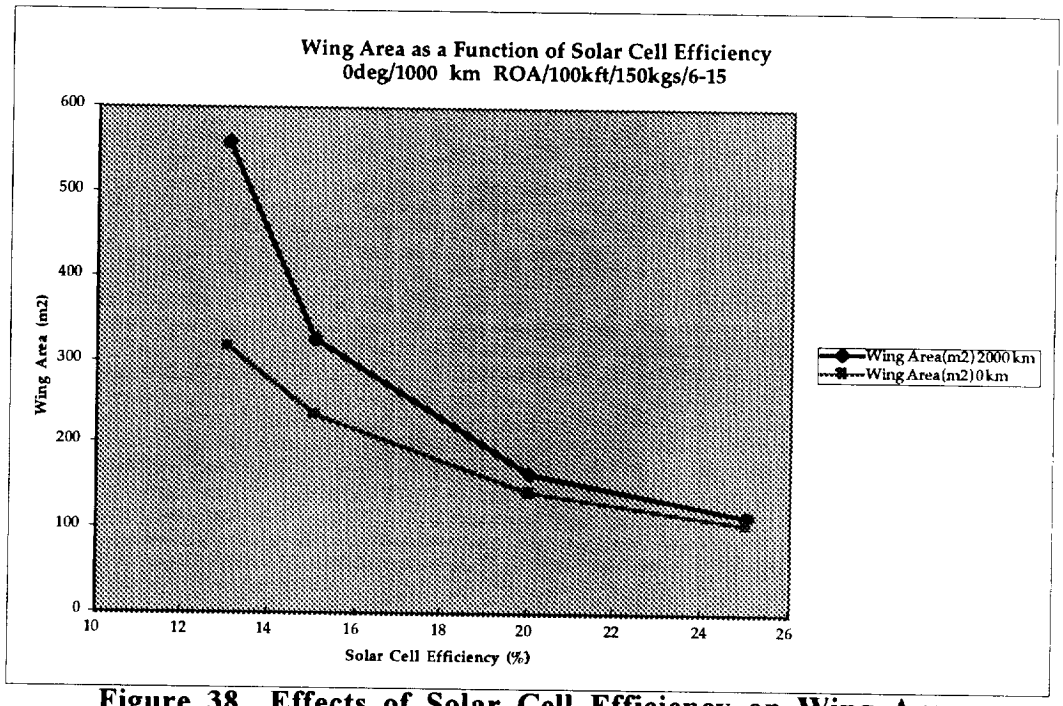

Figure 38 Effects of Solar Cell Efficiency on Wing Area

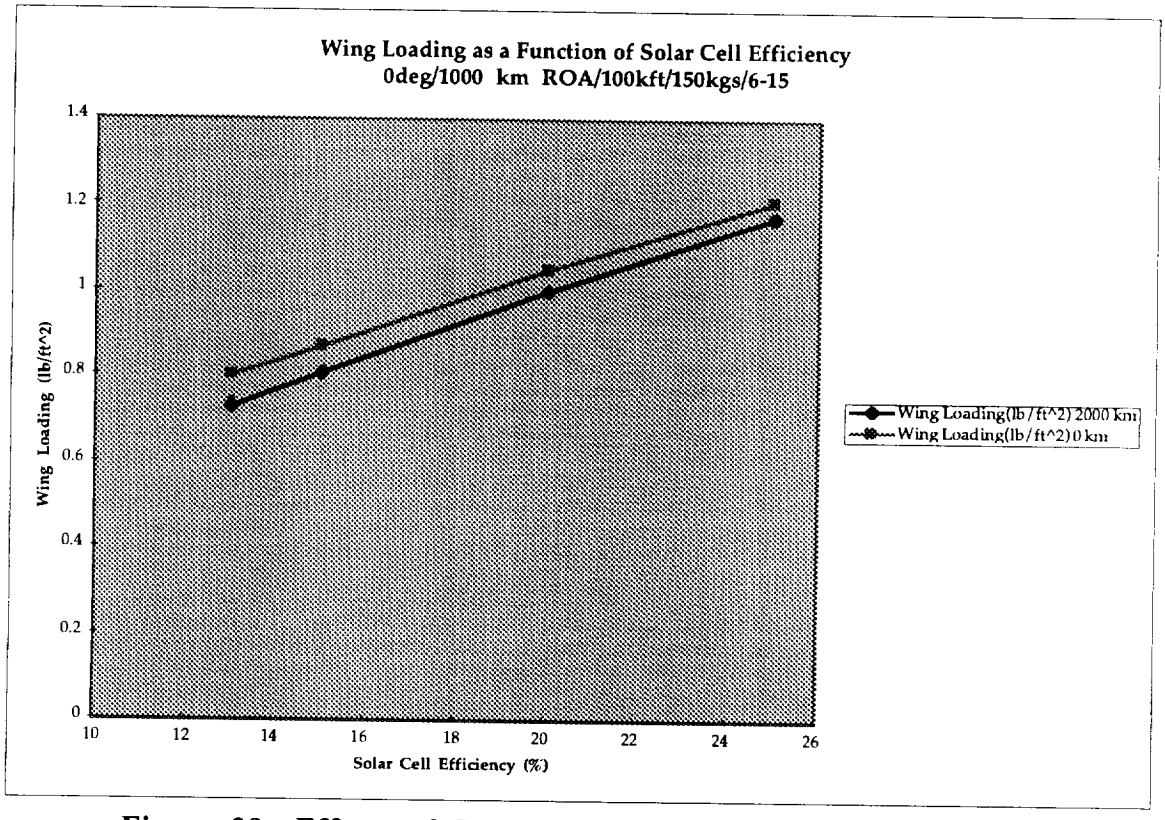

Figure 39 Effects of Solar Cell Efficiency on Wing Loading

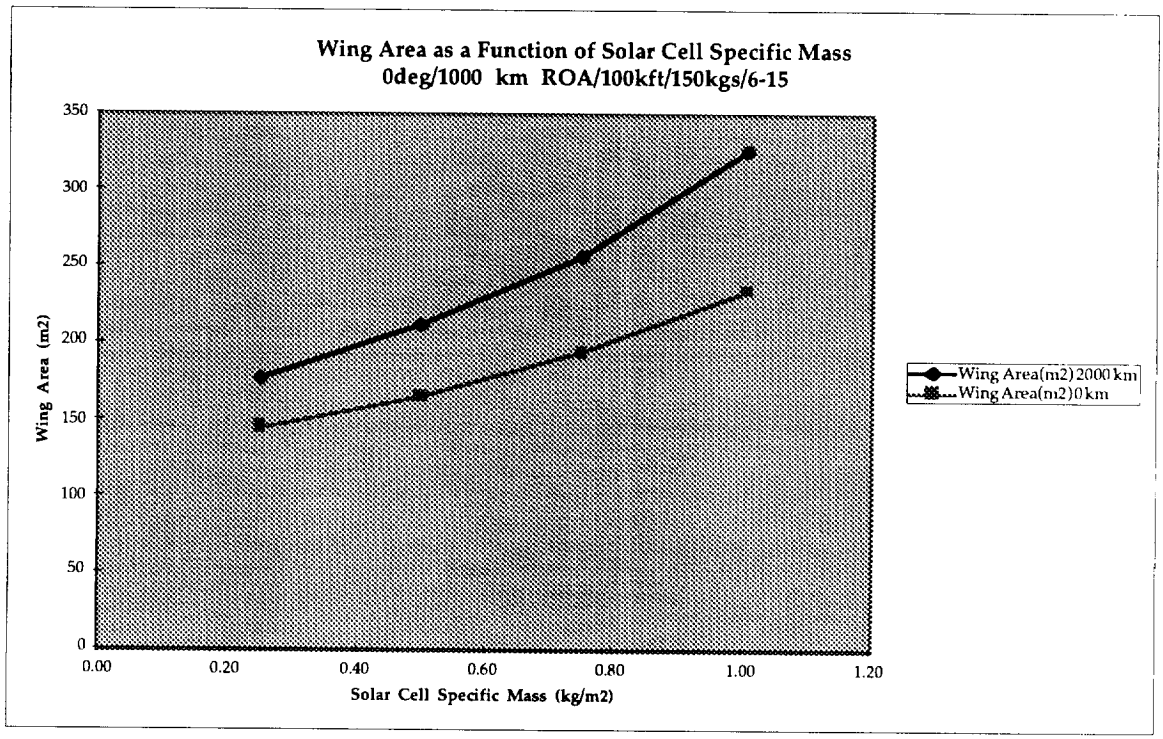

Figure 40 Effects of Solar Cell Specific Mass on Wing Area

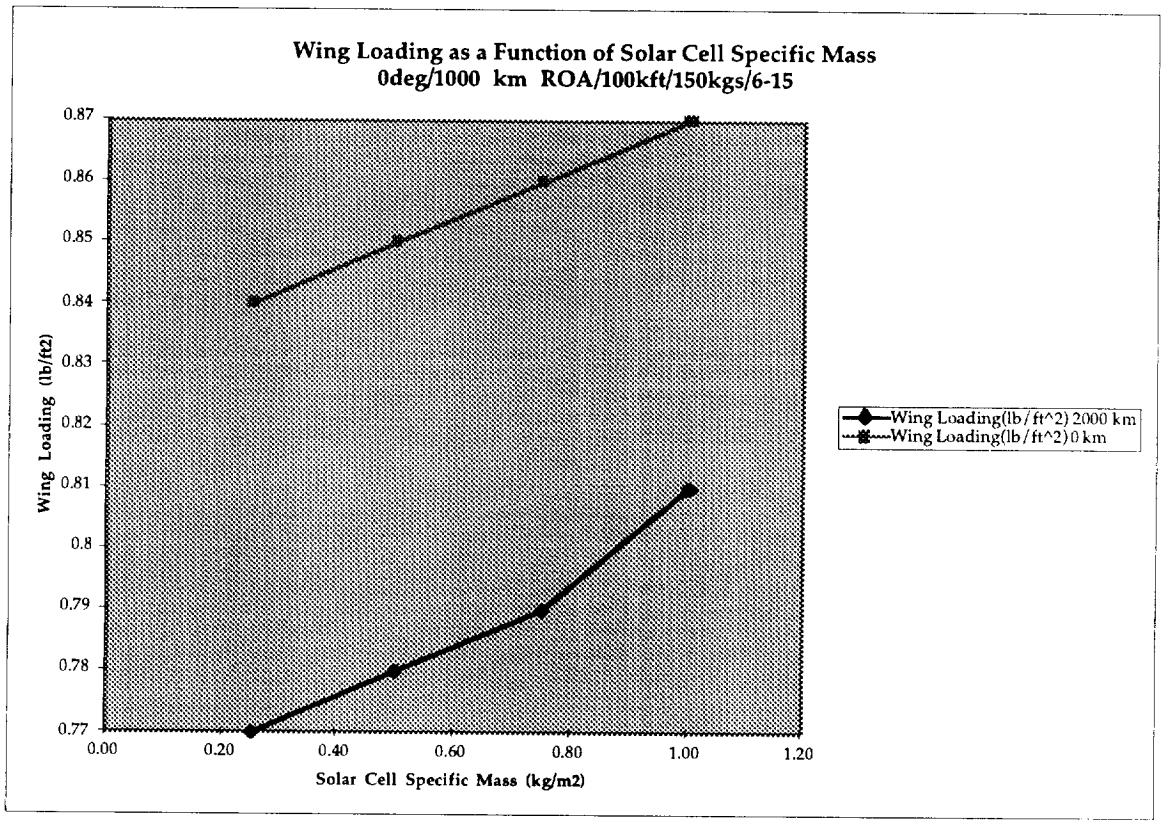

Figure 41 Effects of Solar Cell Specific Mass on Wing Loading

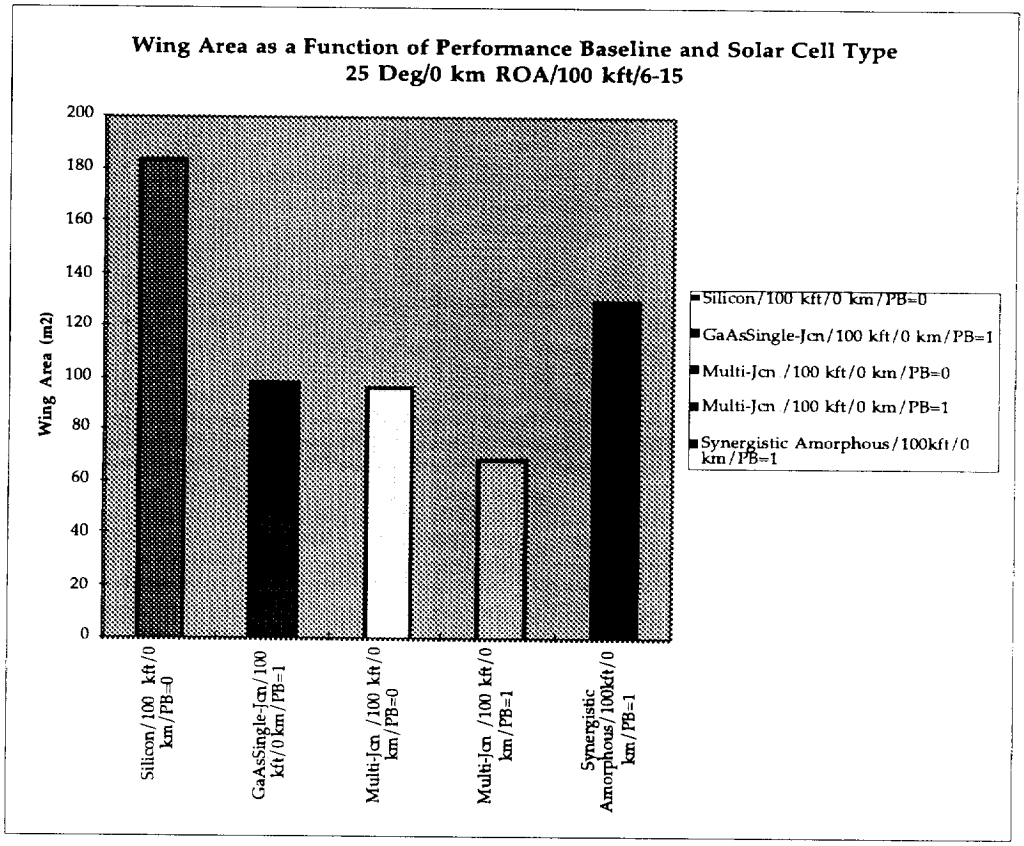

Figure 42 Effects of Performance Baseline on Wing Area (0 km ROA)

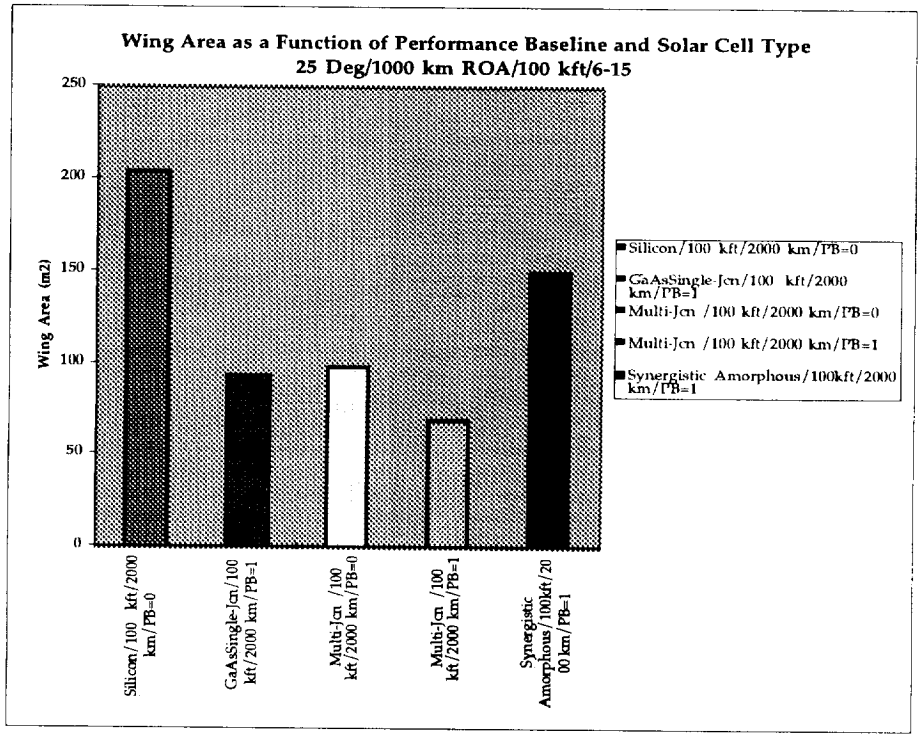

Figure 43 Effects of Performance Baseline on Wing Area (1000 km ROA)

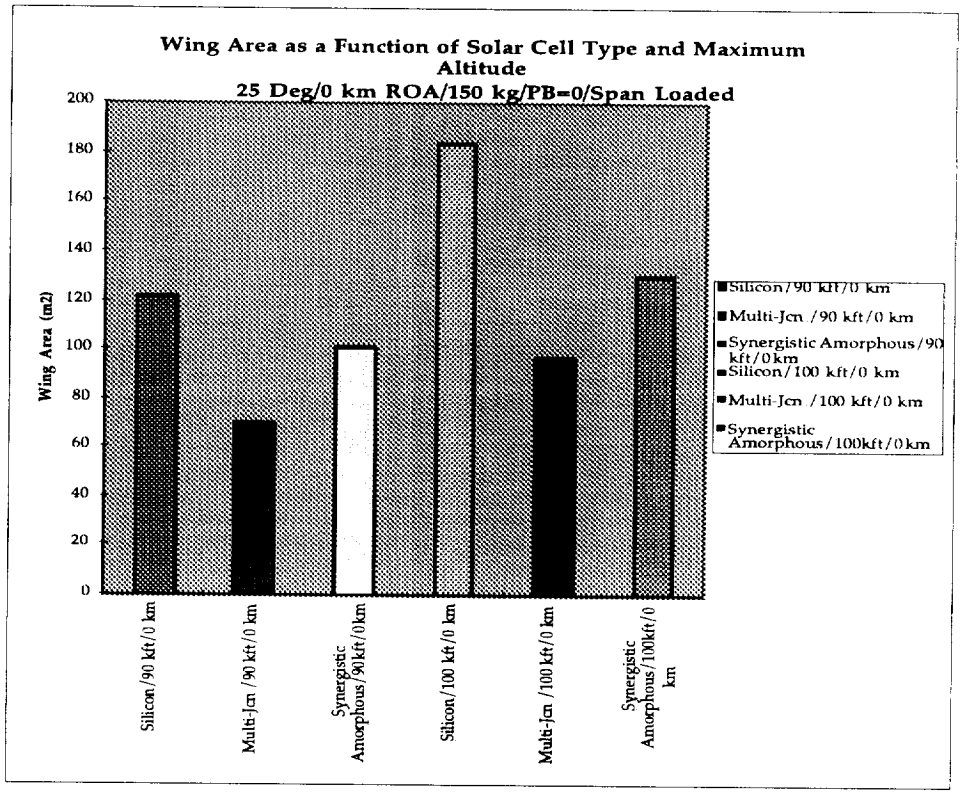

Figure 44 Effects of Maximum Altitude on Wing Area (0 km ROA)

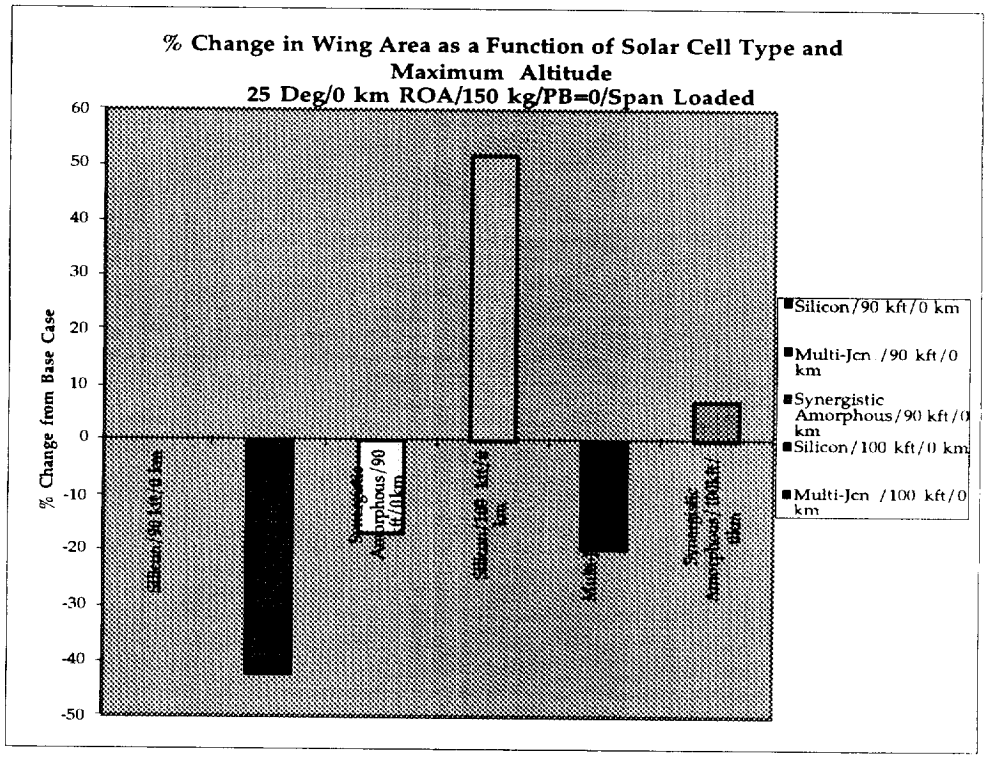

Figure 45 % Change from Baseline as a function of Solar Cell Type on Wing Area (0 km ROA)

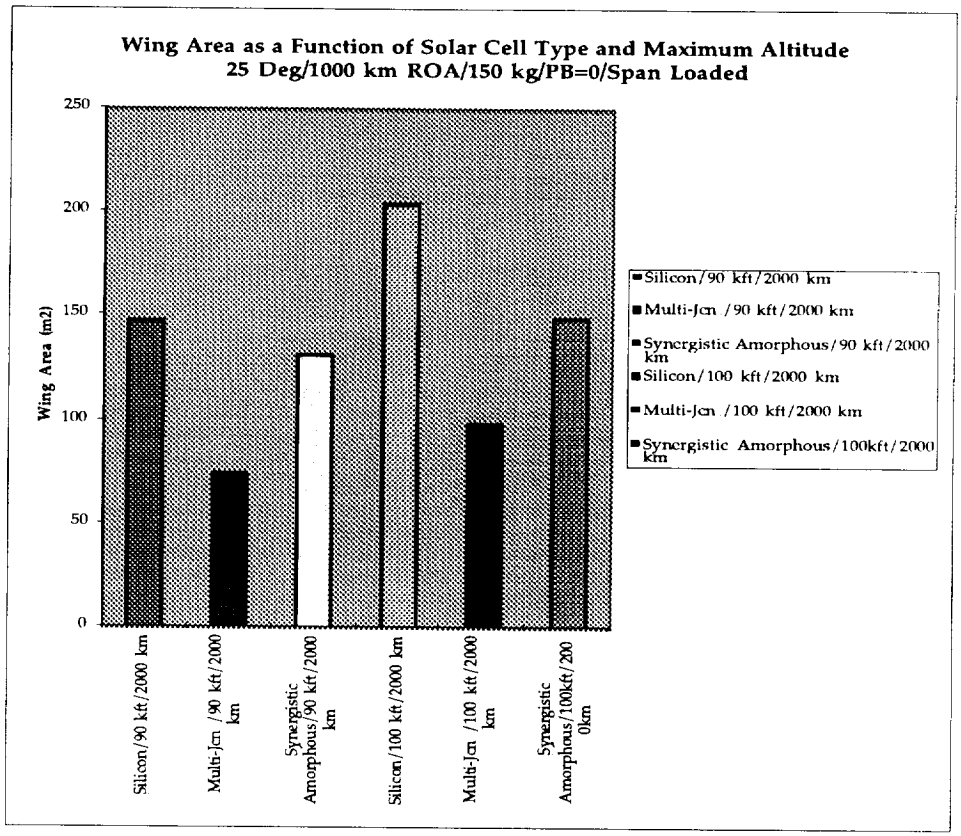

Figure 46 Effects of Solar Cell Type on Wing Area (1000 km ROA)

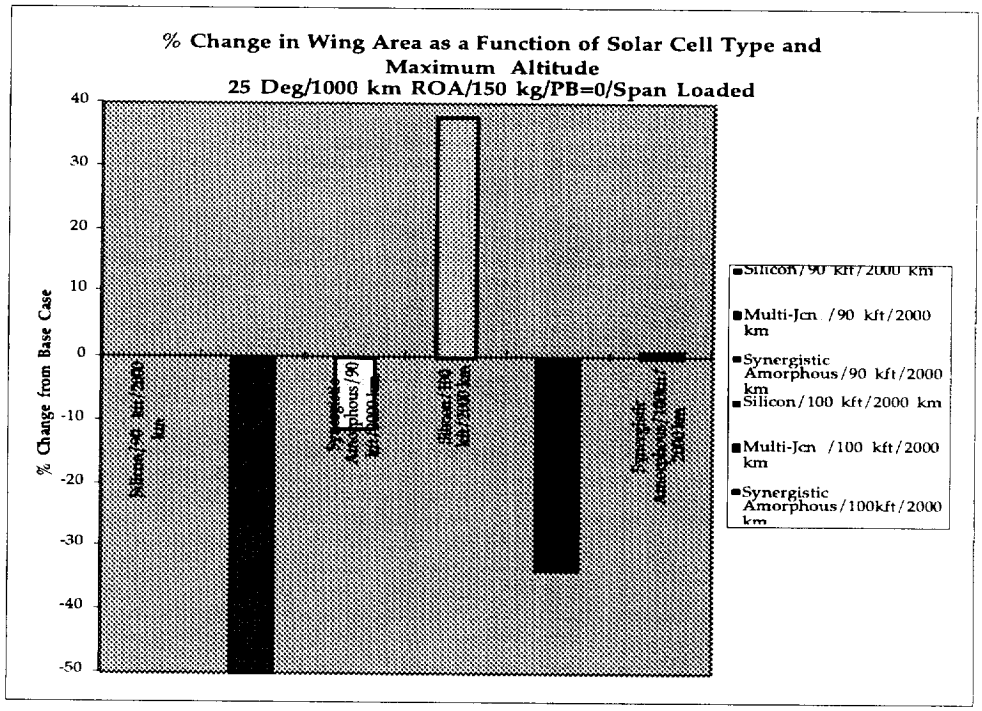

Figure 47 % Change from Baseline as a function of Solar Cell Type on Wing Area (1000 km ROA)

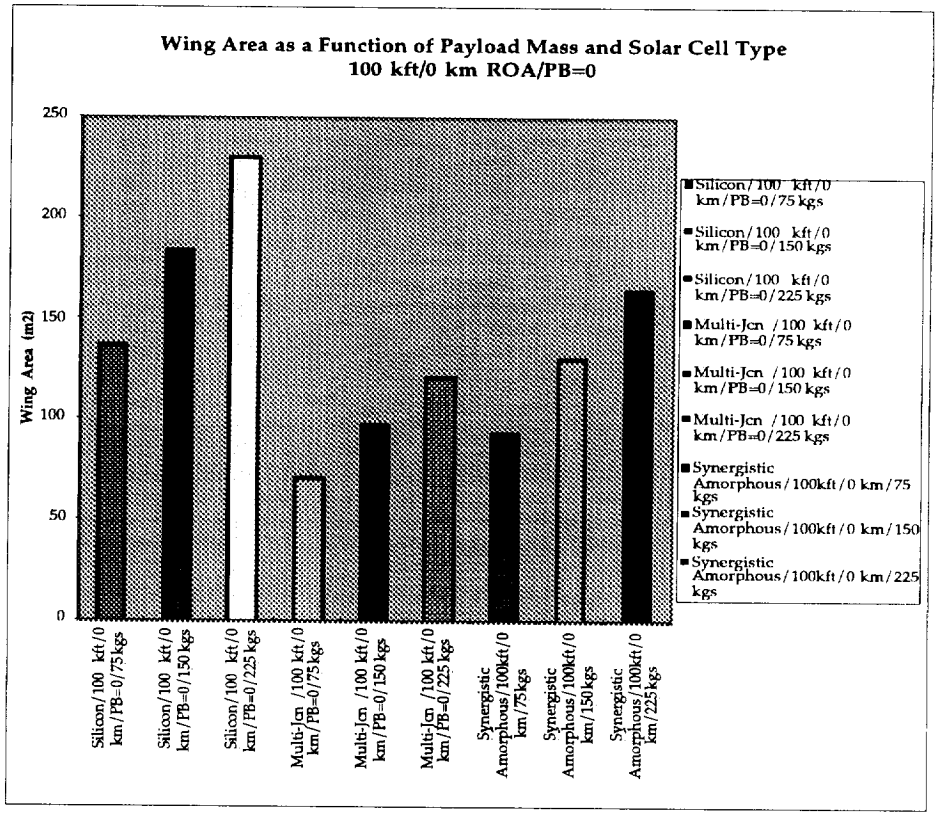

Figure 48 Payload Mass and Solar Cell Effect on Wing Area (0 km ROA)

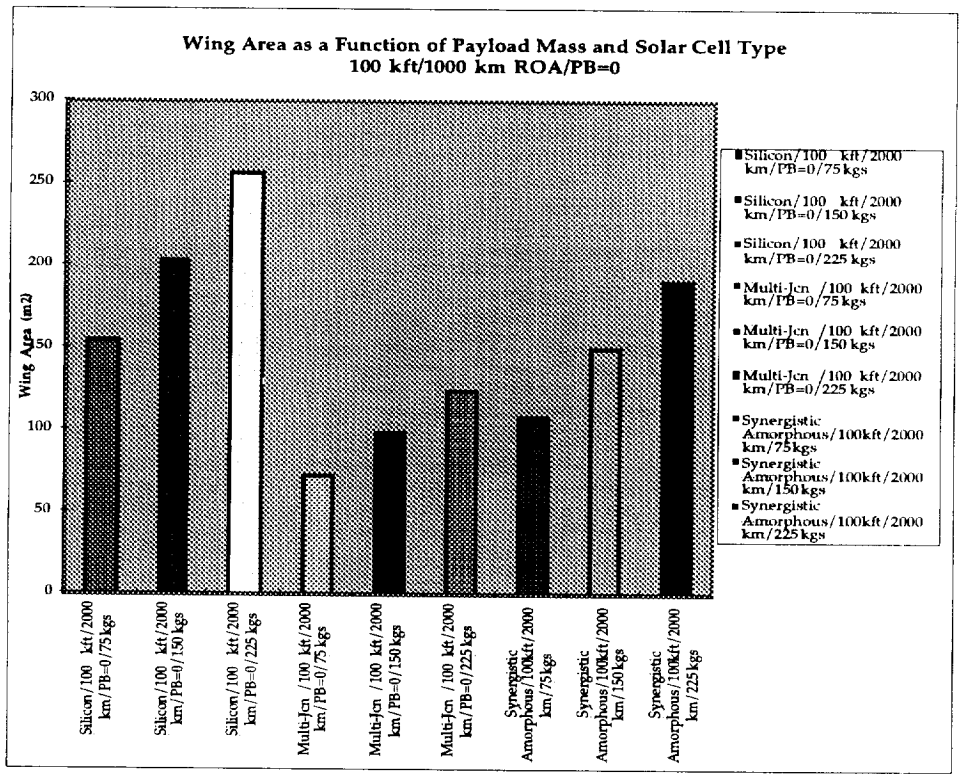

Figure 49 Payload Mass and Solar Cell Effect on Wing Area (1000 km ROA)

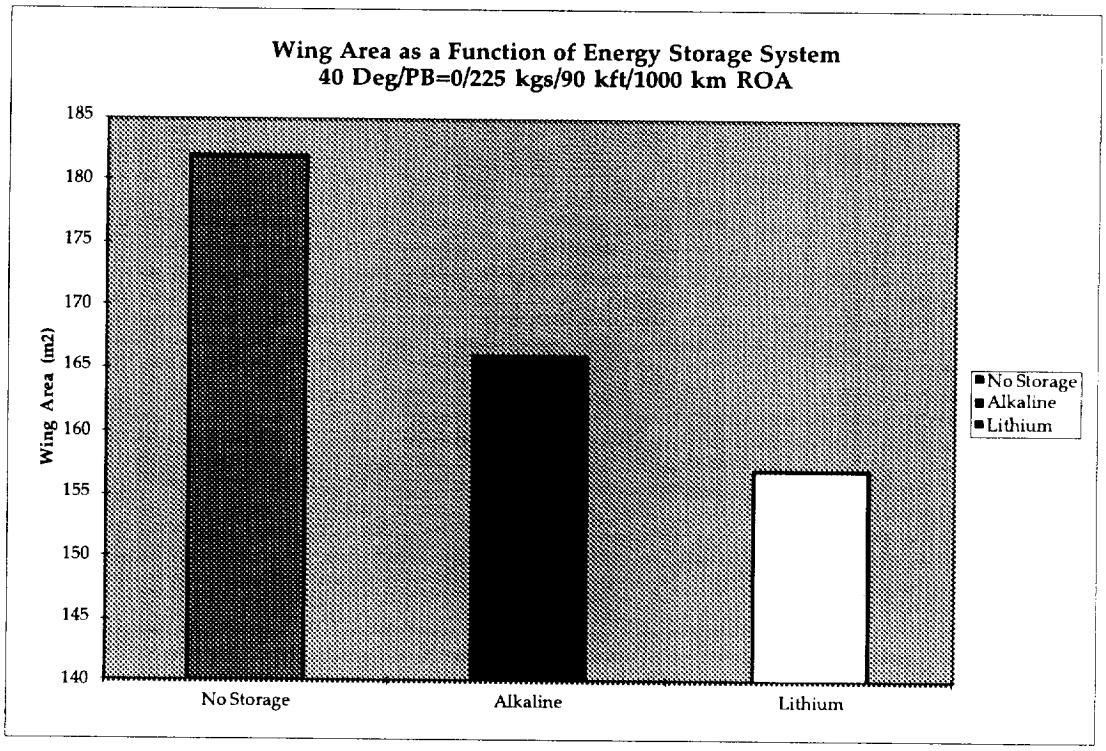

Figure 50 Energy Storage Selection Effect on Wing Area (1000 km ROA)

**********Solar Aircraft Analysis Code(SAAC)**********

Mission Date at Take-off	6\15	
Mission Duration (days)	0.00	
Latitude (deg)	40.00	
Maximum Altitude (km)	27.44	
Minimum Time Duration at Max. Altitude (hrs)	0.58	
Minimum Radius of Action (km)	1000.00	
Payload Mass (kg)	225.00	
Payload Power (W)	0.00	

XXXXXXXXXXXXXX Airframe Output Data XXXXXXXXXXXXXX

Airframe Type:	Span Loaded	
Wing Area	157.00	m^2
Wing Span	56.04	meters
Wing Aspect Ratio	20.00	
Wing Loading	1.09	lb/ft^2
Propeller Type :	Fixed Pitch	
Propeller Efficiency (%)	85.000	
Propeller Diameter (m)	4.40	
Propeller Blade Aspect Ratio	14.00	

XXXXXXXXXXXXXX Power Subsystem XXXXXXXXXXXXXX

Drivetrain Performance Baseline:		1997	
Solar Cell Type : Single Junction			
Solar Cell Efficiency (%)		15.000	
Solar Cell Specific Mass (kg/sq m)		1.005	
Solar Cell Approximate Cost (1997 $)		$ 3.3 Million	
Type of Energy Storage System :		Nonrechargeable LiSOCl	
Energy Storage System Efficiency(%)		90.0000	
Motor Type : Induction Motor			
Motor Efficiency (%)		95.000	
Power Conditioning Efficiency (%)		95.000	
Electrical Power Generated at Mid-Day		20099.29	
Engine Mass (kg)		41.72	kg
Propeller Mass (kg)		39.39	kg
Solar Cell Mass (kg)		157.79	kg
Fuselage Mass (kg)		51.62	kg
Spar Mass	85.55 kg		
Rib Mass	11.52 kg		
Leading Edge Mass	64.52 kg		
Trailing Edge Mass	11.06 kg		
Control Mass	10.55 kg		
Covering Mass	89.47 kg		

Total Wing Mass		272.68	kg
Boom Mass		0.00	kg
Tail Mass (kg)		37.86	kg
Payload Mass		225.00	kg
Energy Storage System Mass (kg)		5.50	kg
Total Mass		832.00	kg
Energy Storage System Volume		2.20	l
Energy Storage System Spec. Energy		363.64	W-h/kg
Energy Storage System Energy Dens.		909.09	Wh/l
Energy Storage System Discharge Time		0.00	hrs
Energy Storage System Re-charge Time		0.00	hrs
Total Energy Available for Discharge		2000.00	W-hr
Total Energy Available for Re-charge		0.00	W-hr
Wing Area		157.00	m^2
Wing Span		56.04	meters
TakeOff Time		5.20	hours

Table 33 SAAC Output for the Lithium Primary Cell Case

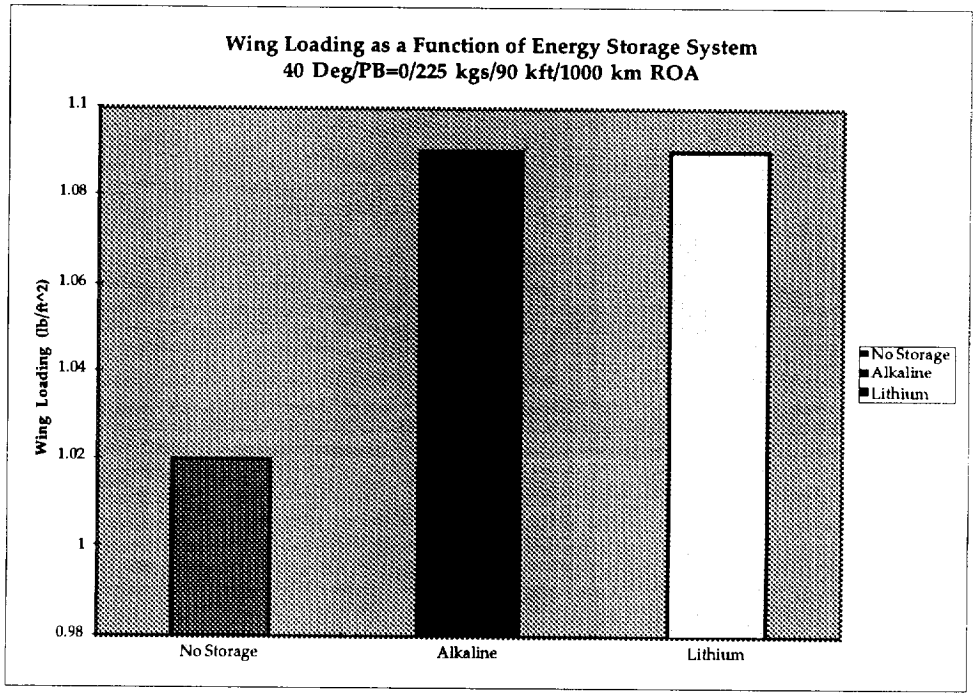

Figure 51 Energy Storage Selection Effect on Wing Loading (1000 km ROA)

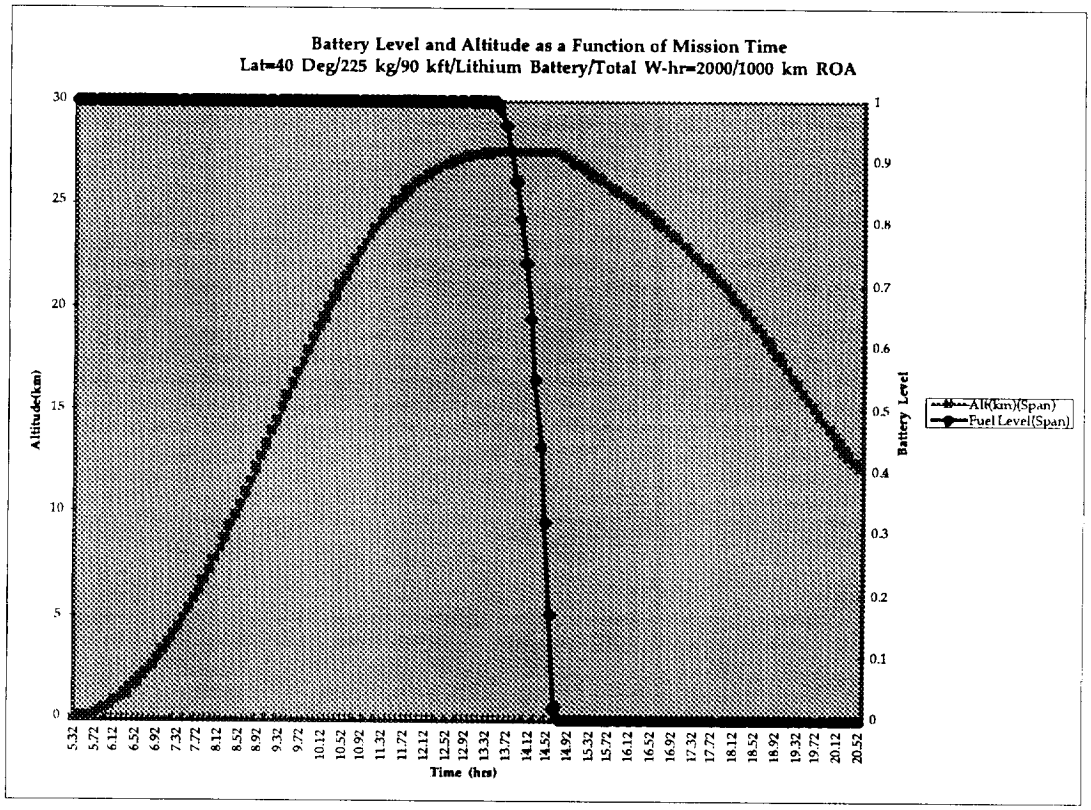

Figure 52 Battery Charge State and Altitude as a Function of Mission Time (1000 km ROA)

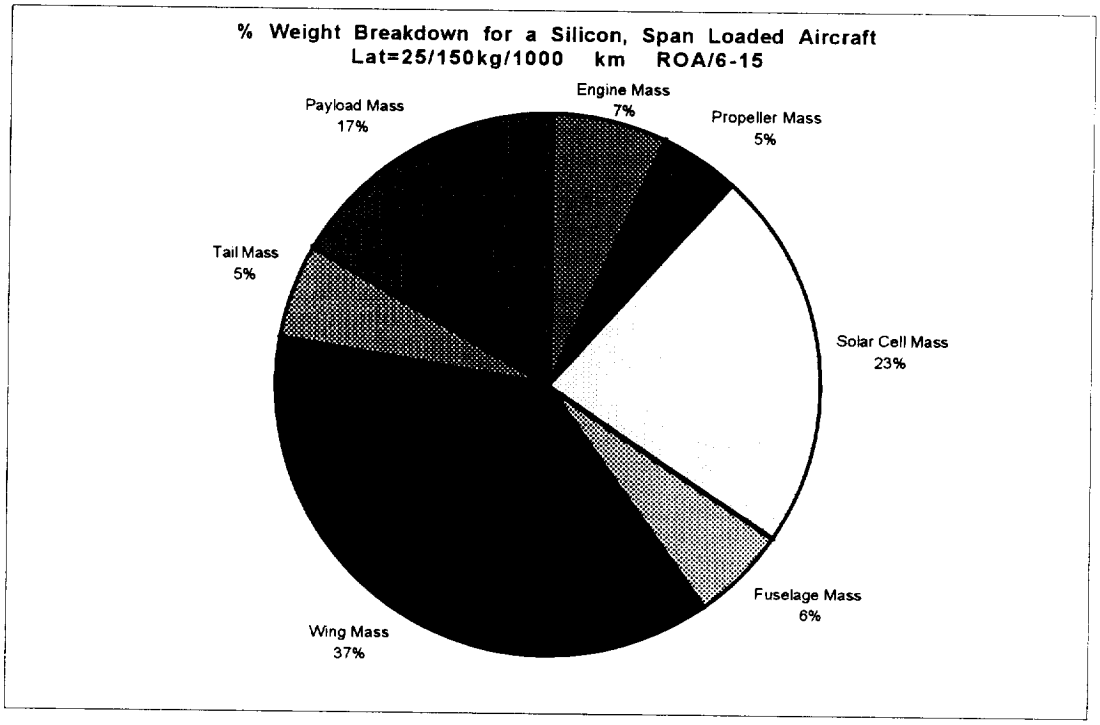

Figure 53 Weight Fraction Breakdown for a Single Junction 1997 Baseline Span Loaded Aircraft

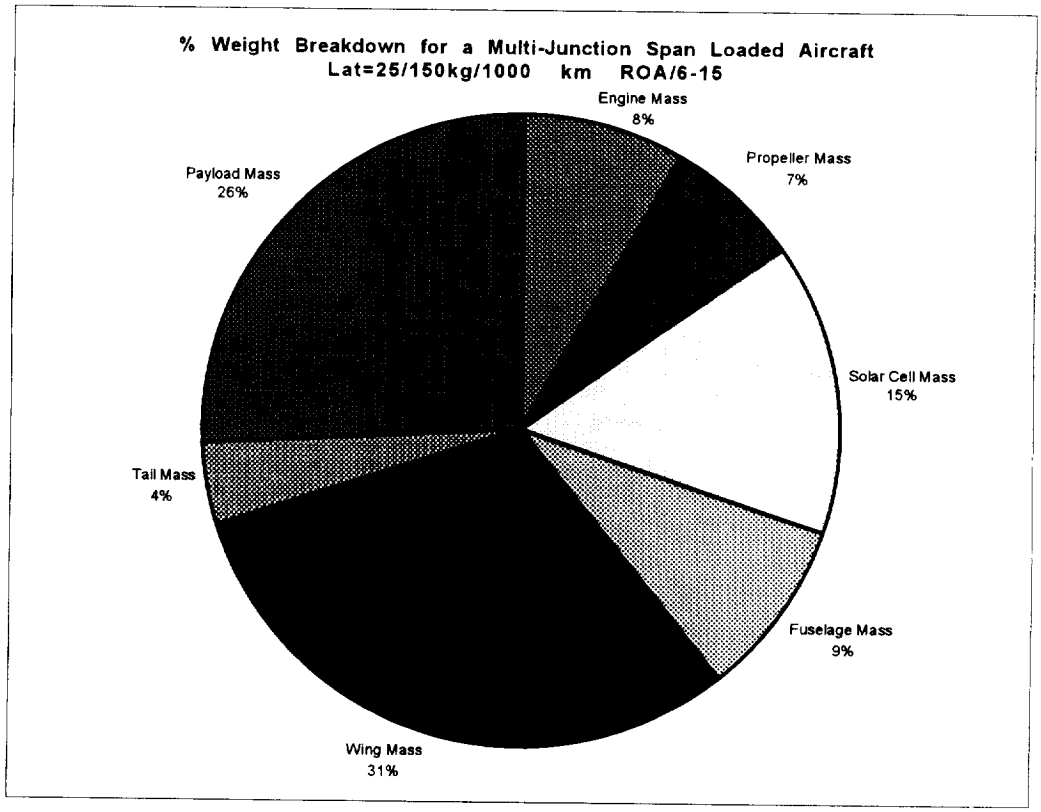

Figure 54 Weight Fraction Breakdown for a Multi-Junction 1997 Baseline Span Loaded Aircraft

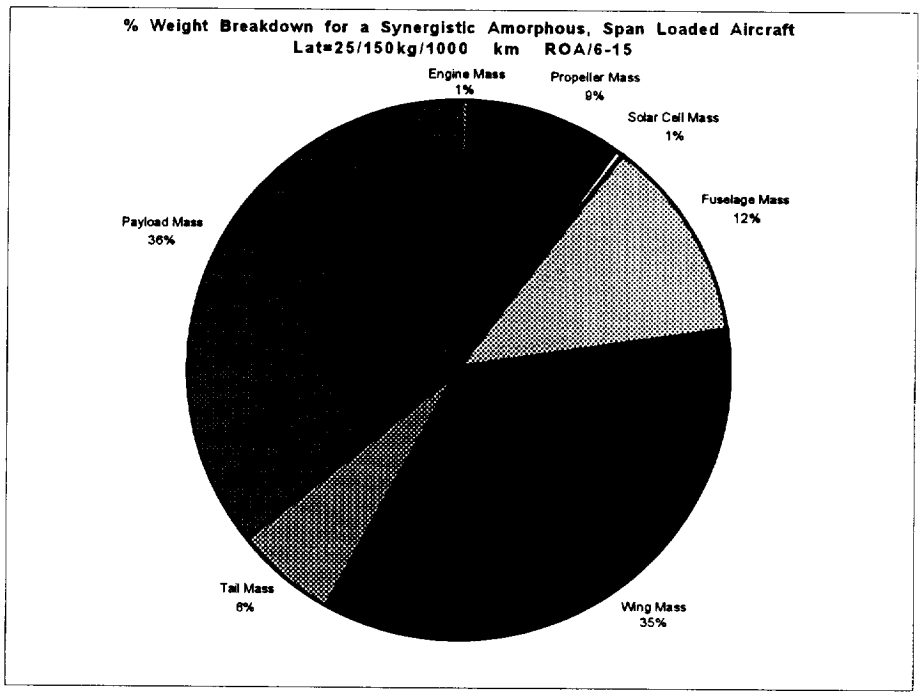

Figure 55 Weight Fraction Breakdown for a Synergistic Amorphous 1997 Baseline Span Loaded Aircraft

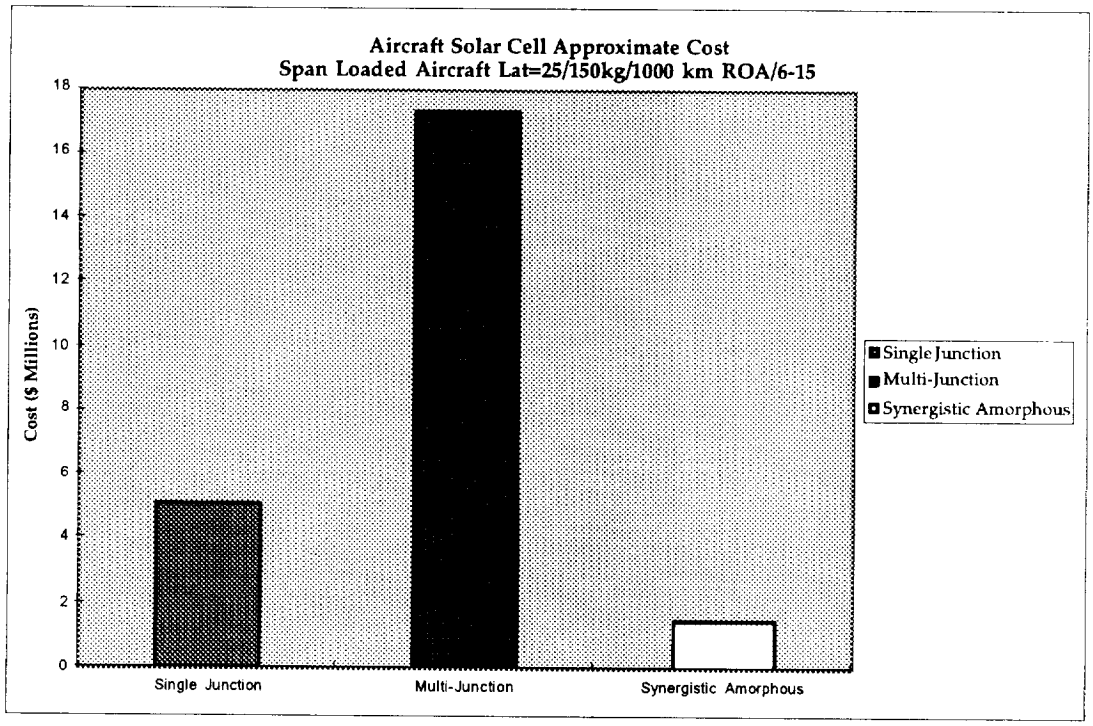

Figure 56 Approximate Cost Comparison of Airframes with Various Solar Cell Types

APPENDIX A: AIRFOIL SELECTION

To show the effects of airfoil choice on aircraft size, three separate airfoils were used in this study. The airfoil data was provided by NASA Ames Research Center. Two of these airfoils were chosen for their ability to demonstrate the tradeoffs between an airfoil with a small pitching moment, requiring a small tail but with poorer performance at low Reynolds numbers versus an airfoil with a large pitching moment requiring a large (and boomed) tail with better low Reynolds number performance. Both the Twin-Boom and the Span loaded aircraft are considered span loaded. The difference in the simulation is that the pitching moment is compensated by a long tail in the twin-boom aircraft and the pitching moment is compensated on the span loaded aircraft by a tail just aft of the wing. This is the basic trade explored for the twin boom versus span loaded aircraft part of the study.

The airfoil chosen for the span loaded aircraft (corresponding to the low pitching moment airfoil) is the Liebeck L1003 20% thick airfoil. Figure 57 shows the basic airfoil geometry used for calculating surface area of the airfoil. Figure 58 shows the Power Factor vs. Cl lines for the airfoil along with the operating line chosen for this airfoil to maximize power factor. Figure 59 and 60 show the regressions and plot of Cl and Cd as a function of Reynolds number for this operating line.

A Wortman FX63, 13.7 % thick airfoil was used for the twin-boom aircraft. It has a much high pitching moment than the Liebeck (about -.12 vs. -.04) but it has better low Reynolds number Cd and Cl performance. Figures 61, 62, and 63 show the power factor, lift, and drag correlation's used for this study.

The Clark Y 5.9% thick airfoil was chosen for the tail section of both the span loaded and twin boom aircraft. Its operation is based on compensating the pitching moment generated by the primary airfoil. Therefore once the moment of the primary airfoil is generated the tail section must compensate for it by exerting an equal and opposite force. Based on the necessary Cl of the airfoil, an interpolation is performed between the Cl vs. Cdprofile at a Cl of 0 and a Cl vs. Cdprofile at a Cl of .45. This provides the profile drag of the airfoil. Figures 64, 65, and 66 show the power factor plot, and the Lift and Drag profiles of the airfoil.

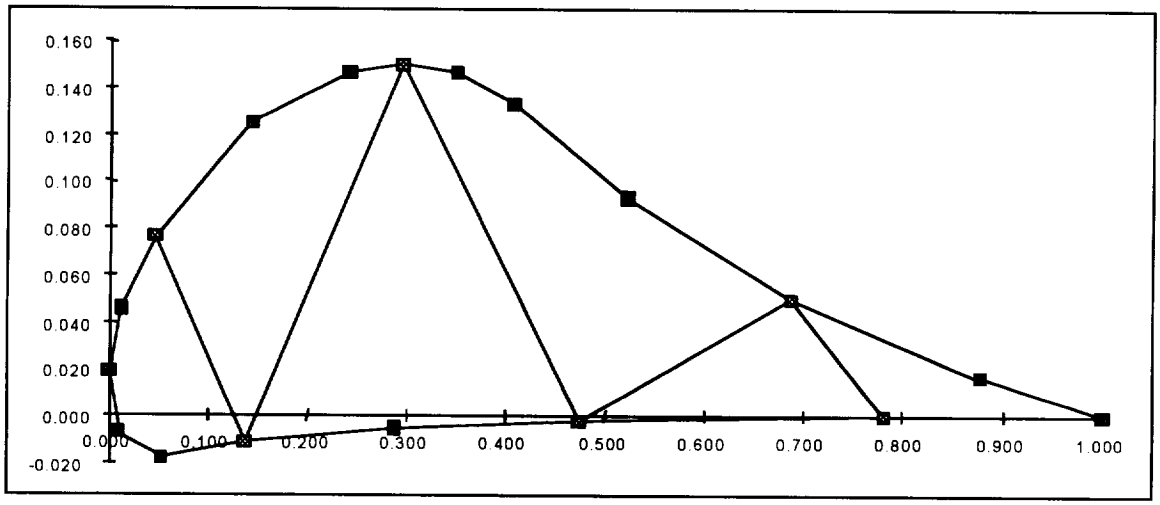

Figure 57 Airfoil Profile for the Liebeck 1003

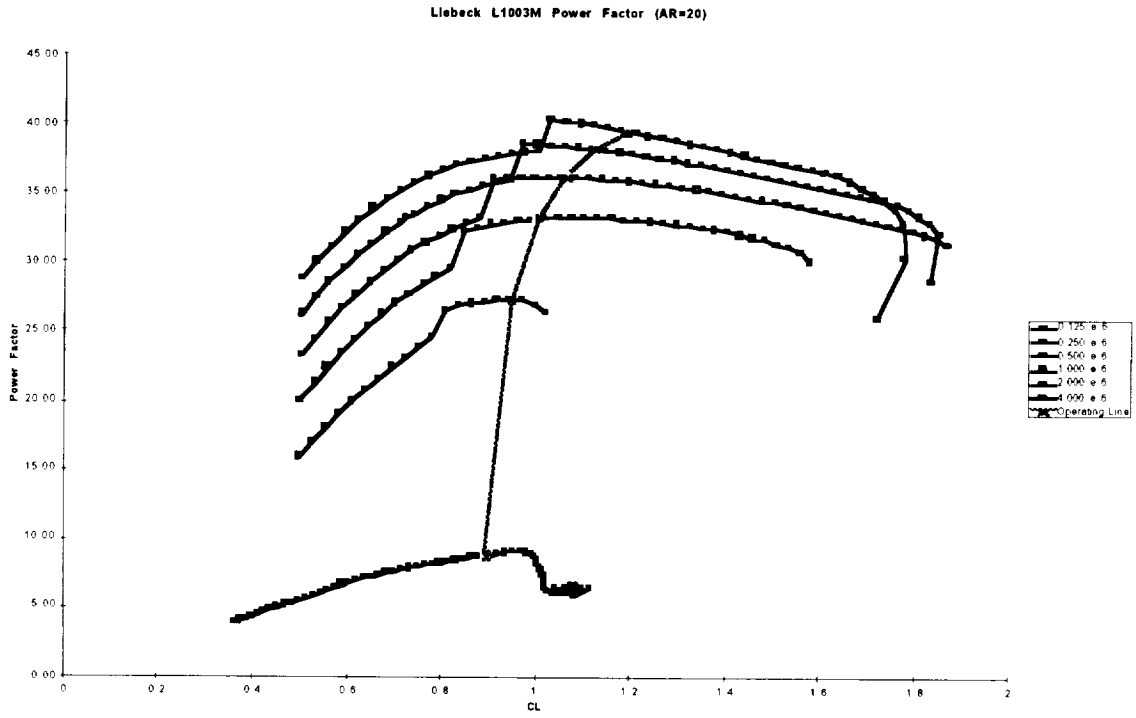

Figure 58 Power Factor as a Function of Cl for the Liebeck L1003M

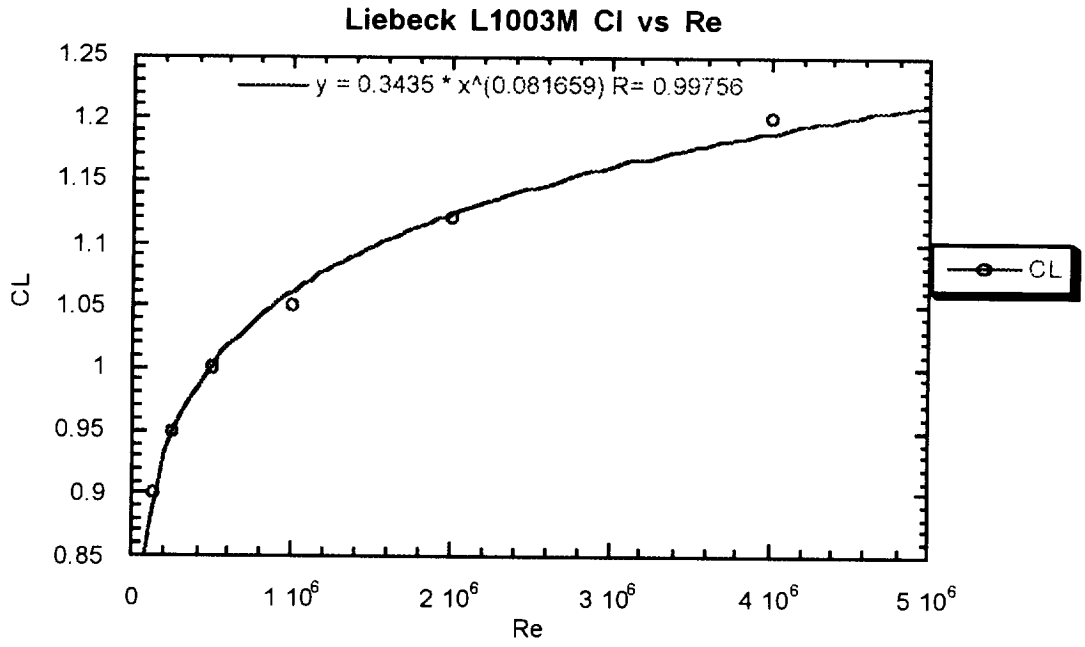

Figure 59 Cl vs Reynolds Number for the Liebeck L1003M

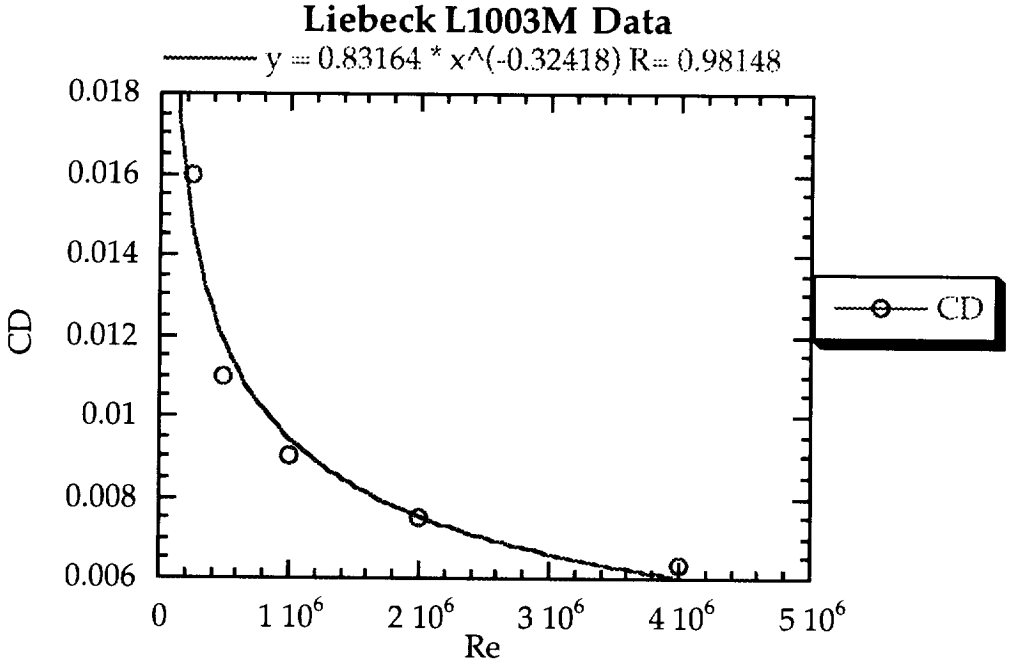

Figure 60 Cd vs Reynolds Number for the Liebeck L1003M

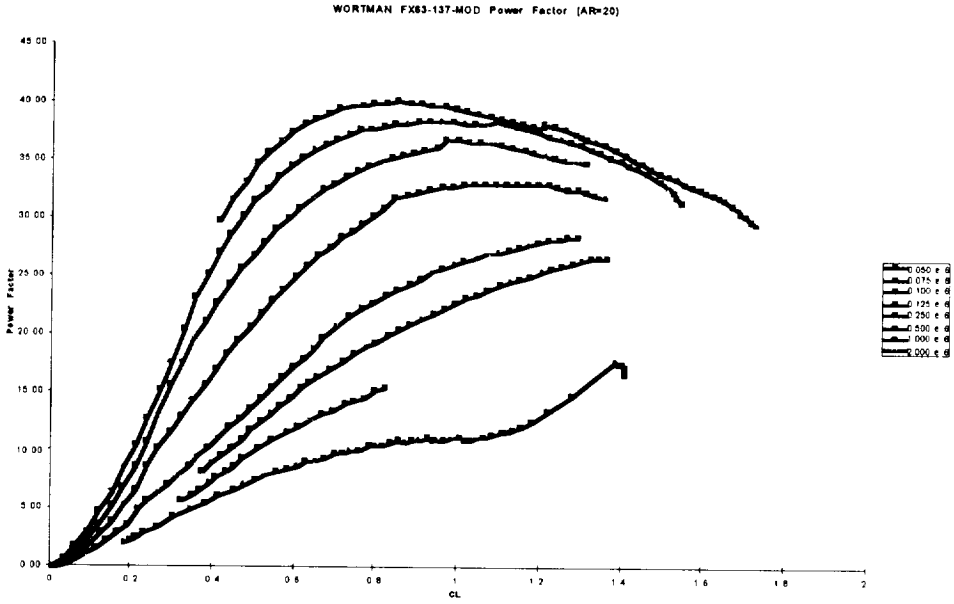

Figure 61 Power Factor for the Wortman FX-63-137-mod

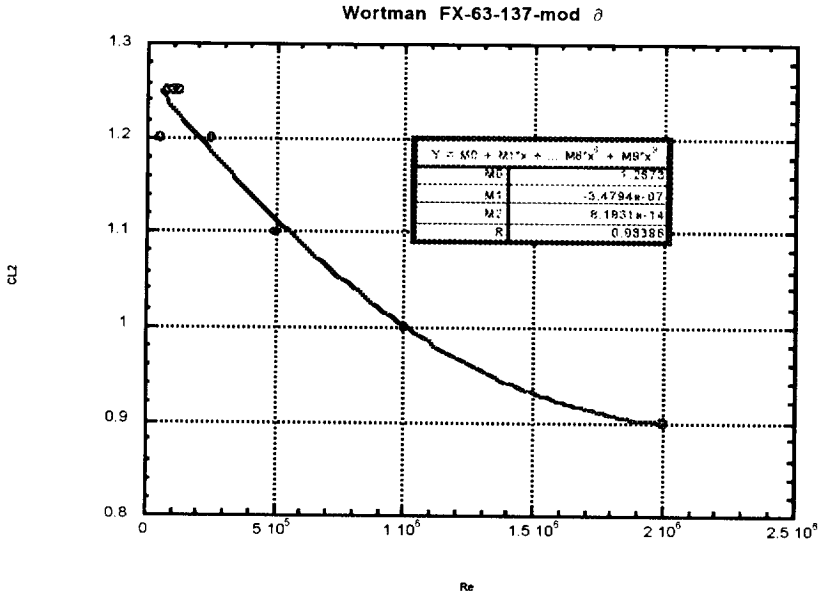

Figure 62 Cl as a Function of Reynolds # for the Wortman FX-63-137-mod

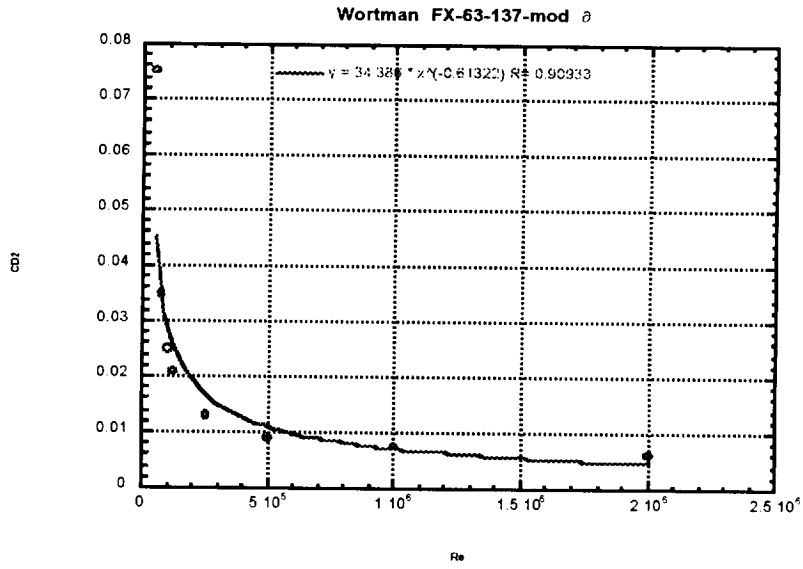

Figure 63 Cd as a Function of Reynolds # for the Wortman FX-63-137-mod

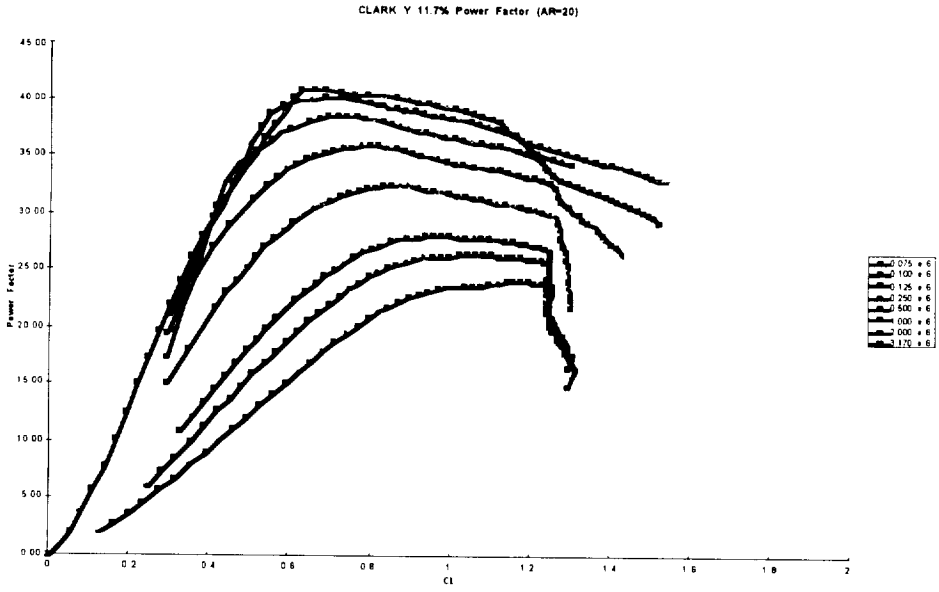

Figure 64 Power Factor for the Clark Y

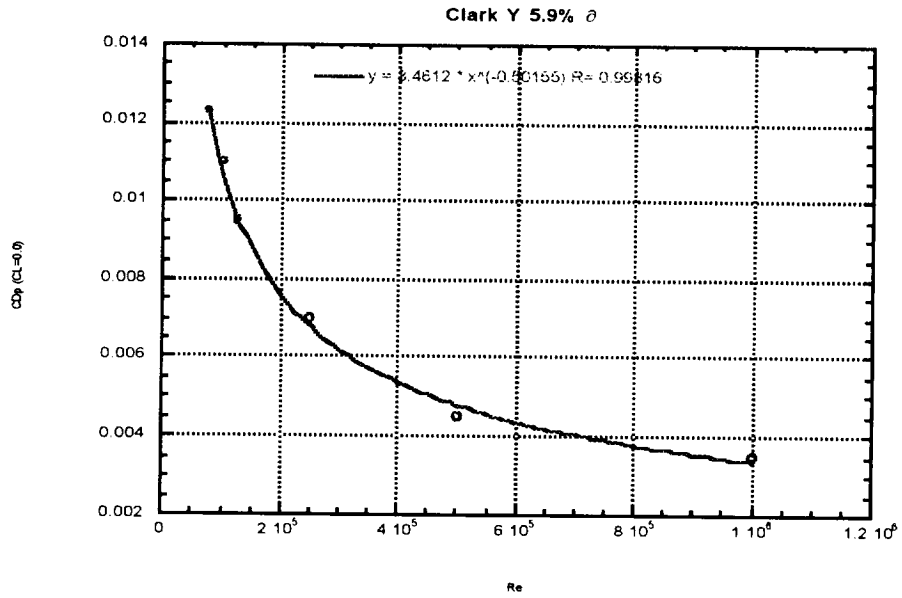

Figure 65 Cd(Cl=0.0) as a Function of Reynolds # for the Clark Y 5.9%

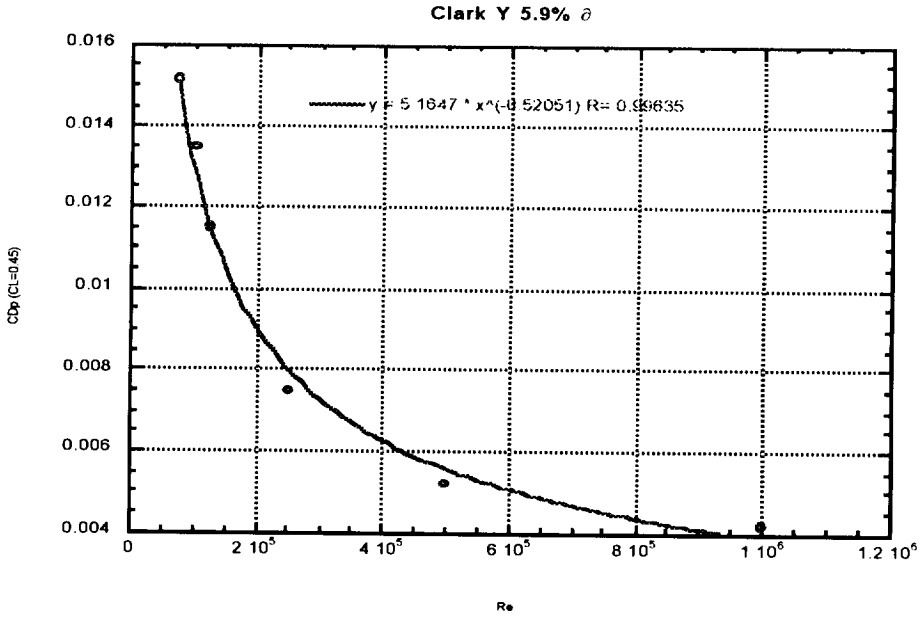

Figure 66 Cd(Cl=.45) as a Function of Reynolds # for the Clark Y 5.9%

APPENDIX B: FLYWHEELS

Energy Storage Rotors

The flywheel rotor stores energy by the rotation of the rotor. The amount of energy stored is proportional to the mass of the rotor, the square of its radius, and the square of the speed of its rotation. Ideally, it is desirable to spin a small rotor at very high speeds, because this maximizes specific energy and minimizes momentum. Practically, the strength of rotor material, the maximum speed capability of the motor/generator, aerodynamic drag, and bearing losses all establish upper limits on the maximum operating speed. For a hollow ring or cylinder (which is representative of an ideal flywheel system) the polar moment of inertia is given by:

$$I=\frac{1}{2}m\left[\left(r_o^2-r_i^2\right)\right]$$

where:

m= mass of the rotor

r_0 = outside radius of the rotor

r_i = inside radius of the rotor

The kinetic energy, E_k, stored in a flywheel is given by the relationship

$$E_k=\frac{1}{2}I\omega^2$$

where:

ω is the angular frequency

The ratio of stored energy to mass is called the specific energy of the flywheel, and the ratio of stored energy to volume is called the energy density. The theoretical maximum specific energy of a candidate flywheel rotor material can be calculated if the maximum strength and density of the material are known. This maximum specific energy is derived from the hoop stress equation and is given by the following:

$$\frac{E_k}{m}=\frac{1}{2}\frac{\sigma}{\rho}$$

where

σ is the material strength

ρ is the material density.

Because all real rotors have some size to them, much of their material is placed away from the outer surface, where it stores less energy than it is theoretically capable of. Therefore, all real flywheels will always have lower specific energy than predicted by this equation. This equation given above is useful when comparing various materials for their potential to flywheel energy storage systems.

Momentum Storage in a Flywheel

The angular momentum, of a rotating body is equal to:

$M=I\omega$

Conservation of momentum of a rotating flywheel tends to maintain the orientation of the axis of spin. If a torque is applied such that it would tend to change the orientation of this axis, conservation of momentum results in another torque acting 90 degrees away from the applied torque, and in the plane of the axis of spin. This phenomenon is called the "gyroscopic effect" and it can produce substantial torque. For aircraft and vehicular flywheels, it is desirable to minimize the momentum of the spinning rotor in order to minimize the gyroscopic effect and its potential effects on vehicle handling.

Specific energy can be maximized and momentum can be minimized by spinning a small rotor, made from a lightweight but strong material, at very high speeds.

Power

The power for a rotating systems is defined by:

$$P=T\omega$$

where:

T is the torque applied by or applied to the motor/generator.

Assuming that the maximum torque of a flywheel's motor/generator at any particular speed is constant, the maximum power will increase in direct proportion to the maximum speed of the rotor. Operation at high speeds therefore increases the specific power and power density of electric motor/generators.

Synergistic Effects

One opportunity was explored for using the flywheel energy storage systems to not only function as an energy storage device but to also eliminate the aircraft control system. Currently, flywheels are under consideration to replace not only the battery energy storage

subsystem on spacecraft, but to also double as control systems for these spacecraft. By appropriate positioning and control of flywheels, a net torque can be placed on the spacecraft by a combination of spin up/spin-down of the flywheels used for energy storage. At most, this could eliminate the need for any control surfaces on the aircraft. The following correlation to estimate control mass for the solar aircraft:

$$Mass_{controls}(kg) = .3006 * \frac{S_W}{AR^{.5}}$$

where:
S_w is the wing area (m^2)
AR is the Aspect Ratio of the aircraft's Wing

Figure 10 shows control system mass as a function of aspect ratio for various aircraft wing areas. Previous studies have shown that for a 200 W-hr/kg energy storage system solar aircraft the total aircraft mass is about 1500 kg.[xxiii] This example shows that, at most the removal of the control system on the aircraft would change the total mass of the aircraft by about 3% to .3%.

Other possibilities for using the flywheels for a second function include using their structure, designed to contain a rotor failure, as part of the aircraft structure itself. Assuming that the energy storage requirements for the aircraft is 6 kW for a 12 hour dark period equates to a energy storage requirement of 72 kW-hr. Using the USFS energy density of 109 W-hr/Liter equates to 660 liters of volume or 23.3 ft^3 needed for energy storage.

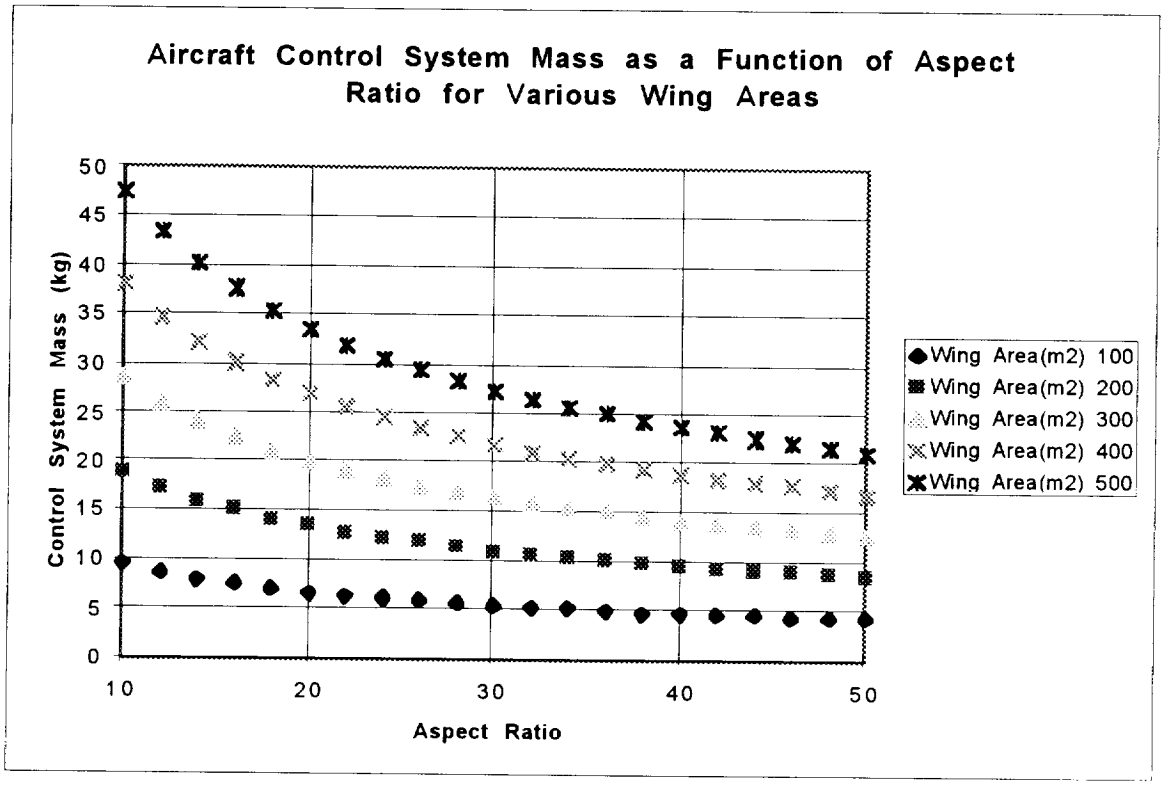

Figure 67 Aircraft Control System Mass vs. Aspect Ratio

[i] Brinker, D. Personal Communication, NASA Lewis Research Center, Solar Cell Research, August 1997.
[ii] Warshay, M. et al., "The NASA Fuel Cell Upgrade Program for the Space Shuttle Orbiter", August 1997, IECEC.
[iii] Power Computing Solutions, Inc. "Component Modules for PEM Fuel Cell System Conceptual Designs", NASA LeRC Contract C-79578-E, August 1997.
[iv] Pow, R., Reindle, M. Tillmetz, W., "1996 Fuel Cell Seminar Abstracts, pages 276-279, November 1997.
[v] Kohout, L., NASA Lewis Research Center, NASA TM 101980, June 1989.
[vi] Mockler T., Maldonado J., Schmitz, P. "A Triply Turbocharged Rotax 912 for High Altitude UAV, 1994, NASA Lewis Internal Document
[vii] McElroy, et al., NASA Space Electrochemical Research and Technology Conference Proceedings, 1991.
[viii] Ibid iii
[ix] California Air Resources Board, CARB Report on Electric Vehicle Batteries, 1995.
[x] Pellerin, Alain, "Are You Talking Batteries", Electric & Hybrid Vehicle Technology '96, pages 68-75.
[xi] Green, Robert, Personal Communiction, NASA Lewis Research Center, March 1997.
[xii] Raymond Beach, NASA Lewis Research Center Flywheel Contact.
[xiii] "An Assessment of Flywheel Energy Storage Technology for Hybrid and Electric Vehicles", Abacus Technology Corporation, Prepared for the U.S. DOE, 1996.
[xiv] Ibid. ii
[xv] Coyner, John V., "Flywheel Energy Storage System for Utilities and Their Customers", lecture notes, Oak Ridge National Laboratory Energineering Technology Division, Oak Ridge, TN
[xvi] Beachley, A Comparison of Accumulator and Flywheel Energy Storage for Motor Vehicle Applications.
[xvii] DOE Hybrid Electric Vehicle Web Site, http://www.hev.doe.gov, 1997
[xviii] Parks, Bill, Personal Communication, Aerovironment, April 1997.
[xix] R. Tew, Personal Communication, NASA Lewis Research Center, April 1997.
[xx] David W. South, Jon R. Mancuso, *Mechanical Power Transmission Components*, Marcel Dekker, Inc. 1994, p589.
[xxi] Richard J. Parker, Stuart H. Loewenthal, George, Fischer, "Design Studies of Continuously Variable Transmissions for Electric Vehicles", NASA TM-81642, 1981.
[xxii] Ibid v.

[xxiii] A. Colozza, "Effect of Power System Technology and Mission Requirements on High Altitude Long Endurance Aircraft", NASA CR-194455, February 1994.